The final

Cassini Science Symposium

12-17 August 2018—University of Colorado, Boulder

PROGRAM

Sponsored by the Cassini Project

The final
CASSINI SCIENCE SYMPOSIUM

August 12-17, 2018
CU's University Memorial Center, Glenn Miller Ballroom, Boulder, Colorado
Sponsored by the Cassini Project
Hosted by Larry Esposito and the organizing committee

Welcome

These invited and contributed talks include the latest Cassini findings on the Saturn system, including the interpretation and synthesis of results. We hope this Symposium can serve as a springboard for future studies and space missions.

The scientific organizing committee was composed of Larry Esposito—Chair, Josh Colwell, Jeff Cuzzi, Scott Edgington, Tamas Gombosi, Candy Hansen, Amanda Hendrix, Andrew Ingersoll, Norbert Krupp, Jonathan Lunine, Francois Raulin, Larry Soderblom, Linda Spilker.

Table of Contents

Schedule

Sunday August 12

RECEPTION	6:00-8:00pm	Hotel Boulderado

—Invited talks 30 minutes, contributed talks 15 minutes (unless noted otherwise) includes time for discussion—

Monday, August 13—*Rings & Icy Satellites*

Prior to session	8:15-8:45	Load presentations
Opening remarks	8:45	Lori Glaze, NASA HQ
RINGS 1	9:00 AM	
(Chairs: Larry W. Esposito, Luke Dones)		
Welcome and housekeeping		Larry W. Esposito
*Saturn's rings after Cassini (**INVITED,** 15 min.)*		Jeff Cuzzi
Shaping Saturn's F ring		Carl Murray
Saturn's outer B ring		Phil Nicholson
Radial distribution of textures in Saturn's main rings		Matthew Tiscareno
Synergy between density waves and viscous overstability in Saturn's rings		Glen Stewart
Break	10:15 – 10:30	Load presentations
RINGS 2	10:30	
(Chairs: Phil Nicholson, Joshua Colwell)		
Analyzing propeller gaps in Cassini NAC images & Hydrodynamic Simulations of Asymmetric Propeller Structures in the Saturnian Ring System		Holger Hoffmann & Michael Seiler
Still more Kronoseismology with Saturn's rings, filling in the spectrum of planetary normal modes		Matthew Hedman
Saturn ring results from the Cassini Composite Infrared Spectrometer		Estelle Deau
Thermal infrared determinations of particle size properties and ring emissivity with Cassini CIRS		Stuart Pilorz
Properties of aggregates and particle sizes in the C ring plateaus		Richard Jerousek
Physical properties of Saturn's Rings from multi-wavelength multi-viewing-geometry extinction and scattering Cassini radio occultation observations.		Essam Marouf
*Lunch (**Group photo first**)*	12:00 – 1:15pm	On your own
ICY SATELLITES 1	1:15	

(Chairs: Andrew Ingersoll, Katrin Stephan)

Paleo non-synchronous rotation (NSR) and true polar wander (TPW) on Enceladus	Paul Helfenstein
Enceladus plumes: Variability on timescales from months to years	Andrew Ingersoll
Using Enceladus's complex surface to reconstruct a complex history	Emily Martin
Temporal variations in Enceladus surface temperature?	Carly Howett
Evolving Enceladus: What Cassini taught me about Saturn's surprising satellite	James Roberts
Cassini ISS photometry of Enceladus' surface and major terrains.	Anne Verbiscer

Break 2:45 – 3:00 Load presentations

ICY SATELLITES 2 3:00

(Chairs: Katrin Stephan, Andrew Ingersoll)

Exploring the oxidation chemistry of Enceladus' ocean	Christine Ray
The structure and composition of Enceladus' plume – Results from Cassini's Ultraviolet Imaging Spectrograph (UVIS)	Candy Hansen
Jets of Enceladus: Cassini's UVIS occultation observations and DSMC model of Enceladus jets	Ganna Portyankina
Resolving Enceladus plume production along the fractures	Ben Southworth

POSTER SESSION – RINGS & ICY SATELLITES 4:00

Crater chronometers and chronos	Kevin Zahnle (M1)
Color mapping of geologic processes on Saturn's icy moons: Enceladus 2018	Paul Schenk (M3)
A new suite of hydrodynamical simulations of collisions between Saturn's icy mid-sized moons	Luis Teodoro (M4)
Texture classification in Cassini ISS images of Saturn's rings	Klaus-Michael Aye (M5)
Particle size and ring structure of Saturn's rings from stellar and solar occultations in the UV	Tracy Becker (M6)
The structure of Saturn's B ring from Cassini CIRS High-resolution scans	Shawn Brooks (M7)
Clues to clumping	Joshua Colwell (M8)
Particle properties in Saturn's rings from skewness of Cassini UVIS stellar occultations	Melody Green (M9)
Analyzing propeller gaps in Cassini NAC images	Holger Hoffmann (M10)
Hydrodynamic Simulations of Asymmetric Propeller Structures in the Saturnian Ring System	Michael Seiler (M11)

Adjourn 6:00

—Invited talks 30 minutes, contributed talks 15 minutes (unless noted otherwise) includes time for discussion—

Tuesday, August 14—*Icy Satellites & Rings*

Prior to session	8:30-9:00	Load presentations
ICY SATELLITES3	9:00 AM	
(Chairs: Paul Schenk, Ganna Portyankina)		
*Icy satellites in the era of Cassini (**INVITED**)*		Bonnie Buratti
Orbital history of Mimas and Enceladus		Matija Ćuk
The big impact of small craters on midsized Saturnian satellites		Sierra Ferguson
Constraints on the recent Saturnian crater flux from Cassini VIMS and ISS: Crater ages on Rhea		Michelle Kirchoff
Break	10:15 – 10:30	Load presentations
ICY SATELLITES 4	10:30	
(Chairs: Ganna Portyankina, Paul Schenk)		
The tide that binds: Stress and tectonics on the mid-sized icy moons of Saturn		Alyssa Rhoden
Multi-wavelength investigation of the co-orbital moons Dione and Helene		Emilie Royer
Surface compositions of the icy satellites from UV spectroscopy		Amanda Hendrix
High energy electron sintering of icy regoliths: Learning from Pac-Man		Micah Schaible
H_2O ice phase measurements and mapping of the Saturn Icy Satellites		Michelle Kirchoff
Saturn's irregular moons: Cassini imaging observation campaign		Tilmann Denk
Lunch	12:00 – 1:15pm	On your own
RINGS 3	1:15	
(Chairs: Jeff Cuzzi, Linda Spilker)		
Exogenous dust at Saturn observed by CASSINI-CDA		Nicolas Altobelli
Implications of the micrometeoroid flux measured by Cassini CDA for ballistic transport in Saturn's rings		Paul Estrada
Modeling the bombardment of Saturn's rings and fit to Cassini UVIS spectra to estimate their age		Joshua Elliott
Viscous spreading and the mass of Saturn's rings		Julien Salmon
A recent origin for Saturn's rings from the collisional disruption of an icy moon		John Dubinski
Recent origin of Saturn's rings: How sure are we?		Luke Dones *(withdrawn)*
Break	2:45 – 3:00	Load presentations
RINGS 4	3:00	
(Chairs: Matthew Hedman, Matthew Tiscareno)		
Cassini's view of the faint D ring and Roche Division		Robert Chancia
The ring atmosphere/ionosphere revisited using results from the Cassini Grand Finale Mission		Wei-Ling Tseng
Cosmic Dust Analyzer onboard Cassini Collects Material from Saturn's Main Rings		H. –W. Hsu

INMS compositional constaints on organics and other volatiles in Saturn ring rain		Kelly Miller
POSTER SESSION –ICY SATELLITES & RINGS	4:00	
The Enceladus auroral footprint – and lack thereof		Abigail Rymer (TH37)
Outstanding problems in understanding Saturn's rings		Jeff Cuzzi (T12)
Spectral properties of fresh impact craters on Dione, Tethys, Rhea and Ganymede		Katrin Stephan (T13)
Enceladus: three-stage limit cycle and current state		Jing Luan (T13b)
Cassini's science data connection: the deep space network		Dave Doody (T14)
Predator-prey analogs for Saturn ring dynamics		Larry Esposito (T15)
rss_ringoccs: An open-source analysis package for Cassini RSS ring occultation observations		Richard French (T16)
Cassini and the PDS Ring-Moon Systems Node		Mitchell Gordon (T17)
Advanced radiative transfer model for closely packed regolith surfaces		Sanaz Vahidinia (T18)
Adjourn	6:00	
PUBLIC TALK	7:30-8:30	Glenn Miller Ballroom

—Invited talks 30 minutes, contributed talks 15 minutes (unless noted otherwise) includes time for discussion—

Wednesday, August 15—*Titan*

Prior to session	8:30-9:00	Load presentations
TITAN 1	9:00 AM	
(Chairs: Veronique Vuitton)		
*Insights into Titan's surface and subsurface methane reservoirs at the end of the Cassini Mission **(INVITED)***		Elizabeth Turtle
*Titan's atmosphere: How to bake a five-layered cake **(INVITED)***		Conor Nixon
Titan's interior structure inferred from analysis of topographic and gravity data		Christophe Sotin (*withdrawn*)
Break	10:15 – 10:30	Load presentations
TITAN 2	10:30	
(Chairs: Veronique Vuitton)		
Frozen hydrocarbons on Titan		Jason Soderblom
Pond hockey on Titan? How to stratify Titan's vernal ponds and form ethane ice deposits		Jordan Steckloff
Radiolysis in Titan's subsurface ocean provides a new source of deep energy for possible life		Chris Glein *(withdrawn)*
Titan surface temperatures through the Cassini mission		Donald Jennings

Seeing Titan with VIMS infrared eyes during 13 years: from changing atmospheric features over the poles to global surface mapping		Stéphane Le Mouélic
Uncovering the influence of surface and subsurface hydrology on Titan's climate system		Juan Lora
Lunch	12:00 – 1:15pm	On your own
TITAN 3	1:15	
(Chairs: Conor Nixon, Sandrine Vinatier)		
Trace organic volatiles in Titan lower atmosphere: Re-interpretation of Huygens/GCMS data		Thomas Gautier
Enhancement of the Huygens DISR dataset		Bjorn Grieger
Regional mapping of aerosol population and surface albedo of Titan by the massive inversion of the Cassini/VIMS dataset		Sebastien Rodriguez
Taking the long view: High resolution MM/SubMM spectral imaging of Titan's atmosphere with ALMA		Mark Gurwell *(withdrawn)*
Seasonal variations in Titan's stratosphere observed with Cassini/CIRS during northern spring		Sandrine Vinatier
Seasonal effects in Titan's stratosphere analyzed through Global Climate Modelling		Jan Vatant d'Ollone
Break	2:45 – 3:00	Load presentations
TITAN 4	3:00	
(Chairs: Sandrine Vinatier, Conor Nixon)		
Seasonal variations of Titan's stratospheric temperatures and winds from Cassini/CIRS observations		Richard Achterberg
Titan's zonal winds from Cassini radio-occultation soundings		F.Michael Flasar
Cassini UVIS observations of Titan airglow		Joe Ajello
Highlights and open questions on Titan's atmospheric chemistry		Véronique Vuitton
POSTER SESSION - TITAN	4:00	
Evolution of aerosols in Titan's ionospheric plasma: An experimental simulation		Audrey Chatain (W19)
Key positive ion precursors to tholin formation		David Dubois (W20)
Photochemical activity of HCN-C4H2 ices in Titan's lower atmosphere		David Dubois (W21)
Infrared spectroscopy support for the Cassini mission		Antoine Jolly (W22)
Visualization and analytics of Saturnian moons data		Emily Law (W23)
Enigmatic electron densities in Titan's ionosphere: Is ion transport a solution?		Stephen Ledvina (W24)
Comparison of modeled alkane abundances in Titan's atmosphere using different spectral windows with Cassini CIRS spectra		Nicholas Lombardo (W25)
Seasonal changes in the middle atmosphere of Titan from 2004 to 2017 using Cassini/CIRS observations		Christophe Mathe (W26)

Is Titan's hemispheric surface-liquid dichotomy an equilibrium state?		Jonathan Mitchell (W27)
Integrated laboratory, modeling and observational investigations of the condensation of benzene on Titan's stratospheric aerosols		Ella Sciamma-O'Brien (W28)
Adjourn	6:00	
BANQUET	7:30-9:00	Hotel Boulderado

—**Invited talks 30 minutes, contributed talks 15 minutes (unless noted otherwise) includes time for discussion**—

Thursday, August 16—Magnetospheres & Saturn

Prior to session	8:30-9:00	Load presentations
MAPS 1	9:00 AM	
(Chairs: Tamas Gombosi, Norbert Krupp)		
*An overview of Cassini's major findings regarding Saturn's magnetosphere (**INVITED**)*		Xianzhe Jia
Saturn's magnetic field observations from the Cassini Grand Finale		Michele Dougherty
The legacy of Cassini RPWS: Radio and plasma waves at Saturn		William Kurth
New insights into Saturn's inner magnetosphere during Cassini's Grand Finale: MIMI		Norbert Krupp
Break	10:15 – 10:30	Load presentations
MAPS 2	10:30	
(Chairs: Norbert Krupp , Tamas Gombosi)		
Saturn's internal magnetic field revealed by Cassini Grand Finale		Hao Cao
Global maps of energetic charged particles at Saturn and their relation to the magnetic field		James Carbary
Evidence for a ring-driven current system		Willliam Farrell
Relative fractions of water-group ions in Saturn's inner magnetosphere		Mark Perry
Saturn's ionosphere: Electron density altitude profiles and ring shadowing effects from the Cassini Grand Finale		Lina Hadid
A large seasonal variation of energetic C+ and CO+ abundances in Saturn's magnetosphere probably resulting from changing ring illumination		Douglas Hamilton
Lunch	12:00 – 1:15pm	On your own
SATURN 1	1:15	
(Chairs: Valery Lainey, Christopher Mankovich)		

Constraints on Saturn's deep interior from seismic inversions		Ethan Dederick
Saturn's deep atmosphere revealed by the Cassini Grand Finale gravity measurements		Eli Galanti
Determination of tidal parameters at multiple frequencies within Saturn from ground and space data		Valery Lainey
Ring seismology as a probe of Saturn's rotation		Christopher Mankovich
Saturn density profiles from gravity data with minimal assumptions		Naor Movshovitz
A refined measurement of Saturn's gravity environment		Luciano Iess
Break	2:45 – 3:00	Load presentations
SATURN 2	3:00	
(Chairs: Zarah Brown, Scott Edgington)		
*Saturn: Cassini explores the giant planet (**INVITED**)*		Andrew Ingersoll
Polar temperature profiles of Saturn from Grand Finale UVIS stellar occultations		Zarah Brown
Saturn's stratospheric dynamics and chemistry revealed by CIRS limb observations		Sandrine Guerlet
POSTER SESSION – MAPS & SATURN	4:00	
The induced magnetosphere of Titan: characterizing its outer edge		Cesar Bertucci (TH29)
Planetary Exploration, Horizon 2061: Some proposed next steps for Giant Planets Systems exploration		Michel Blanc (TH30)
A statistical picture of interchange injections at Saturn through energetic H+ flux intensifications		Abigail Azari (TH31)
The meridional magnetic field of Saturn: a new analytical model		James Carbary (TH32)
Re-examining the ordering of injection events within Saturnian SLS5 longitude		George Hospodarsky (TH33)
A diffusive equilibrium model for the plasma density from 2.4 to 10 RS		Ann Persoon (TH34)
Auroral hiss emissions during Cassini's Grand Finale: Diverse electrodynamic coupling between Saturn, its rings, and Enceladus		Ali Sulaiman (TH35)
Dust observation by the Radio and Plasma Wave Science instrument during the Cassini Mission		Shengyi Ye (TH36)
The Enceladus auroral footprint – and lack thereof		Abigail Rymer (TH37)
TEXES Saturn's observations in support of the Cassini mission		Thierry Fouchet (TH38)
Saturn Ring Seismology: Saturn's Normal Modes and Forcing of the Slowest Density Waves in the C Ring		Jim Friedson (*withdrawn*)
A Concept for a Future Entry Probe Mission to Saturn – The Saturn PRobe Interior and aTmosphere Explorer (SPRITE)		Amy Simon (TH40)
Adjourn	6:00	

—Invited talks 30 minutes, contributed talks 15 minutes (unless noted otherwise) includes time for discussion—

Friday, August 17—*Saturn*

Prior to session	8:30-9:00	Load presentations
SATURN 3	9:00 AM	
(Chairs: Kevin Baines, Scott Edgington)		
Potential vorticity of Saturn's polar regions		Arrate Antuñano Martin
The eye of Saturn's north polar vortex: Surprising diversity of cloud structures observed at high spatial resolution by Cassini/VIMS during the Grand Finale		Kevin Baines
Saturn photochemistry and ring shadow		Scott Edgington
A survey of slowly moving thermal waves in Saturn from Cassini CIRS and ground-based thermal observations from 2003 to 2017		Glenn Orton
Saturn's south polar cloud structure inferred from 2006 Cassini VIMS spectra		Lawrence Sromovsky
Break	10:15 – 10:30	Load presentations
SATURN 4	10:30	
(Chairs: Tommi Koskinen, Robert West)		
Saturn in Lyman a: A comparison of Cassini and Voyager observations		Tommi Koskinen
Monitoring Saturn's upper atmosphere density variations and determination of the Saturnian He mixing ratio using helium 584 Å airglow		Christopher Parkinson
Characteristics of the neutral influx from Saturn's rings		Mark Perry
The composition of Saturn's upper atmosphere from Cassini/INMS measurements		Joseph Serigano
Exploring low-latitude electrodynamics in Saturn's thermosphere		Jess Vriesema
Cassini UV reflection spectra of Saturn: Acetylene and haze		Robert West
Adjourn	12:00pm	

Abstracts

Alphabetical within each discipline: *Icy Satellites, Magnetospheres, Rings, Saturn, Titan*

Icy Satellites

Icy satelites in the era of Cassini

B. J. **Buratti**[1] and the *Cassini* Science Teams.
[1]Jet Propulsion Laboratory, California Institute of Technology (4800 Oak Grove Dr. Pasadena, CA 91109 (bonnie.buratti@jpl.nasa.gov);

Introduction: The *Cassini* spacecraft performed the first in-depth study of the moons of Saturn. The discovery and characterization of ongoing activity on Enceladus and a liquid global ocean sustaining it was one of the crowning achievements of the mission. We will present the most important discoveries of the mission and discuss the main open questions. Emphasis will be put on the final year of the mission.

Main Results: Among *Cassini's* prime discoveries was a heavily cratered surface on Phoebe; the unique equatorial ridge on Iapetus; a possible subsurface ocean on Dione; a Rhea not in hydrostatic equilibrium; strange red streaks of unknown origin on Tethys; equatorial bulges of accreted ring material on the ring moons; the existence of one or more low-albedo reddish chromopheres that color the moons and rings; the importance of plasma-surface interactions, and ring-surface interactions, on determining the albedo and color patterns of the moons' surfaces; unresolved evidence for activity on moons other than Enceladus; evidence for thermal migration of volatiles on Iapetus; the discovery of CO_2 and organic molecules in the system; the characterization of craters found uniquely on the surface of Hyperion, which are believed to be similar to terrestrial "suncups"; "blue pearls" on Rhea of unknown origin; and the discovery of new small moons.

Remaining questions: Even though the mission fulfilled all the science goals for icy moons, a number of questions remain outstanding. Among them are: 1. What is the identity of the red chromophore(s) in the system? 2. Do the surfaces of any of the moons contain ammonia or ammonia hydrate? 3. What causes the red streaks on Tethys and the "blue pearls" on Rhea? 4. What is the total heat production on Enceladus and what are its long-term variations? Does the plume vary with the seasons of Saturn? 5. Are any of the other moons active, particularly Dione or Tethys? 6. Why are some of the moons not in hydrostatic equilibrium? 7. Is the ridge on Iapetus evidence for a past ring? 8. How old are the moons? Could they possibly have had a relatively recent origin? 9. Why does the origin of the moons of Jupiter and Saturn seem to diverge, with the jovian moons being formed relative to their position from Jupiter, and the Saturnian moons being formed by stochastic events? All these unknowns will serve as a guide for future explorations of Saturn, when a new generation will continue where this great mission left off.

Acknowledgments: This work was funded by the *Cassini* Project. Part of this research was carried out at the Jet Propulsion Laboratory, California Institute of Technology, under contract to the National Aeronautics and Space Administration.

Orbital history of Mimas and Enceladus

M. **Ćuk**[1], M. El Moutamid[2] and M. S. Tiscareno[1].
[1]SETI Institute, 189 N Bernardo Ave, Mountain View, CA 94032, [2]Cornell University, Space Sciences Building, Ithaca, NY 14853, (mcuk@seti.org).

Background: Saturn's moon Enceladus is currently in the 2:1 mean-motion resonance (MMR) with a larger moon Dione. This resonance excites the eccentricity of Enceladus and apparently plays an integral role in Enceladus's intense internal heating. While older estimates of tidal heating, based on lower tidal evolution rates, could not account for the observable heat flux (assuming equilibrium, Meyer and Wisdom 2007), the recently proposed lower tidal Q of Saturn would naturally resolve this discrepancy (Lainey et al 2012, 2017). The most important remaining problem concerning Enceladus's resonance is that the current e-Enceladus sub-resonance is the last of the six sub-resonances that Enceladus would encounter as its orbit was converging with that of Dione. Prior calculations have shown that capture into the e-Dione resonance would be very robust and hard to avoid (Meyer and Wisdom 2008), and our own numerical tests have confirmed that result. The very low inclination of Enceladus (0.003 deg) also makes it likely to be captured in the inclination-type sub-resonances (most notably the pure i-Enceladus one). However, these inclination-type resonant captures certainly did not happen, or the inclinations of either Enceladus or Dione would be higher than we observe them to be.

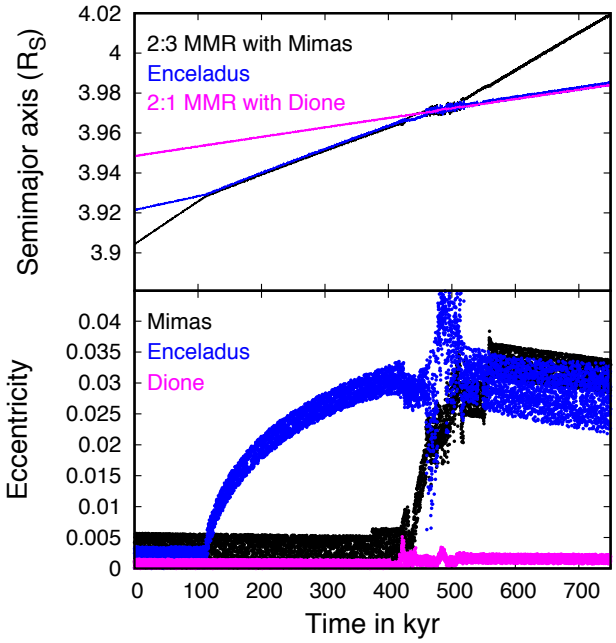

Our work: We propose to test a hypothesis that there was a "handoff" between the Mimas-Enceladus and Enceladus-Dione resonances. The Mimas-Enceladus 3:2 MMR would be established first, after which the pair would encounter the MMR with Dione (3:1 for Mimas, 2:1 for Enceladus). During the handoff, the presence of Mimas affects the dynamics of capture into the Enceladus-Dione MMR in two ways. First, the presence of Mimas creates resonance overlap and chaos. Second, Mimas "pushes" Enceladus outward much faster than it otherwise would evolve. The figure below shows a preliminary accelerated simulation of such a scenario, where Mimas first captures Enceladus into 3:2 e-Enceladus resonance, then the pair captures Dione into a e-Dione resonance. A chaotic resonance overlap ensues, during which the eccentricity of Mimas is excited to just above its current value. Eventually Mimas breaks from the triple resonance, moving on to encounter the MMR with Tethys. Enceladus and Dione remain in the 2:1 e-Enceladus MMR observed today. This scenario is very promising for explaining the capture into the current Enceladus-Dione MMR, as well as the currently unexplained eccentricity of Mimas. Additionally, the "handoff" explains how Enceladus and Dione were captured into their MMR in less than 100 Myr, despite their slow orbital convergence.

H_2O ice phase measurements and mapping of the Saturn icy satellites

C.M. **Dalle Ore**[1,2], F. Scipioni[1], K. Stephan[3], and D.P. Cruikshank[1]. *[Presented by Michelle Kirchoff, Southwest Research Institute, kirchoff@boulder.swri.edu]*

[1]NASA Ames, MS 245-6, Moffett Field, CA 94035, (Dale.P.Cruikshank@nasa.gov), (francesca.scipioni@nasa.gov) [2]SETI Institute,183 Bernardo Ave, Mountain View, CA 94043, (cmdalleore@gmail.com), [3]Institute of Planetary Research, DLR, 12489 Berlin, Germany (Katrin.Stephan@dlr.de)

Introduction: In spite of having been the focus of many thorough studies since the arrival of the Cassini spacecraft at Saturn, the surfaces of the icy satellites continue to intrigue. Temperature maps of the satellites show anomalous and unexpected distributions on two of the satellites (Howett et al 2011, 2012, 2013 and references therein) attributed to changes in thermal inertia due to the high energy electron bombardment affecting the surfaces. Color maps of Mimas and Tethys also show patterns (Schenk et al. 2011) that are indicative of interaction between the ice and the very high-energy electrons. Dione shows patterns, the Wispy Terrains, that are reminiscent of the fractures, the 'Tiger Stripes' that distinguish Enceladus

At the typical average temperature, ~80 K, amorphous ice is stable against thermal recrystallization for long timescales (Mastrapa et al. 2013). Nevertheless, surfaces are generally observed to be crystalline.The phase of the ice records information on the local physical conditions, such as temperature, irradiation, and bombardment changes. Crystalline ice is usually associated with ice formation in warmer temperatures (above ~135 K) (Mastrapa & Brown 2006). Amorphous H_2O ice, on the other hand, implies colder temperatures (below 135 K) and can result from irradiation from sufficiently energetic photons or charged particle bombardment of the crystalline phase (Baragiola et al. 2003). Amorphous H_2O ice will convert back to the crystalline phase at ~135 K (Mastrapa & Brown 2006). Because both phases are stable at Saturn's icy satellites, then the presence of one phase versus the other can trace the history of the ice on the surface.

Enceladus, Dione, Rhea and Mimas orbit Saturn at different distances and sample different parts of its magnetosphere experiencing varying degrees of exposure to high-energy electrons. We use measurements of crystallinity looking for possible explanations for some of the phenomena characterizing these surfaces.

Method: To measure the crystalline to amorphous ratios we apply the methods from Dalle Ore et al. (2015). The first step consists in determining variations in the 1.5-µm band indicative of changes in grain-size/temperature/composition on the surface, which could mistakenly be interpreted as phase variations. We then model the 2-µm band shape with varying amounts of crystalline to amorphous ice to calibrate the effect on the spectral signature. The calibration is applied to the measured 2.0 µm band asymmetry to gauge the phase change. The resulting ice phase ratio were mapped, compared, and contrasted among the satellites.

References:

Baragiola, R.A., 2003 Planet. Space Sci. 51, 953–961; Dalle Ore, C.M., Cruikshank, D.P., Mastrapa, R.M.E., Lewis, E., and White, O.L. 2015. Icarus, 261, 80-90; Filacchione, G., D'Aversa, E., Capaccioni, F., et al. 2016. Icarus, 271, 292-313; Howett, C.J.A., Spencer, J.R., Schenk, P., et al. 2011. Icarus, 216, 221; Howett, C.J.A., Spencer, J.R., Hurford, T., Verbiscer, A., & Segura, M. 2012. Icarus, 221, 1084; Howett, C.J.A., Spencer, J.R., Paranicas, C., & Schenk, P.M. 2013. LPI Contributions, 1719, 2824; Mastrapa, R.M.E., Brown, R.H., 2006. Icarus 183, 207–214; Mastrapa, R.M.E., Grundy, W.M., and Gudipati, M.S. 2013. The Science of Solar System Ices, 371-408.

Saturn's irregular moons: Cassini imaging observation campaign

T. **Denk**[1] and S. Mottola[2].

[1]Freie Universität Berlin, Malteserstr. 74-100, 12249 Berlin, Germany (tilmann.denk@fu-berlin.de), [2]Deutsches Zentrum für Luft- und Raumfahrt (DLR), Rutherfordstr. 2, 12489 Berlin, Germany (Stefano.Mottola@dlr.de).

Introduction: With 38 known members, the outer or irregular moons constitute the numerically largest group of satellites in the Saturnian system. Their orbital semi-major axes range between 11.4 and $25.2 \cdot 10^6$ km. Nine objects occupy prograde, the other 29 retrograde orbits.

All but exceptionally big Phoebe (ø = 213 km) were discovered between year 2000 and 2007 and thus after the launch of Cassini-Huygens. Except Phoebe (targeted flyby on 11 June 2004 at ≈2070 km altitude), they were not part of the original science goals of the mission.

Ground-based vs. Cassini: As seen from Earth, Phoebe reaches a brightness of ≈16 mag. Approximately 30-40 km sized objects Albiorix and Siarnaq barely scratch the 20-mag mark, while the rest (≈4-25 km) does not exceed 21 to 25 mag. Therefore, obtaining high-quality lightcurve or color data requires very large telescopes or smaller distances between observer and moons.

The ISS-NAC (Imaging Science Subsystem Narrow Angle Camera; aperture 0.19 m) onboard Cassini was ≈40-300 times closer to the irregular Saturnian moons than Earth and thus well suited for a survey. The apparent brightness of the irregulars reached up to 10 mag (Phoebe ≈6 mag), and most objects were within the observation limit of the NAC (≈16 mag for lightcurve studies). Other advantages for Cassini were the large range of accessible phase angles (0°-180° in principle), or the potential option to observe a single object continuously for up to ≈37 h. Thus, we initiated an observation campaign which has been performed mainly during the Cassini Solstice mission.

Cassini observation campaign: All nine prograde plus 16 of the 29 retrograde irregular moons of Saturn were successfully observed with ISS. Since the objects (except Phoebe) were not resolved by the NAC, the prime observation goal was to obtain lightcurves to determine rotational periods, shape models, pole-axis orientations, possible global color variegations, etc.

The measured lightcurves are very likely shape-driven (except for Phoebe). Most show either four or six extrema (2-maxima/2-minima or 3-maxima/3-minima patterns), indicative for very different shapes among Saturn's irregular moons. Rotational periods were derived for all 25 observed moons (for 20 with errors <2%); the fastest is 5.45 h (moon Hati). Although this is the fastest reliably known rotational period of all moons in the solar system, it is still slower than about one third of the asteroid spins at the size range 4-45 km, indicating that the outer moons may have rather low densities, possibly as low as comets.

Talk: Our talk will give a short overview of the observation campaign and of some results. These include lightcurves at various phase angles, rotational periods, shape and pole-axis determinations, colors, and the search for binary moons. Furthermore, likely non-random correlations between the object ranges to Saturn, their orbit directions, sizes, and rotational periods were found.

Reference: Denk, T., Mottola, S., Tosi, F., Bottke, W.B., Hamilton, D.P. (2018): The Irregular Satellites of Saturn. Chapter in: Enceladus and the Icy Moons of Saturn, Schenk, P.M., et al. (eds.), Space Science Series, The University of Arizona Press, Tucson, AZ.

Cassini's science data connection: the Deep Space Network

D. **Doody**[1]

[1]Jet Propulsion Laboratory, 4800 Oak Grove Drive, Pasadena, CA 91109

(dave.doody@jpl.nasa.gov).

The DSN served as Cassini's science and engineering connection for the twenty years beginning in ATLO and ending with the Grand Finale dive. The project scheduled DSN resources approximately 8,700 times since launch, averaging roughly once a day using one or more apertures. This poster illuminates facets of the DSN connection as follows:

RS experiment and ORT passes, TCM and OTM passes, DSN engineering demonstration passes, and anomaly-response passes all involved significant realtime direction of DSN activities. Outside of those, guided automation evolved to become the norm.

Typical link operations with DSN via Cassini RTO are described, and DSN subsystems and their operations are characterized. Included are: predicts, precal setup, coherent radiometric TRK data acquisition, locking, decoding and delivering science and engineering playback TLM, data-gore prevention tactics, use of "wedding-cake" TLM bit rates, CMD protocols and cautions, the limited VLBI and TLM components of navigation input, selected use of full-spectrum arraying to improve TLM bit-rate margins, and MON data which reflected performance in the DSN subsystems and assemblies. The new DSN capabilities driven by Cassini's requirements are mentioned, as is the independent evolution of DSN capabilities during Cassini's tenure. Data losses are categorized, and data-capture performance is evaluated.

The big impact of small craters on midsized Saturnian satellites

S. N. **Ferguson**[1] and A. R. Rhoden[1].
[1]Arizona State University, School of Earth and Space Exploration, 781 E Terrace Mall, Tempe AZ, 85287, (sierra.ferguson@asu.edu) and (alyssa.rhoden@asu.edu).

Introduction: Tethys and Dione are two of Saturn's midsized icy satellites, which differ in the geology that is observed on their surfaces. Tethys is well known for the Odysseus basin and the Ithaca Chasma canyon system, whereas Dione is well known for its wispy terrain and a variety of tectonic terrains. However, both moons have substantial populations of impact craters, and they are the only moons known to have co-orbital satellites of their own. Within the Saturnian system, it has been suggested that the satellites are bombarded by planetocentric debris in addition to the heliocentric debris that is generally expected. We are investigating the populations of craters on the midsized satellites to constrain the source populations of impactors, with particular emphasis on planetocentric, co-orbital, secondary, and sesquinary populations. We have utilized high resolution images taken by the Cassini spacecraft to catalog the craters observed on the surface. The images used have an average spatial resolution of 150 m/pix, which enables the study of the 1-2 km craters that are most likely to be associated with the populations of interest. Because we are focusing on high-resolution images, we are limited to small regional images and mosaics. A global study is not currently possible with the available data. To date, we have mapped and analyzed the crater populations on Tethys and have expanded our study to Dione. Our mapped regions on Tethys include a mosaic near the Odysseus basin centered at 6.95° S, -178.9°W (region 1), two regions near Ithaca Chasma centered at 5.05°N, -27.23°W and 19.26° N, -11.462° W respectively (regions 2 and 3), and one region near the antipode of Odysseus centered at 28.31° S, -42.18° W (region 4). On Tethys we found a large number of small impact craters across the four mapped regions. In each region, craters with diameters between 1-2 km were the most frequently observed, followed by craters between 3 and 4 km. In addition to the crater mapping on Tethys, we have also mapped linear features that may also have impact origins such as scours or pit chains. Interestingly, region 1 has the largest number of small craters, whereas the other regions have much more similar population statistics. This could meant that region 1 is slightly older, or it could be a signature of a regionally-variable impactor flux. Analysis of secondary craters from the Odysseus-forming event shows that they do not explain the increase in region 1. We will continue to assess potential sources that would predominantly affect a region at the anti-Saturn point. We will also present a comparison between the populations on Tethys and our on-going mapping on Dione.

The Structure and Composition of Enceladus' Plume – Results from Cassini's Ultraviolet Imaging Spectrograph (UVIS)

C. J. **Hansen**[1], L. W. Esposito[2], A. Hendrix[1], G. Portyankina[2], J. Colwell[3].
[1]Planetary Science Institute, 1700 E. Fort Lowell, Tucson, AZ 85719, (cjhansen@psi.edu), [2]University of Colorado, Laboratory for Atmospheric and Space Physics, Boulder, CO, [3]University of Central Florida, Orlando, FL.

The geologically youthful surface of Saturn's moon Enceladus, and the association of Enceladus' orbit with Saturn's E ring, made it an important target for investigation by the Cassini mission to Saturn. Four close flybys of Enceladus were planned for Cassini's prime mission. In July 2005, on the third flyby, Cassini's instruments definitively detected a water vapor plume with jets of ice particles erupting from Enceladus, implicated in Magnetometer data returned at Cassini's first flyby in Febuary 2005 [1, 2, 3]. More flybys were planned into Cassini's extended mission to study this remarkable discovery.

Stellar occultations observed by Cassini's Ultraviolet Imaging Spectrograph (UVIS) show that the gas composition of the plume is dominated by water [2] with other molecular constituents such as CO_2, NH_3, CH_4 and various other hydrocarbons detected by Cassini's Ion Neutral Mass Spectrometer (INMS) providing the identification of the remaining ~5-10% [4]. The occultations also revealed highly collimated supersonic gas jets embedded within the overall plume [5]. Assuming a source temperature of at least 170K [6], all gas molecules leave with thermal velocities greater than escape velocity. Occultations observed from 2005 to 2017 show source rates varying just 15% in over 12 years, at a rate adequate to populate and maintain the torus of neutral water products OH, detected by Hubble Space Telescope [7], and O, observed on approach by Cassini [8], against loss [2].

Tidal energy has long been theorized as the source of Enceladus' eruptive activity, but tides were finally implicated as the driving force by the variability observed in particle flux by VIMS [9]. The number of particles expelled from Enceladus varies diurnally as Enceladus orbits Saturn. UVIS results show that the supersonic collimated gas jets imbedded in the plume are the likely source of the variability in dust output, rather than overall flux from the tiger stripe fissures. An occultation of epsilon Orionis observed in 2016 when Enceladus was near apokrone showed that although the bulk flux changed little the amount of water vapor coming from the Baghdad I jet increased by 25%. The Baghdad I jet was observed again in the 2017 epsilon CMa occultation, with a column density half that of 2016, bolstering the conclusion that the gas jets change output as a function of orbital longitude.

Other observational techniques have been applied, e.g. Enceladus was observed in transit across Saturn in 2009 (the plume was not detected). We will describe the observations made by Cassini's UVIS from 2004 to 2017, and what the results tell us about the composition and structure of Enceladus' plume.

References:

[1] Dougherty, M. et al. (2006) *Science* 311:1406; [2] Hansen, C. J. et al. (2006) *Science* 311:1423; [3] Porco, C. et al. (2006) *Science* 311:1393; [4] Waite, J. W. et al. (2011) *EPSC-DPS* 2011-61-4; [5] Hansen, C. J. et al. (2008) *Nature* 456:477; [6] Spencer, J. et al. (2006) *Science* 311:1401; [7] Shemansky, D. E. et al. (1993) *Nature* 363:329; [8] Esposito, L. W. et al., (2005) *Science* 307:1251. [9] Hedman, M. et al. (2013) *Nature* 500:182.

Paleo non-synchronous rotation (NSR) and true polar wander (TPW) on Enceladus

P. **Helfenstein**[1], R. Tajeddine[1] , P. C. Thomas[1], B. Giese[2], T. Roatsch[2] and T. Denk[3].
[1]CCAPS, 320 Space Sciences Bldg. Cornell University, Ithaca, NY 14853-6801 (helfenst@astro.cornell.edu), [2]Institute of Planetary Research, DLR, Rutherfordstr.2, 12489 Berlin, Germany (bernd.giese@dlr.de), [3]Freie Universität Berlin, Malteserstr. 74-100 Berlin, 12249, Germany, (tilmann.denk@fu-berlin.de)

Introduction: Tajeddine *et al.* [1] discovered a global pattern of topographic depressions which imply that Enceladus's crust has undergone TPW by ~55° roughly about the tidal axis, i.e. (0° N, 11° W). They also identified a sparse collection of geological features that are plausible degraded morphologic analogs to present day structures in the South Polar Terrain (SPT) province. We examine the change in position and orientations of mapped terrain units and tectonic structures predicted by TPW. We identify an ancient system of quasi-parallel fractures that appear to be relict tiger stripe rifts which likely originated near the geographic location now occupied by the active *Baghdad Sulcus* tiger stipe.

Approach, Results, and Analysis: We projected terrains given in an updated unit map of Enceladus [2] to south polar stereographic (Fig.1). The active SPT (Fig. 1A) is presently centered on the south pole and includes S.P. Funiscular Plains, active tiger stripe units and examples of relic tiger stripes. Of special interest is an annulus of highly-fractured S.P. Reticulated Plains surrounding the active SPT and a partial annulus of stratigraphically older W.H. Reticulated Plains that is offset toward the northeast.

The proposed backward TPW rotation of 55° would center the south pole on the easternmost section of W.H. Reticulated Plains (Fig. 1B). This terrain unit is characterized by highly overprinted, cross-cutting fracture segments. We identified a pair of piecewise continuous fractures that are forked at the same end and lie close to the paleo south pole. Because they are remarkably similar to active tiger stripe rifts in shape, scale, and length we propose that they may be relic tiger stripe rifts that were displaced from their original orientation by NSR prior to the TPW event. Indeed, rotating Fig. 1B westward by ~75° about the paleo south pole (Fig. 1C), places them at the same geographic location and orientation occupied today by *Baghdad Sulc*us.

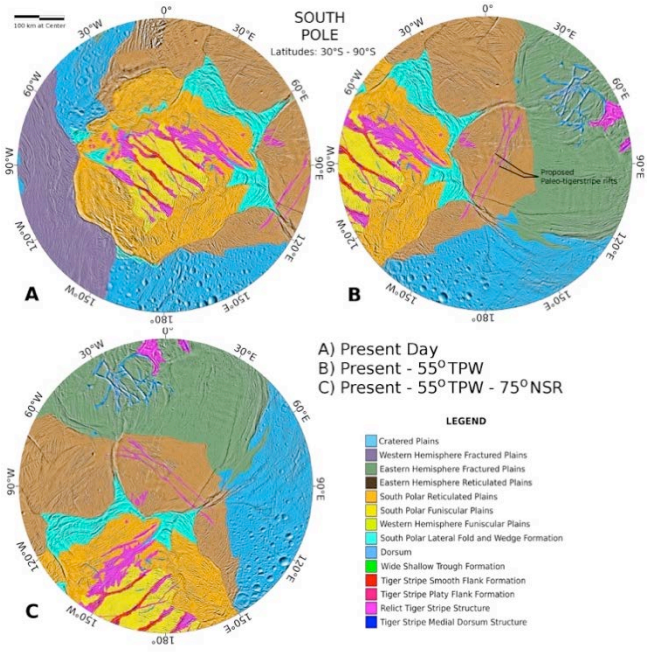

Figure 1: Three South Polar stereographic projections of Enceladus terrain units [2] that show the modeled backward progression through time starting from A) present day to B) just prior to 55° True Polar Wander about (0°N,11°W), and C) with 75° of eastward non-synchronous rotation subtacted from *B*. (See text for discussion).

Discussion and Conclusions: The geometric similarity to

Baghdad Sulcus of the proposed paleo tiger stripe rifts, including their bifurcations suggest that all formed under similar conditions of lithospheric stress. If stresses due to tidal deformation played a major role, then the paleo rifts likely had similar placement and orientations to their modern counterparts. Our evidence supports the TPW hypothesis [1] and further implies that NSR has persisted much longer in Enceladus's history than suggested from present stratigraphic patterns of SPT fractures [3].

References: [1] Tajeddine *et al*. 2017. *Icarus* 295. 46–60; [2] Patterson *et al.* (2018). In *Enceladus and the Icy Moons of Saturn.* Space Sci. Series, Univ. of Ariz. Press, Tucson, AZ. (in press); [3] Patthoff & Kattenhorn, 2011 *GRL* 38, L18201.

Surface Compositions of the Icy Satellites from UV Spectroscopy

Amanda R. **Hendrix**[1] and Candice J. Hansen[1].
[1]Planetary Science Institute (Tucson, AZ; arh@psi.edu).

The Ultraviolet Imaging Spectrograph (UVIS) (Esposito et al., 2004) on *Cassini* provided the first-ever opportunity to do far-UV (110-190 nm; 0.1-0.19 μm) spectroscopic investigations of icy moons in the solar system. In addition to studying atmospheres and plumes, this capability extends the spectral coverage from the traditional visible-near-infrared range to allow for further identification of surface compositional species, and in particular allows for studies of the character of the top-most few microns of the surface (due to the shallow sensing depths of these wavelengths), which reveal information about the weathering effects on the surface. In the Saturn system, key weathering processes include plasma and energetic electron bombardment, as well as interactions with E ring grains (in the inner system) and interactions with Phoebe ring grains (in the outer system). Prior to *Cassini*, near-UV observations (0.2-0.35 μm) of some of Saturn's moons had been made using *Hubble Space Telescope (HST)* (Noll et al., 1997). *Cassini* UVIS observations demonstrate the ubiquitous presence of the far-UV water ice absorption edge (165 nm) (e.g. Hendrix and Hansen, 2008; Hendrix et al., 2010); prior to *Cassini*, this strong water ice absorption had only ever been observed in a set of *International Ultraviolet Explorer (IUE)* observation of Saturn's rings (Wagener and Caldwell, 1986).

The UVIS data have also strengthened the knowledge of the significance of the "UV absorber(s)" in the Saturnian system. The Saturnian moons are known to have relatively high visible albedos (e.g. Buratti and Veverka, 1984), linked to E ring grain bombardment (e.g. Verbiscer et al., 2007); however despite their dominant water ice component, all of the icy Saturnian moons are absorbing in the ~0.2-0.5 μm region, making them dark at FUV wavelengths. Filacchione et al. (2012) used *Cassini* VIMS data to show that the spectral slope (0.35-0.55 μm) increases (becomes redder) with distance from Enceladus. The visibly-reddish material is present on both the leading and trailing hemispheres, with increased abundances (i.e. increased absorption strength) on the trailing hemispheres and with distance from Enceladus as shown using combined UVIS and *HST* data (Hendrix et al., 2015; 2017). The exact nature of the absorbing species is not completely understood but has been widely discussed in the literature as related to carbonaceous/organic species (perhaps associated with E ring grains), nano-grains of iron and/or E ring grain salts.

Much of our work has focused on understanding large scale results from disk-integrated observations; new results from more recent work using disk-resolved observations will be presented as well. We address remaining questions, including: What is the reddish UV-visible absorber? Is there a connection between the composition of the plume and the regions on Enceladus where plume deposits exist (e.g. Schenk et al., 2011)? How are the plume fallout zones compositional different from the other (E ring) zones on Enceladus? What is the chemical make-up of the trailing side of Tethys, and why is it so reddish (Schenk et al., 2011) compared to regions dominated by the infall of E-ring grains?

Temporal Variations in Enceladus Surface Temperature?

C.J.A. **Howett**[1], J.R. Spencer[1], A. Verbiscer[2]
howett@boulder.swri.edu, [1] Southwest Research Institute, 1050 Walnut Street, Suite 300, Boulder, CO, 80301
[2] University of Virigina, Charlottesville, VA, 22904

Introduction: Enceladus' plume mass varies as a function time and of orbital position (Ingersoll and Ewald, 2017). CIRS observations of Enceladus' active south polar region during Cassini's F-Ring and Proximal Orbits (FRPO) were designed to investigate whether Enceladus' surface temperatures also vary with time. Preliminary results indicate that Enceladus' surface temperatures do vary with mean anomaly, but lag in time behind the plume change.

Method: To properly account for Enceladus' poles the CIRS data were binned into triangles, which are tessellated across the sphere. The area of each triangle is almost constant. The triangles are much smaller than the size of a single FP3 field of view, but since CIRS scans FP3 slowly across the disk sub-pixel resolution is achieved. The integrated radiances of all the high SNR observations were totaled for all bins inside of 70° S. Only mean anomalies between ~270 and 10° are covered by these observations,

Results: Preliminary results appear to show the flux from Enceladus' surface decrease by about a factor of 2 from mean anomalies ~270 and 10°. This is smaller than the 3-5x decrease observed in the plume mass, and occurs at slightly higher mean

anomalies. However, the difference is notable and tentatively implies that the temperature of Enceladus' surface in its active region does vary with its orbital location, but the change lags the plume emission change. More work is required to firm up this preliminary result, and analyze the lower signal-to-noise observations to fill in the mean anomaly coverage.

Enceladus plumes: Variability on timescales from months to years

A. P. **Ingersoll**[1], S. P. Ewald[2] and S. K. Trumbo[3].
Caltech mail 150-21, 1200 E. California Blvd., Pasadena, CA, 91125, USA, [1](api@gps.caltech.edu), [2](spe@caltech.edu), [3](strumbo@caltech.edu).

In their paper, "Decadal timescale variability of the Enceladus plumes inferred from Cassini images," Ingersoll and Ewald (hereinafter IE17) presented data showing that plume brightness decreased by roughly a factor of two during much of the period 2005-2015 [Icarus 282, 260-275 (2017)]. They offered three hypotheses to explain this result. One was a long-period tide – the decreasing phase of an 11-year cycle in orbital eccentricity; another was buildup of ice at the throats of the vents; and the third was seasonal change – the end of summer in the southern hemisphere.

The tidal hypothesis rests on the fact that the diurnal opening and closing of the cracks depends on the orbital eccentricity, which peaked at a value of 0.00485 in 2009 and dropped to a minimum of 0.00460 in 2015 as part of an 11-year cycle. Therefore one might expect that plume brightness would increase during the period 2005-2008 and would decrease during the period 2009-2015. Such a decrease did occur during the later period, as shown in the attached figure [Fig. 8 of IE17], but a corresponding increase seems not to have occurred in the earlier period. On the other hand, there are very few data from the earlier period, not enough to rule out an 11-year cycle. Another problem is that the effect is small, namely a ±2.5% change in eccentricity, which itself is less than 0.5%.

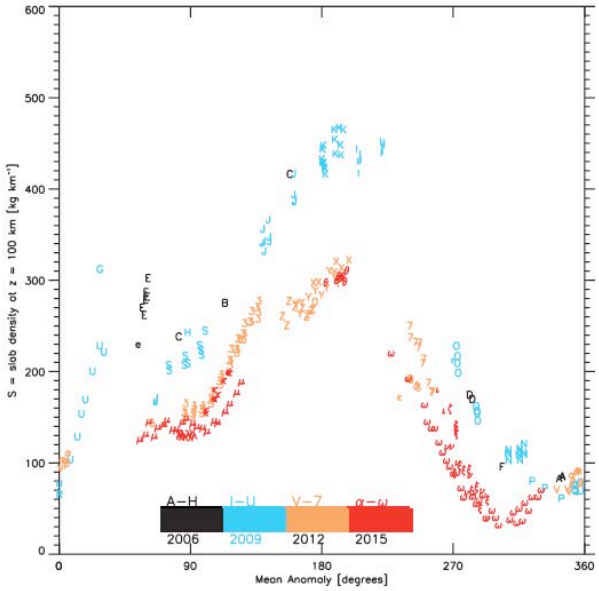

Fig. 8. Plume mass vs. position in the orbit labeled by year of observation. The ordinate is slab density—the mass of particles in a horizontal slab one km thick 100 km above the south pole. The abscissa is mean anomaly—time from pericenter divided by the orbit period expressed as an angle. The symbols give the date of observation starting with the English alphabet in 2005, then the single digit numbers, and finally the lower case Greek alphabet in 2015. Table 1 gives a summary of the observations. Colors and shading give a coarse version of the same information in 3-year intervals centered on the years 2006, 2009, 2012, and 2015. In addition to the 4–5-fold variation with mean anomaly, the graph shows a 2-fold decline in slab density from 2005 to 2015.

The stochastic variability hypothesis rests on the fact that if latent heat of the vapor coming up from below is supplying the power that is radiated to space, ice must be building up on the walls of the cracks as the vapor condenses. If condensation is occurring to a depth of 100 m, the cracks must be closing at a rate of 1.4 m/year. If the depth is less, the closing rate is greater. Some mechanism must be keeping the cracks open or causing new ones to form as the old ones die. Since the cracks are thought to be less than 1 m wide, this is a fundamental problem. The third hypothesis, seasonal change, could contribute if the temperature of ice at the surface is affecting plume activity. IE17 noted that sunlight is fairly weak at Saturn and is unlikely to affect the opening and closing of the cracks in any significant way.

In this study, we have extended the data analysis to observations taken in 2015-2017. We use the same software and the same methods to subtract the E ring background from the plume images. The period 2015-2017 is crucial because it fills in the sparsely observed period from 2005-2008, assuming the 11-year cycle is controlling the long-term variability. Second, we have heightened our efforts to monitor individual plumes, assuming ice buildup is causing them to turn on and off on timescales less than a year. Our observations provide critical tests of theories of long-term plume variability and help us understand the plumes in general.

Reprinted from Ingersoll and Ewald, Icarus 282, 260-275 (2017).

Constraints on the recent saturnian crater flux from Cassini VIMS and ISS: Crater ages on Rhea

M. R. **Kirchoff**[1], C. M. Dalle Ore[2], E. G. Rivera-Valentín[3].
[1]Southwest Research Institute, 1050 Walnut St., Suite 300, Boulder, CO, 80302, (kirchoff@boulder.swri.edu), [2]SETI Institute, 189 N Bernardo Ave suite 200, Mountain View, CA 94043, Mountain View, CA, (cristina.m.dalleore@nasa.gov), [3]Lunar and Planetary Institute (USRA), 3600 Bay Area Boulevard, Houston, TX, 77058, (ervalentin@usra.edu).

Introduction: During a hypervelocity impact onto an icy satellite, a shallow melt region is produced [e.g., 1], and during cooling H_2O solidifies into its crystalline form [2]. Over time bombardment by ions disrupts the crystalline structure producing

amorphous ice [e.g., 3], which is stable over the age of the Solar System for the surface temperatures of Saturn's mid-sized moons [4]. The local abundance of amorphous ice with respect to crystalline ice within and surrounding craters thus allows for an estimate of absolute crater formation age [5], which when paired with cumulative crater densities, gives new constraints on the recent crater flux at Saturn.

Methods: *Ice Phase.* The 2.0-µm band shape is affected by changes in H_2O phase [6] in a consistent way. By measuring the distortion on band shape models with varying amounts of crystalline to amorphous ice, we calibrate the effects of phase change on the VIMS spectra. The calibration is applied to distortion measurements of the data to obtain a crystallinity fraction. From the relative amount of ice phases and information about the energetic particle flux, we can estimate the age of large craters.

Crater Statistical Analysis. High-resolution ISS image(s) of the large craters are integrated into JMARS. We use the 3-point crater tool to measure the small, superposed craters located on the large crater floors. Cumulative crater size-frequency distributions (SFDs) are generated using a new, more statistically robust technique [7].

Preliminary Results and Discussion: We have thus far analyzed two craters on Rhea: Obatala and Inktomi. Inktomi shows ~20% more crystalline ice than Obatala, indicating it is younger. Furthermore, the lower cumulative crater density ($D \geq 1$ km) for Inktomi (0.6×10^{-2} km^{-2}) than Obatala (1.4×10^{-2} km^{-2}) also indicates Inktomi is younger. We derive a recent cratering rate for $D \geq 1$ km craters by combining the absolute ice phase age of Obatala (~450 Ma [5]) with its cumulative crater density. This value is ~3×10^{-5} per 10^6 km^2 per year, which agrees with Case B on Rhea from [8]. Case B is the expected crater SFD for $D < 10$ km as constrained by Triton's crater distribution. Case A is instead constrained by the crater distributions on the jovian satellites. Indeed, the shapes of the superposed crater SFDs for Obatala and Inktomi both best fit Case B. The continuing analysis of more craters on Rhea and other saturnian mid-sized satellites will also be discussed.

References: [1] Barr, A. C. and Citron, R. I. (2011) *Icarus*, 211, 913-916. [2] Baragiola, R. A., et al. (2013) *The Science of Solar System Ices*, 356, 527-549. [3] Mastrapa, R. M. and Brown, R. H. (2006) *Icarus*, 183, 207-214. [4] Mastrapa, R. M., et al. (2013) *The Science of Solar System Ices*, 356, 371-408. [5] Dalle Ore, C. M., et al. (2015) *Icarus*, 261, 80-90. [6] Grundy, W. M. and Schmitt, B. (1998) *JGR*, 103, 25809-25822. [7] Robbins, S. J. et al. (2018) *MAPS*, 53, 931. [8] Zahnle, K. et al. (2003) *Icarus* 163, 263–89.

Enceladus: three-stage limit cycle and current state

Jing **Luan**[1] and Peter Goldreich[2], [1]
Campbell Hall, 605H, UC Berkeley, Berkeley, CA 94720 (jingluan@berkeley.edu), [2]MC 350-17, Caltech, 1200 East California Blvd, Pasadena, CA 91125 (pmg@ias.edu).

Introduction: Enceladus is one of the most popular worlds that might accommodate life outside our own earth. We study its evolutionary path, especially focus on the physical processes that drive Enceladus to its current state. I will also discuss possible applications of these physical processes to other bodies in our solar system. Below is a brief summary of the evolution path for Enceladus.

Eccentricity (e) growth as Enceladus migrates deeper into mean motion resonance with Dione results in increased tidal heating. As the bottom of the ice shell melts, the rate of tidal heating jumps and runaway melting ensues. At the end of run-away melting, the shell's thickness has fallen below the value at which the frequency of free libration equals the orbital mean motion and e has damped to well below its current value. Subsequently, both the shell thickness and e partake in a limit cycle. As e damps toward its minimum value, the shell's thickness asymptotically approaches its resonant value from below. After minimum e, the shell thickens quickly and e grows even faster. This cycle is likely to have been repeated multiple times in the past.

Currently, e is much smaller than its equilibrium value corresponding to the shell thickness. Physical libration resonance resolves this mystery, it ensures that the low-e and medium-thickness state is present for most of the time between consecutive limit cycles. It is a robust scenario that avoids fine tuning or extreme parameter choice, and naturally produces episodic stages of high heating, consistent with softening of topographical features on Enceladus.

Using Enceladus's complex surface to reconstruct a complex history

E. S. **Martin**[1] and D. A. Patthoff[2].
[1]Center for Earth and Planetary Studies, National Air & Space Museum, Smithsonian Institution (Washington DC, 20013 martines@si.edu), [2]Planetary Science Institute (apatthoff@psi.edu).

Introduction: Saturn's small moon Enceladus has proven to be a geologically dynamic world. Large fissures near Enceladus's south pole, numerous globally-distributed fractures and ridges, and heavily relaxed craters all which suggest a period of intense heating. Taken together, these feature preserve evidence of discrete stages of deformation in Enceladus's past.

Results: We completed detailed geological mapping, interpretation, and modeling, from which we observe five periods of distinct episodes in Enceladus's geologic history that represent either the build-up or the release of heat:

Episode I: Formation of ancient tectonic structures in the Saturnian and Anti-Saturnian cratered terrains, many of which likely preserve a signature consistent with nonsynchronous rotation.

Episode II: Cratering event occured globally but is only preserved through the present-day in the Saturnian and Anti-Saturnian cratered terrains.

Episode III: Formation of ridges on the leading and trailing hemispheres that uggest hemispherical contractional. The distribution of the ridges is evocative of loading models including a plate response (narrow load on a thick lithosphere) or a membrane response (wide load on a thing lithosphere).

Episode IV: Formation of pit chains in the Saturnian and Anti-Saturnian cratered terrains. Pit chains are some of the youngest structures observed on the surface of Enceladus, and the patterns of pit chains across the surface are consistent with formation due to stresses caused nonsynchronous rotation. The relative ages of pit chains with respect to the tiger stripes is unclear however, crosscutting relationships suggest that pit chain formation may be ongoing.

Episode V: The geologically active south polar terrains with erupting jets of water from large ridges (tiger stripes). Detailed observations of the surrounding fractured south polar terrains show evidence of ancient tiger stripes that have changed orientation through time, suggesting that nonsynchronous rotation has been ongoing during the history of the presently active SPT.

Discussion: The aforementioned five episodes in Enceladus's geologic history suggest that Enceladus has experienced multiple episodes of intense geologic activity associated with a dramatic release of heat. Between those episodes, Enceladus experienced a time of relative tectonic quiescence and impact bombardment. Presently, the satellite is reaching the end of the latest episode of heat release allowing the ice shell to thicken as a result of the freezing of the subsurface ocean.

We will present the detailed mapping and modeling results used to establish each episode and how they demonstrate the interesting and dynamic history that has resulted in the dynamic state of Enceladus as it is observed today.

Jets of Enceladus: Cassini's UVIS occultation observations and DSMC model of Enceladus jets

Ganna **Portyankina**[1], L. W. Esposito[1], K-M. Aye[1], and C. J. Hansen[2]
[1]Laboratory for Atmospheric and Space Physics, University of Colorado, Boulder, 1234 Innovation Dr. 80303, Boulder, CO, USA; (Ganna.Portyankina@lasp.colorado.edu), [2]Planetary Science Institute, 1700 E. Fort Lowell, Tucson, AZ 85719, USA.

Introduction: During Cassini mission UVIS observed jets of Enceladus seven times. Using occultation mode, UVIS tracked a star while it passed behind the jets. It took spectroscopic measurements in its Far UltraViolet (FUV) channel and photon counts in High Speed Photometer (HSP) channel to determine absorption by the water vapor along its line of sight. Each observation had a specific geometry: at each time step of the observation, UVIS line of sight crossed multiple jets that possibly erupt from different tiger stripes and thus integrated contributions from multiple sources. The acquired profile of absorption by water vapor was converted to water vapor column density. Together with the geometry of each observation, these data hold the information about relative strengths of the jets, the total amount of material in the plume, and the flux rates of the ejected water vapor.

Model: We use 3D Direct Simulation Monte Carlo (DSMC) model to simulate the distribution of water vapor along the line of sight of UVIS during occultation observations. The model tracks water vapor molecules from sources on Enceladus surface [Porco et al. 2014] into the space, taking into account gravity of Saturn and Enceladus, Coriolis, centrifugal, and tidal forces, and accounting for molecular collisions when appropriate. Total flux is used to calibrate the model [Hansen et al., 2006]. The exact geometry is calculated using SPICE and a synthetic profile of water vapor column density mimicking the specific observation is generated. The comparison of the synthetic profile to the one acquired by UVIS provides us the information about relative strengths of the jets and an estimate of the water vapor vertical velocity in the most collimated jets.

Fitting procedure of the synthetic to observed profiles is used to infer which jet sources contributed to the signal and at what relative strengths.

Results: For each of seven occultation observations we produce maps of the active sources including their relative strengths. Because the geometry and spatial resolution of each

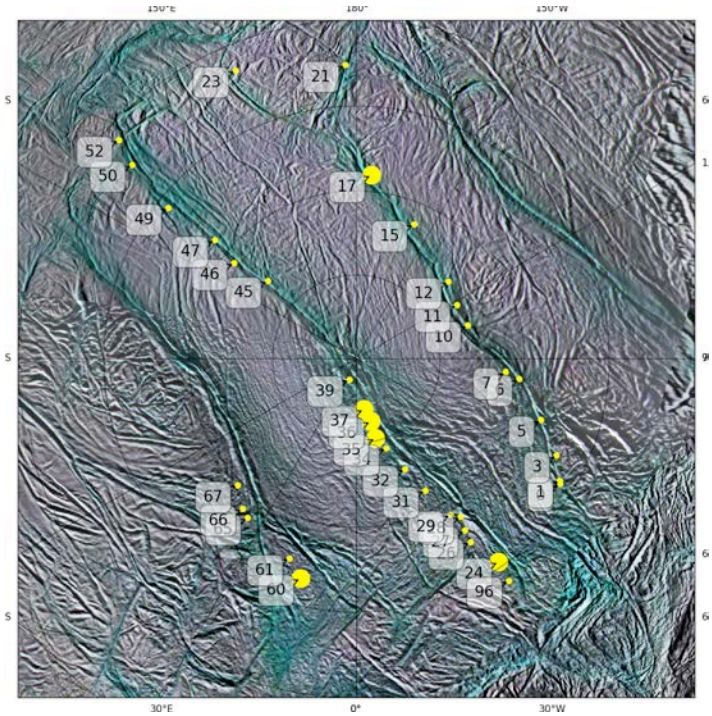

Figure 1: View to the Enceladus south pole with jet sources that appear repeatedly in several UVIS occultation observations. Source number is according to Porco et al., 2014.

observation is unique, the resulting distribution of jet sources is unique as well. Occultations in 2007, 2010, 2011, and 2017 cut through the plume horizontally providing information about the complete plume. While the observation in 2016 had only partial spatial coverage. Over-all, each observation shows a specific set of active sources that only partially repeat.

We determine the minimum vertical velocity that is required to fit the most narrow features in each of the occultation observations. We detect several sources that appear in different UVIS observations over the years (Fig. 1) and thus have high probability to be constantly active.

References: Porco, C., DiNino, D., Nimmo, F. (2014) How the geysers, tidal stresses, and thermal emission across the south polar terrain of Enceladus are related. The Astronomical Journal 148, 45. Hansen, C. J., Esposito, L, Stewart, A. I. F., Colwell, J., Hendrix, A., Pryor, W., Shemansky, D., and West, R. (2006) Enceladus' Water Vapor Plume. Science 311, 1422–1425.

Exploring the oxidation chemistry of Enceladus' ocean

C. Ray[1,2], C. R. Glein[2], J. H. Waite[2,1], B. D. Teolis[2], and J. A. Huber[3].
[1]The University of Texas at San Antonio, Department of Physics and Astronomy, San Antonio, TX 78249 [2]Southwest Research Institute, San Antonio, TX 78228 [3]Josephine Bay Paul Center, Marine Biological Laboratory, Woods Hole, MA 02543 (cray@swri.edu).

Introduction: The detection of molecular hydrogen in the plume of Saturn's icy moon Enceladus implies that there is free energy available for methanogenesis, the metabolic reaction of hydrogen with carbon dioxide to form methane and water [1]. Methanogenesis, however, is just one of many possible metabolic pathways that could be utilized by putative microorganisms. While reduced species are abundant in the plume, CO_2 was the only oxidant observed.

Approach: To constrain the amount of metabolically important oxidants including sulfate (SO_4^{2-}), molecular oxygen (O_2), and ferric iron in Enceladus' ocean, we present a geochemical model of the ocean based on detections made by the Cassini INMS instrument [1] and likely equilibrium mineralogies of Enceladus' core. We use a model of radiolysis on the surface of Enceladus to estimate the amount of molecular oxygen contained in the ice, and calculate the delivery rate of O_2 from the surface ice to the ocean using previous estimates of the rate of ice deposition on the south polar region [2]. Assuming this activity has occurred over ~4.5 billion years, we obtain an upper limit of $\sim 10^{16}$ moles of O_2 delivered to the ocean over Enceladus' lifetime. We also consider O_2 produced radiolytically in the ocean from electrons and gamma rays released by the decay of ^{40}K atoms, and calculate an upper limit of another $\sim 10^{16}$ moles of O_2 produced this way.

Results and Discussion: The produced oxygen could react with sulfides and ferrous iron dissolved in the ocean to produce SO_4^{2-} and ferric iron, respectively. We estimate upper limits on the concentrations of these species from the solubilities of a number of possible ocean floor minerals. We find that the abiotic oxidation of these species could yield a dissolved sulfate concentration as high as 1.75 mmol/(kg H_2O), and a ferric iron bulk concentration as high as 0.55 mmol/(kg H_2O).

We determine the amount of chemical energy that could be available from metabolic reactions involving the considered oxidants, and compare it with the energy available from methanogenesis reported in [1]. From these results, we suggest that that these oxidation reactions could provide an important additional source of chemical energy available for possible life, unless Enceladus is much younger than the age of the solar system or if the plume has been far less active over the course of its lifetime. Finally, we consider how the production of oxidants from radiolysis of pore water in the core, and how the abiotic consumption of oxidants by reduced minerals in the core, could affect the reported results.

References: [1] Waite et al. (2017) *Science, 356,* 155–159. [2] Kempf et al. (2010) *Icarus, 206,* 446-457.

The tide that binds: Stress and tectonics on the mid-sized icy moons of Saturn

A. R. Rhoden[1], M. Neveu[2], T. A. Hurford[3], W. G. Henning[3,4], J. N. Spitale[5], and E. M. Huff[6].
[1]Arizona State University, School of Earth and Space Exploration, 781 E Terrace Mall, Tempe AZ, 85287, (Alyssa.Rhoden@asu.edu), [2]NASA HQ, 300 E St. SW, Washington DC, 20546, [3]Planetary Geology, Geophysics, and Geochemistry Lab, NASA Goddard Space Flight Center, 8800 Greenbelt Rd., Greenbelt, 20771, [4] Dept. of Astronomy, University of Maryland, College Park, MD, 20742, [5]Planetary Science Institute, Tucson, AZ, [6]NASA JPL, Pasadena, CA.

Introduction: Data acquired by the *Cassini* spacecraft has provided important constraints on the interiors and geologic histories of the mid-sized icy moons (MIMs) of Saturn - Mimas, Enceladus, Tethys, Dione, and Rhea – but many open questions remain. These moons display the full spectrum of tectonic activity, from Enceladus' crater-free south pole, riddled with fractures, to Mimas' heavily cratered surface with only a few dozen tectonic features globally. Tethys, Dione, and Rhea all display some tectonism, but the extent of faulting and its characteristics vary widely. Currently, there is no clear explanation for this geologic diversity. The interiors of the moons are also variable, and some are only weakly constrained. Global, subsurface oceans have been proposed for all the MIMs. An ocean within Enceladus is supported by model fits to gravity, shape, and libration measurements, and the composition of plume

material. An ocean in Mimas has been proposed based on model fits to observed librations, although ocean-free interiors can also explain the data. Gravity and shape measurements support an ocean within Dione but are ambiguous for Rhea. Relaxation of craters on Tethys, Dione, and Rhea suggest higher heat flows than expected and point to a weak, subsurface layer; taken together, these results suggest the presence of oceans within these moons now or in the recent past. Finally, much is still unknown about the thermal-orbital evolution of the moons, resulting in age estimates spanning four orders of magnitude and a large uncertainty as to the likelihood or longevity of sub-surface oceans.

Our approach: Tides on icy satellites can supply the heat necessary to preserve an ocean and generate stresses that lead to fracturing, depending on the orbit, rotation, and interior structure of the satellite. The extensive tectonism on Jupiter's ocean-bearing moon, Europa, exemplifies this process. Tidal stresses appear to control eruptions along the Tiger Stripe Fractures on Enceladus, but the role these stresses have played in the creation of the fractures, and fracture systems on the other MIMs, is uncertain. Tidal stresses are greatly enhanced by the presence of an ocean and by higher-eccentricity orbits, for which there is indirect evidence within the surface ages of all five moons. We analyze tidal stresses, compared with observed fracture systems, to derive additional constraints on the orbits and interiors of the MIMs and the extent of tidally-driven tectonic activity in the Saturnian system. We test present-day orbital configurations and determine the past conditions that would have likely resulted in fracturing. We also test various interior models to determine whether current or recent oceans are consistent with the geologic records of the MIMs. We limit analyses to interiors and orbits consistent with *Cassini* measurements and their interpretations. We will discuss implications for the Mimas ocean hypothesis and the role of tides in forming the Tiger Stripe Fractures on Enceladus. We will also discuss the potential for recent/current oceans and tidally-driven activity on Tethys, Dione, and Rhea based on new coupled thermal-orbital evolution models. This work benefitted from interactions with the Ocean Worlds Cooperative.

Evolving Enceladus: What Cassini taught me about Saturn's surprising satellite

J. H. **Roberts**[1].
[1]Johns Hopkins Applied Physics Laboratory, 11100 Johns Hopkins Road, Laurel, MD 20724, James.Roberts@jhuapl.edu

Introduction: Cassini has brought us a wealth of information has been acquired about Enceladus. This small moon of Saturn was shown to be surprisingly active. As observations accumulated, it seemed increasingly likely that Enceladus must be far from steady-state. In particular, the observed thermal radiation far exceeded the long-term level of dissipation then thought to be sustainable by orbital dynamics. Models of the internal dynamics showed that heat is removed from the interior faster than it can be produced by tidal dissipation, and a subsurface ocean would freeze in tens of My.

This conundrum started my decade-long journey into the long-term evolution of Enceladus, in which the south polar region, the interior, the associated activity, and our understanding of these, were shown to be constantly evolving. Here, I discuss the questions this discovery inspired me (and others) to investigate, the assumptions we questioned and what we learned.

South polar region: The south polar location of the plume and thermal anomaly is also curious, and hints at an episode of true polar wander, but significant reorientation which would require compositional density variations. This may be unnecessary, as others have shown that patterns of tidal dissipation predict maximum at the poles. However, the tidal potential is always symmetric about the equator. The real question then is not why there is so much activity at the south pole, but why is there not also activity at the north pole.

Interior structure: The difficulty of preventing the ocean from freezing alternatives to explain how tidal dissipation in the ice shell could be sustained. I considered that the core of Enceladus was a "rubble pile" rather than a monolith, and found that ice in the pore spaces could weaken the core to where the entire satellite could undergo significant tidal heating even when completely frozen. Others discovered that excitation of the ocean by orbital resonances when the ocean becomes thing could dramatically increase heating in the ocean, preventing total freezing. Thus, the ocean is at once not strictly necessary and easier to sustain, although it is likely to be constantly evolving.

High heat flux: The apparent incompatibility between the observed heat flux and the available energy suggested the south polar thermal anomaly was a transient phenomenon. I explored the effects of heating by a large impact in the recent past. I confirmed prior conclusions that the impact heating would be dissipated rapidly, but found that the projectile could penetrate through the entire ice shell, fundamentally altering the region, enabling regionally increased tidal dissipation, promoting fracture formation, and addressing the symmetry problem.

Discussion: Ironically, my original motivation for this investigation, to reconcile the observed high heat flux with the sustainable level of dissipation has been obviated, as is has since been shown that Saturn is far more dissipative than originally appreciated, and the heat flux at Enceladus is sustainable. Nevertheless, this drove me to reconsider my assumptions. Cassini's legacy extends beyond the Saturn system and challenges us to think differently about how we do planetary science.

Multi-Wavelength investigation of the co-orbital moons Dione and Helene

E. M. **Royer**[1], A. Hendrix[2], C. Howett[3] and L. Spilker[4].
[1]University of Colorado-Boulder, 3665 Discovery Dr., Boulder, CO, (emilie.royer@lasp.colorado.edu), [2]Planetary Science Institute (PSI), Tucson, AZ, [3]Southwest Research Institute (SwRI), Boulder, CO, [4]Jet Propulsion Laboratory (JPL), La Cañada, CA.

Introduction: The icy satellites Dione and Helene share the same orbit, at 6.26 Saturn radii from the giant planet, which is within Saturn's diffuse E ring. Helene is one of Dione's two Trojan moons, located in the leading Lagrangian point L4 of Dione's orbit. We present here preliminary results on the investigation of the Dione-Helene duo in term of origin, formation and evolution. Specifically, the key objectives are to retrieve the photometric properties and composition of the moons to answer questions such as: *Are the Dione and Helene surfaces made of the same material? Did they form in the same region of the Solar System? Is one satellite older than the other? Have they experienced the same amount of space weathering?*

Methods: To provide the most complete evaluation of the Dione and Helene surfaces and advance our understanding of how exogenic processes affect the surfaces of icy satellites we use the synergy of four of the Cassini instruments: UVIS (Ultraviolet Imaging Spectrograph), ISS (Imaging Science Subsystem), VIMS (Visual and Infrared Mapping Spectrometer) and CIRS (Composite Infrared Spectrometer). Composite disk-integrated spectra of both moons have been produced to conduct spectral modeling. Using a k-nearest neighbors (k-nn) algorithm, we accounted for differences in instrument resolution and preserved spectral fearures across a large wavelength range from the ultraviolet to the infrared, from 111nm to 1mm. We used simultaneous observations of Dione and Helene by all four instruments when available.

Expected Results: Until now, most investigations have focused only on one wavelength domain, telling only part of the story. A multi-wavelength analysis allows an in-depth investigation of the surfaces of the Saturnian satellites as each wavelength probes a different layer of the surface. Special attention is directed toward the search for correlations of basic properties (albedo, scattering properties, texture, grain size, composition, porosity, thermal properties) between Dione and Helene.

The Enceladus auroral footprint – and lack thereof.

A. M. **Rymer**[1].
[1]JHU/APL 11101 Johns Hopkins Road, Laurel, MD 21032, USA, (abigail.rymer@jhuapl.edu), [2]D. G Mitchell[1] and [3]W. Pryor[2], Central Arizona College, AZ, USA.

Perhaps the most significant and surprising discovery of the Cassini mission to date is that of significant geysers of water vapour and ice grains from the South polar region of Enceladus (Science, 311, 2006), possibly from a subsurface ocean. These icy 'plumes' make the tiny moon the dominant source of plasma, neutral gas, and E-ring particles in Saturn's magnetosphere. This source far outstrips that from the moon Titan, despite Titan having the densest atmosphere of any moon in the solar system.

It is well known that mass loading near Io produces strong UV auroral emission at Io's magnetic footprint in Jupiter's ionosphere. Wannawichian et al. [2008] analyzed Hubble Space Telescope (HST) UV observations to search for an analogous auroral footprint at Saturn associated with plasma loading at Enceladus. Their negative result indicated that Birkeland currents associated with mass loading at Enceladus are too weak to produce UV auroral emissions that are detectable by HST.

Pryor and Rymer [2010] reported magnetic-field aligned ion and electron beams near Enceladus using two of the Cassini charged-particle sensors, the Ion and Neutral Camera (INCA) [Krimigis et al., 2004] and the Electron Spectrometer (ELS) [Young et al., 2004]. A subsequent search revealed the expected Enceladus auroral footprint at exactly the expected location.

We review these results in context of prior and subsequent non-observations of the Enceladus footprint and implications for Enceladus activity.

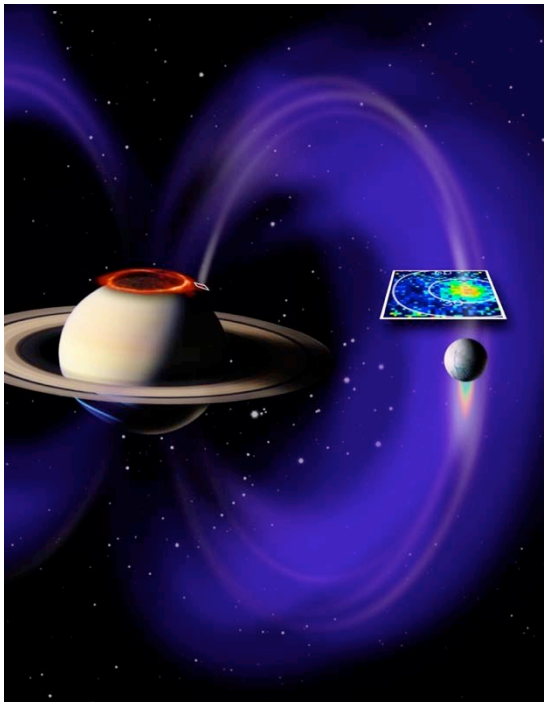

Figure 2. The Enceladus-Saturn interaction. Pryor and Rymer et al., 2010.

High energy electron sintering of icy regoliths: Learning from Pac-Man

M.J. **Schaible**[1], R.E. Johnson[2], L.V. Zhigilei[2], T.M. Orlando[1].
[1]Georgia Institute of Technology, 901 Atlantic Drive, Atlanta, GA 30332, (mjschaible@gatech.edu). [2]University of Virginia, 395 McCormick Road, Charlottesville, VA 22904, (rej@virginia.edu).

Introduction: The lens shaped 'Pac-Man' features identified on the leading hemispheres of the icy Saturnian moons Mimas, Tethys and Dione are found to have an anomalously high thermal inertia as compared with the surrounding regions [1] and

additionally show enhanced UV reflectance [2]. The locations of these anomalies were discovered to closely match the expected deposition profiles of high energy (~ MeV) electrons moving counter rotational to the moons [3,4]. Ultimately, it was shown that radiation enhanced diffusion of water molecules near intergrain contacts can explain the anomalous thermal conductivity [5] and is likely also the source of enhanced UV scattering due to radiation-driven formation of submicron sized voids in the bulk grains and at grain interfaces. The coincidence of a strongly observed signal with a well characterized energetic driver for their formation provide a unique opportunity to study energetic radiation on ice bodies in space. Since ionizing radiation (IR_p) processing of surfaces on airless bodies orbiting both stars and planets with extended magnetospheres is near universal, with differences consisting simply in the composition of the irradiated surfaces and the details of the incident radiation energy loss processes, the well-defined Saturnian environment provides a unique opportunity to move toward a general model for energetic radiation processing of icy bodies. This work outlines a physical model by which electron radiation can produce changes in the thermal conductivity of an icy regolith and provides analysis of the available theoretical and experimental estimates for enhanced diffusion produced by MeV electron irradiation in ~um sized water ice grains. The calculated sintering rate estimates for electron sintering are compared with rough estimates of the dust grain impact resurfacing timescales for the icy Saturnian moons. This analysis can provide unique physical constraints on the size and structure of icy regolith grains.

Analysis: Electron interactions with the grains can both create and anneal defects in the crystalline lattice, and energy deposited by radiation drives enhanced molecular diffusion. Molecules mobilized in the regions surrounding the grain contacts preferentially migrate to the surface energy minimum located at the 'pinch point' between grains, and thus slow migration of molecules driven by radiation enhanced diffusion yield increases in grain contact volume, effectively sintering the grains as shown schematically in Figure 1 and providing an explanation for the enhanced thermal inertia in the anomalous regions. Here, molecular dynamics simulations are used to provide a physical estimate of the defect creation and surface sputtering rates produced by high energy electron ionization of water ice molecules. Using accurate molecular water ice potentials and configurations [6, 7], the number of defects created and the average diffusion lengths of the molecules surrounding an excitation event can be determined. Figure 2 shows a typical thermal profile surrounding an excitation event ~30fs after the initial ionization event and the average radiation induced diffusion of molecules after return to steady state. The molecular excitation effects were studied in bulk hexagonal, cubic, and amorphous ices. Additionally, secondary sputtering and surface diffusion produced by molecular excitations proximal to both flat and curved grain surfaces were considered. Sintering timescale estimates suggest a regolith composed of ~5um spherically shaped grains. Larger grains sizes are possible if they are irregularly shaped, contain high surface defect densities, or are connected by numerous small contact regions.

References:

1. C.J.A. Howett, et al., 2012. "PacMan returns: An electron-generated thermal anomaly on Tethys. Icarus 221
2. P. Schenk, et al., 2011. "Plasma, plumes and rings: Saturn system dynamics as recorded in global color patterns on its midsize icy satellites." Icarus 211
3. C. Paranicas, et al., 2014. "The lens feature on the inner saturnian satellites." Icarus 234
4. T.A. Nordheim, et al., 2017, "The near-surface electron radiation environment of Saturn's moon Mimas." ,Icarus, 286
5. M.J. Schaible, et al., 2017, "High energy electron sintering of icy regoliths: Formation of the PacMan thermal anomalies on the icy Saturnian moons.", Icarus, 285

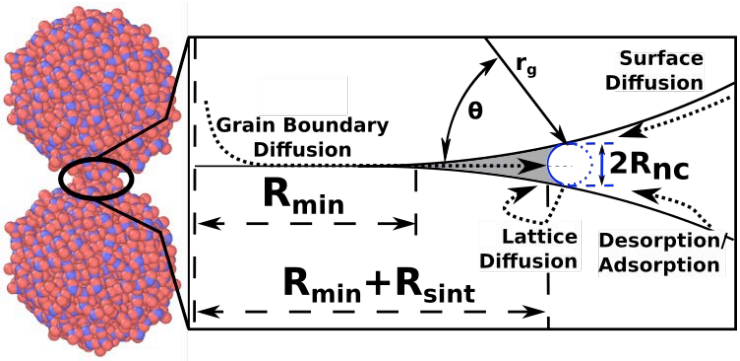

Figure 1: Molecular configuration of roughly spherical water ice grains in Hertzian contact and the typical radiation-induced diffusion pathways that can lead to enhanced grain-grain contact area and corresponding increases in thermal conductivity.

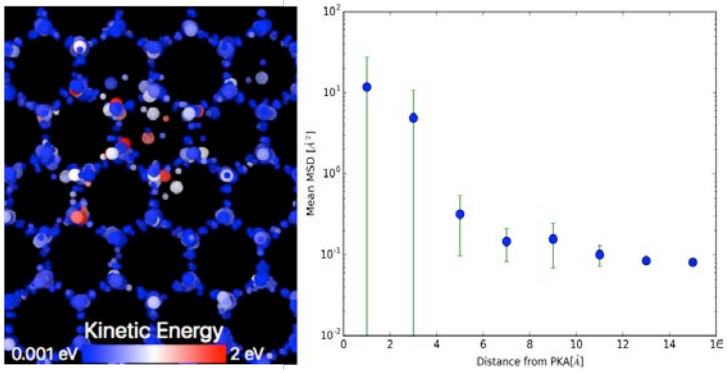

Figure 2: Molecular dynamics simulations allow sub-femtosecond resolution of excitation and diffusion dynamics within bulk crystalline ice grains, near grain surfaces, and in intergrain contact regions. Analysis of the molecular positions before and after the excitation events allows the number of defects and the mean squared displacement (MSD) of molecules as a function of distance from the primary knock on atom (PKA) to be determined.

6. J.L.F. Abascal, et al., 2005, "A potential model for the study of ices and amorphous water: TIP4P/Ice." JChemPhys, 122
7. V. Buch et al, 2005, "A new molecular-dynamics based approach for molecular crystal structure search. JChemPhys, 12.

Color mapping of geologic processes on Saturn's icy moons: Enceladus 2018

P. **Schenk.**
Lunar and Planetary Institute, Houston TX 77508 (schenk@lpi.usra.edu).

Introduction: Color mapping of Saturn's icy moons (Schenk, et al., 2011) revealed a wealth of phenomon hitherto poorly defined or even unknown. These include magnetospheric and E-ring bombardment on trailing and leading hemispheres, respectively, satellite ring reaccretion on Rhea (the Blue Pearls), and high-energy electron alterationof the leading equatorial regions of the inner moons. Also discovered wwas the plume fallout pattern on the surface of Enceladus, creating a pattern now attributed to the concentrated deposition of large salt-rich grains. Subsequently, unusual reddish arcuate lineations were discovered on Tethys (Schenk, et al., 2016). Here we describe the current state of mapping based on data acquired since these reports, with emphasis on the northern regions and on Encealdus, including high resolution color mapping.

Enceladus Global: The global-scale IR/G/UV color patterns on Enceladus (Schenk, et al., 2011) match well the predicted patterns for plume redeposition (Kempf et al., 2010). This pattern consists of an axisymmetric pair of deposits extending northward from the south polar terrains (the source region of the plumes). Mapping coverage in 2011 did not include the north polar regions, where plume deposition tapers off in two distinct 'hooked' patterns. Color mapping covereage was acquired in 2016 and has been processed. These maps confirm the general expected polar deposition pattern but are more diffuse than expected, perhaps as a result of the higher phase angle than typically used for color mapping.

Enceladus Local: In addition, high resolution color imaging of equatorial and north polar terrains was acquired revealing kilometer-scale varigations in color signature, in the form of small discrete patches. Some ofthese are associated with slopes but not all. Fresher (and presumably more recently formed) crater rims and fractures also display the 'bluish' color signature found on other icy moons and may indicate larger grain sizes exposed below the surface. These color signatures will be compared with those of materials in the southern regions, including funicalar terrains in between the tiger stripes, which have a unique color signature indicative of a lack of plume deposition despite their proximal location. This is interpreted as due to convective overturn of these terrains at a rate sufficiatne to prevent plume accumulation.

References: [1] Kempf, S., Beckmann, U., Schmidt, S., 2010. How the Enceladus dust plume feeds Saturn's E ring, Icarus, 206, 446-457; Schenk, P.M., D.P. Hamilton, R.E. Johnson, W.B. McKinnon, C. Paranicas, J. Schmidt and M.R. Showalter, 2011. Plasma, plumes and rings: Saturn system dynamics as recorded in global color patters on its midsize icy satellites, Icarus, 211, 740-757, doi:10.1016/j.icarus.2010.08.016; Schenk, P., B. J. Buratti, P. K. Byrne, W. B. McKinnon, F. Nimmo and F. Scipioni, 2011. "Blood Stains" on Tethys: Evidence for Recent Activity? EPSC abstract.

Resolving Enceladus plume production along the fractures

Ben **Southworth**[1] and Sascha Kempf[2]
[1]University of Colorado, Department of Applied Mathematics (ben.s.southworth@gmail.com)
526 UCB, University of Colorado, Boulder, CO 80309-0526; [2]University of Colorado, Laboratory for Atmospheric and Space Physics (sascha.kempf@mac.com).

Abstract: With the NASA-ESA Cassini mission complete, there remain open questions and interest in better understanding the Enceladus water-vapor plume. "Large particles," on the order of um-sized and larger, are of particular interest, because such particles likely originate from the subsurface ocean, and are most likely to contain organics and signatures of biological activity. Here, we look at data from large-scale parallel simulations of the Enceladus plume, compared with data from the Cassini Cosmic Dust Analyzer (CDA), the primary source of data on large plume particles. In particular, simulation data is able to reproduce CDA impact rates from the two lowest-altitude Cassini flybys with a single set of parameters: mass production is on the order of 25 kg/s, and plume particles take on a power-law size distribution slope with slope ~3. Moreover, data from the lowest-altitude flyby, E21, indicates that not all fractures were producing significant amounts of dust during the time of the flyby. Data from E7 further demonstrates that different fractures appear to be emitting particles with different size distribution slopes. These results are compared with recent results from Hedman et al. on a spatially varying dust-to-gas ratio, providing new insight into plume production.

Spectral properties of fresh impact craters on Dione, Tethys, Rhea and Ganymede

K. **Stephan**[1], C. Dalle Ore[2,3], R. Jaumann[1,4], D. Cruikshank[2], G. Filacchione[5] and M. Ciarniello[5].
[1]Institute of Planetary Research, 12489 Berlin, Germany (Katrin.Stephan@dlr.de); [2]NASA Ames, MS 245-6, Moffett Field, CA 94035, [3]SETI Institute,183 Bernardo Ave, Mountain View, CA 94043; [4]Freie Universität Berlin, 12249 Berlin, Germany; [5]INAF-IAPS, 00133 Rome, Italy.

Introduction: The imaging instruments onboard the Cassini spacecraft detected the icy satellites of Saturn allowing the study of their geological and spectral surface properties. Especially Cassini ISS and VIMS data acquired during few targeted flybys at relatively low latitudes enable a detailed investigation of individual impact craters on Tethys, Dione and Rhea. Although, the surfaces of the icy satellites in the Saturnian system are known to be dominated by H_2O ice, they experienced different geological evolutions and exhibit different environmental conditions. Especially the composition of fresh (more or less un-weathered) impact craters with their recently excavated ejecta material could provide compositional information of the satellites' upper crustal material. Since the spectral signature of H_2O ice is also known to be very sensitive to physical properties such as the size of the individual particles as well as surface temperature, their association to fresh impact material could also reveal information about the impact event itself and/or the surface temperature at the crater's location. Investigations of available Galileo SSI and NIMS observations of the Jovian satellite Ganymede (1) have been included in the investigation in order to compare the spectral properties of fresh impact craters on icy bodies in two different planetary systems.

All investigated impact craters are composed of relatively pure H_2O ice confirming an uppermost layer of all investigated satellites dominated by H_2O ice. The sizes of the H_2O ice particles, however, vary dramatically and have been found rather to be an indicator for the environmental conditions. The fresh impact craters on the Saturnian satellites exhibit relatively small (~5 – 40 µm) H_2O ice particle sizes. In contrast, the H_2O ice particle sizes of fresh impact craters on Ganymede partly increase up to 2mm. The comparison of the H_2O-ice particle sizes with the maximum surface temperatures at the approximate location of the impact site (2, 3) reveals a direct correlation between the H_2O ice particle sizes and surface temperature. The smallest H_2O ice particle sizes (~5µm) are confined to Creusa located on Dione at ~50°N and a surface temperature of ~80 K and the largest H_2O ice particle sizes (~1mm) are associated with impact crater Tammuz located close to Ganymede' equator (~13°N) characterized by a surface temperature of at least 150 K). Thus, the derived particles sizes are apparently rather influenced by the surface environment than reflect the crustal properties. Nonetheless, at similar surface temperatures the H_2O ice particles on Ganymede and the Saturnian satellites are quite similar.

References: (1) Stephan et al. (2017) Ice particle size variations and candidate non-ice materials on Ganymede and Callisto, EPSC abstracts, Vol. 11, EPSC2017-350-2. (2) Howett et al. (2010) Thermal inertia and bolometric Bond albedo values for Mimas, Enceladus, Tethys, Dione, Rhea and Iapetus as derived from Cassini/CIRS measurements, Icarus, 206, 573-593. (3) Squyres (1980) Surface temperatures and retention of H_2O frost on Ganymede and Callisto, Icarus, 44, 502-510.

Cassini ISS photometry of Enceladus' surface and major terrains

A. J. **Verbiscer**[1], P. Helfenstein[2].
A. M. Annex[3] [1]University of Virginia, P.O. Box 400325, Charlottesville VA 22904-4325 (verbiscer@virginia.edu), [2]Cornell University, 320 Space Science Building, Ithaca NY 14853 (helfenst@astro.cornell.edu), [3]Johns Hopkins University, 3400 N Charles St, Baltimore, MD 21218 (aannex1@jhu.edu).

Cassini images reveal in exquisite detail the complex and varied terrains found on Saturn's sixth largest satellite. The geologically active south polar terrain (SPT) is dominated by four parallel rifts or sulci, informally known as tiger stripes, from which plumes comprised primarily of water vapor erupt (Porco et al. 2006, Spencer et al. 2006, Dougherty et al. 2006, Hansen et al. 2006). The rich data set of Cassini images acquired at high spatial resolution (< 0.5 km/pixel) and a variety of viewing and illumination geometries enables the quantitative analysis of surface scattering properties through disk-resolved photometry. We have investigated the photometric properties of individual terrain units (Spencer et al. 2009) through fits of the Hapke photometric model (Hapke 2012) to data acquired in the clear (CL1 CL2), UV3, GRN, and IR3 filters, centered at 0.61, 0.34, 0.57, and 0.93 µm, respectively. South Pole Terrain units include the tiger stripe smooth and platy plank formations, tiger stripe medial dorsum structures, relict tiger stripe structures, south pole funiscular (ropy) plains, south pole lateral fold-and-wedge formations, and the south pole reticulated plains. Despite the constant, ubiquitous infall of plume particles onto the SPT, differences in scattering properties, texture, and albedo among terrain units can be discerned Our preliminary work was exclusively focused on south polar terrains, for which observed photometric geometries are often too limited to constrain the Hapke model fully. To overcome these limitations, we explore a new hierarchical strategy (Figure 1) in which we first obtain well-constrained fits to broad classes of terrains. These fits serve as progressively better first approximations for fitting specific

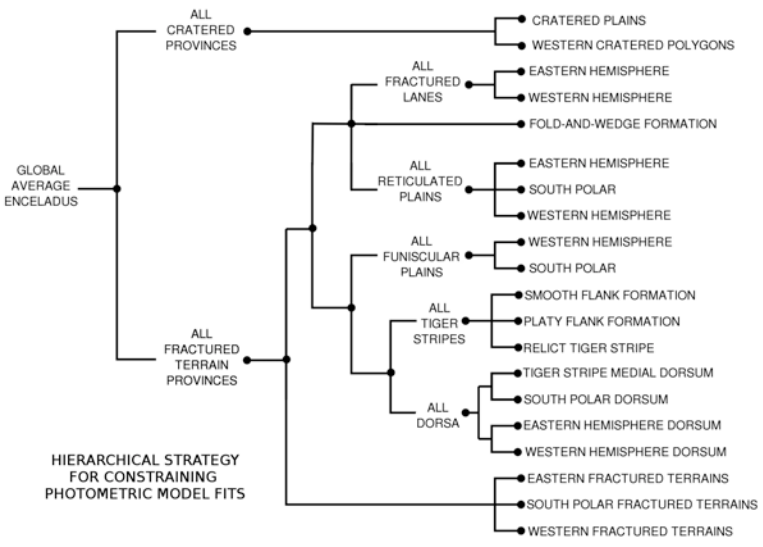

units and localized examples for which available photometric coverage is more restricted. Work supported by NASA's Cassini Data Analysis Program.

Figure 1: Hierarchical strategy for constraining fits of Hapke's (2012) photometric model to Enceladus ISS and VIMS spectrophotometric data base. Photometric angle coverage for the top two-tiers of the dendrogram provides strong constraints on all of the model parameters. The range of available photometric geometries becomes progressively more restricted at the lower tiers. At those levels, the limitations are overcome by fixing the values of the least-well constrained parameters to higher-tier values and fitting only the remaining parameters that are sensitive to the limited coverage.

References: Dougherty et al. 2006. Science 311, 1406-1409l; Hansen et al. 2006. Science 311, 1422-1425; Hapke 2012. *Theory of Reflectance and Emittance Spectroscopy*. 2nd Edition. Cambridge University Press, Cambridge, United Kingdom; Porco et al. 2006. Science 311, 1393-1401; Spencer et al. 2006. Science 311, 1401-1405; Spencer et al. 2009. In *Saturn from Cassini-Huygens* (M. K. Dougherty et al., Eds.) 683-724

Magnetospheres

A statistical picture of interchange injections at Saturn through energetic H+ flux intensifications

A. R. **Azari**[1], X. Jia[1], M. W. Liemohn[1], M. F. Thomsen[2], D. G. Mitchell[3], N. Sergis[4, 5], A. M. Rymer[3], G. B. Hospodarsky[6], C. Paranicas[3], G. Provan[7], S. Ye[6], S. W. H. Cowley[7], and J. Vandegriff[3].
[1]Department of Climate and Space Sciences and Engineering, University of Michigan, Ann Arbor, Michigan, USA, correspondence to (azari@umich.edu). [2]Planetary Science Institute. [3]Johns Hopkins University, Applied Physics Laboratory. [4]Office of Space Research and Technology, Academy of Athens. [5]Institute for Astronomy, Astrophysics, Space Applications and Remote Sensing, National Observatory of Athens.[6]Department of Physics and Astronomy, University of Iowa. [7]University of Leicester, Department of Physics and Astronomy.

Saturn's magnetic and plasma environment has been extensively studied over the past decade and a half with the recent conclusion of the Cassini mission. Periodicities in the plasma properties and magnetic field have been observed at periods closely related to those of the emission power of Saturn Kilometric Radiation (SKR), leading to the hypothesis that the process controlling SKR modulation also controls aspects of magnetospheric physics. Here, we comment on our previous work identifying interchange injections from high-energy (3-22 keV) H+ intensifications and investigate whether interchange injections display periodicities similar to either SKR modulation or other phenomena.

Interchange injections are Rayleigh-Taylor like plasma instabilities and a primary source of mass transport in Saturn's middle magnetosphere. Our previous work found that energetic proton injections are strongly organized by local time and radial distance. We first review our statistical study of interchange injections in Saturn's inner and middle magnetosphere focusing on the dependence of occurrence rate and properties on radial distance, partial pressure, and local time distribution. We analyze the entirety of the Cassini mission's equatorial orbits between 2005 and 2016. In which we identify interchange events from CHarge Energy Mass Spectrometer (CHEMS) H+ data using a trained and tested automated algorithm, which has been compared with manual event identification for optimization. We provide estimates of interchange based on intensity, which we use to investigate current inconsistencies in local time occurrence rates. We find the peak rates of interchange occur between 7 - 9 Saturn radii and that this range coincides with the most intense events as defined by H+ partial particle pressure. We determine that nightside occurrence dominates as compared to the dayside injection rate, supporting the hypothesis of an inversely dependent instability growth rate on local Pedersen ionospheric conductivity. Additionally, we observe a slight preference for intense events on the dawn side, supporting a triggering mechanism related to large-scale injections from downtail reconnection. Our observed local time dependence paints a dynamic picture of interchange triggering due to both the large-scale injection driven process and ionospheric conductivity.

Second, we consider the organization by several different periodic fluctuation-based longitude systems building off our statistical survey of interchange. If organized by planetary oscillation phase, then interchange would assist in communicating these periodicities between the inner and outer magnetosphere of Saturn. We take advantage of the recently updated and near-continuous defined Saturn longitude system (SLS-5), which is based on the modulation phase of SKR, along with the planetary – period oscillations longitude system (PPO), which is based on magnetospheric magnetic field measurements. We analyze the phase system distribution for equatorially observed interchange in 2005 – 2016 and compare this to previous studies.

The induced magnetosphere of Titan: characterizing its outer edge

C. **Bertucci**[1], G. Boscoboinik[1], R. Modolo[3], and N. Edberg[4].
[1]Instituto de Astronomía y Física del Espacio, CC67, Suc. 28, 1428 Buenos Aires, Argentina, (cbertucci@iafe.uba.ar), (gabybosc@gmail.com), [3]LATMOS (11 boulevard d'Alembert, Quartier des Garennes, 78280 - Guyancourt, France, ronan.modolo@latmos.ipsl.fr), [4]Swedish Institute of Space Physics, Swedish Institute of Space Physics, Box 537, SE-751 21, Uppsala, Sweden, (ne@irfu.se).

Plasma boundaries are known to be the loci where significant transfer of momentum and energy exchange between plasma populations can occur. In this work, we analyze the magnetic morphology of the outer limit of Titan's induced magnetosphere. In particular, we apply minimum variance analysis to Cassini MAG data in order to study the role of the magnetic field in the dynamics of charged particles from local and external origin. We examine the properties of Titan induced magnetospheric boundary for different upstream conditions and discuss the role of fossil fields in its formation. These results intend to shed light on the role of the magnetic field in the processes of transfer of energy and momentum between Titan´s ionosphere and exosphere, and the external (Kronian, Solar Wind) plasma.

Planetary Exploration, Horizon 2061: Some proposed next steps for giant planets systems exploration

Michel **Blanc**[1], Ari-Matti Hari[2], Rafael Rodrigo[3], Norbert Krupp[2], Karolyn Szego[2], John Zarnecki[3], the H2061 W.G., Air and Space Academy[4] and the Planetary Exploration Horizon 2061 team[3].
[1]Institut de Recherche en Astrophysique et Planetologie, (michel.blanc@irap.omp.eu), [2]Europlanet Research Infrastructure, [3]International Space Science Institute, [4]http://www.issibern.ch/forum/europlanetforum/, [5]http://www.academie-air-espace.com.

The assembly of magnetospheres, satellites, rings, small bodies, dust, gas and plasma tori that co-orbit Giant Planets form with the central body fascinating "small planetary systems" in the Solar System at large. The lessons we learn from their exploration can be extrapolated to provide us with a better understanding of the Solar System as a whole and of the more than 500 already discovered exoplanetary systems.

We will present the results of a foresight exercise jointly implemented by the Europlanet Research Infrastructure project of the European Union and by the International Space Science Institute (ISSI) to produce a community Vision of Planetary Exploration up to the 2061 horizon (the return of Halley's comet into the inner Solar System and the centennial of the first Human space flight). An international community forum convened by them in Bern, Switzerland on September 13th to 15th, 2016 tentatively identified the key questions of the science of planetary systems and a set of representative planetary missions that we found should be flown to the different objects of the Solar System by 2061 to answer these "big questions".

We will focus this communication on the future of the scientific exploration of giant planets. Starting from the legacy of the Cassini-Huygens mission, which brilliantly addressed several of our key science questions in the Saturn system, we will first focus on the major science questions to be answered in the Jupiter system beyond those addressed by the currently flying (Juno) and planned (JUICE and Europa Clipper) missions. Then we will describe the scientific needs for a new post-Cassini mission to the Saturn System, and place the well-needed future exploration of the ice giants, Uranus and Neptune, in the broader perspective of the interdisciplinary study of planetary systems.

Saturn's Internal Magnetic Field Revealed by Cassini Grand Finale

Hao **Cao**,[1,2] Michele K. Dougherty,[3] Krishan K. Khurana,[4] Gregory J. Hunt,[3] Gabrielle Provan,[5] Stephen Kellock,[3] Marcia E. Burton,[6] Thomas A. Burk [6] and the Cassini Magnetometer Team.
[1]Department of Earth and Planetary Sciences, Harvard University, 20 Oxford Street, Cambridge, MA 02138, (haocao@fas.harvard.edu), [2]Division of Geological and Planetary Sciences, California Institute of Technology, 1200 E California Blvd, Pasadena, CA 91125, USA [3]The Blackett Laboratory, Imperial College London, London SW7 2AZ, UK [4]Department of Earth, Planetary, and Space Sciences, University of California, Los Angeles, 90025, USA [5]Department of Physics and Astronomy, University of Leicester, Leicester, UK 6Jet Propulsion Laboratory, California Institute of Technology, 4800 Oak Grove Dr, Pasadena, CA 91109, USA

Saturn's intrinsic magnetic field continues to offer surprises since the first in-situ measurements during the Pioneer 11 Saturn flyby. The Cassini spacecraft entered the Grand Finale phase in April 2017, during which time the spacecraft dived through the gap between Saturn's atmosphere and the inner edge of the D-ring 22 times before descending into the deep atmosphere of Saturn on Sep. 15th 2017. The unprecedented proximity to Saturn (reaching ~ 2550 +/- 1290 km above the cloud deck) and the highly inclined nature of the Grand Finale orbits provided an ideal opportunity to decode Saturn's internal magnetic field. The fluxgate magnetometer onboard Cassini made precise in-situ vector magnetic field measurements during the Grand Finale phase. Magnetic signals from the interior of the planet and various magnetospheric currents were observed during the Grand Finale phase. Here we will report new features of Saturn's internal magnetic field revealed by measurements from the Cassini Grand Finale phase. We will show the directly determined northward offset of Saturn's magnetic equator and it variations. Small-scale yet highly consistent magnetic structures were detected along every Grand Finale orbits. When expressed in spectral space, intrinsic magnetic moments up to at least degree 9 are needed to describe these magnetic structures. Implications for the deep interior of Saturn will be discussed.

Global maps of energetic charged particles at saturn and their relation to the magnetic field

J.F. **Carbary**[1], D.G. Mitchell[1], P. Kollmann[1], E. Roussos[2], N.Krupp[2], and D.C. Hamilton[3].
[1]Johns Hopkins University Applied Physics Laboratory, Laurel, MD, 20723, USA (james.carbary@jhuapl.edu), [2]Max-Planck-Institute für Sonnensystemforschung, Göttingen, Germany, [3]University of Maryland Department of Physics, College Park, MD, 20742, USA.

The combined datasets of the Low Energy Magnetospheric Measurement System (LEMMS) and the Charge-Energy Mass Spectrometer (CHEMS), of the Cassini Magnetospheric Imaging Instrument (MIMI), are combined from SOI in July, 2004, to the Final Orbit in September, 2017, to render global maps of electrons (18-2000 keV) and ions (3-225 keV) within Saturn's magnetosphere. Generated at a resolution of 1x1 R_S (1 R_S = 60268 km) for the dayside and nightside magnetosphere, the maps reveal charged particles concentrated in a magnetodisk near the equatorial plane for cylindrical ranges from ~10 R_S to the magnetopause, while inside this distance their distributions bifurcate along field lines to a northern and southern branch. The bifurcation location is similar on the dayside and nightside and probably signals a plasma-pause boundary. Fluxes of all species are generally greater on the nightside than the dayside, a result of particle injections from the magnetotail or a noon-midnight electric field. The magnetodisk thickness is greater on the dayside than nightside, which implies compression by the solar wind. The figure below shows a detailed map of the lowest energy CHEMS H+ ions accumulated over the whole Cassini mission, displayed in cylindrical coordinates where the z axis is the spin (magnetic) axis of Saturn. Non-dipolar field lines are those from a force-balance model. On the dayside, a model magnetopause has also been drawn. Crosses indicate bins with few or no samples.

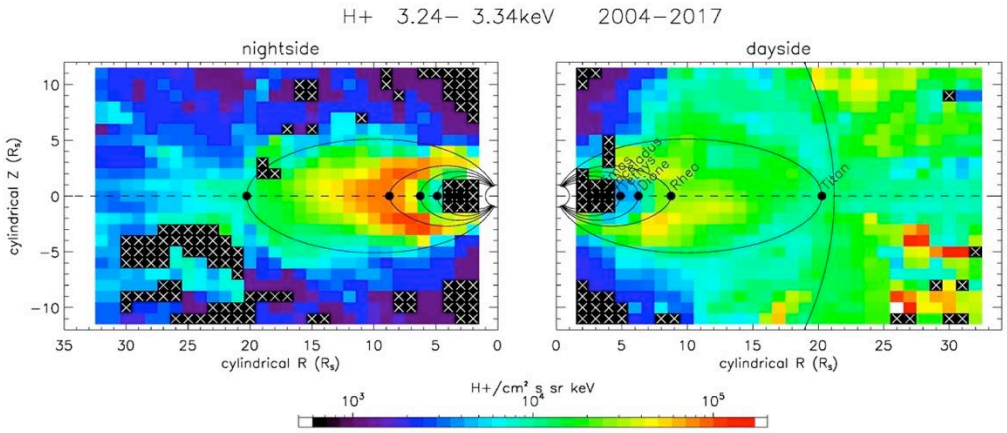

The meridional magnetic field of saturn: a new analytical model

J.F. **Carbary**[1].
[1]Johns Hopkins University Applied Physics Laboratory, Laurel, MD, 20723, USA (james.carbary@ jhuapl.edu).

The magnetometer (MAG) data for the Cassini mission (2004-2016) is used to derive an analytical model of Saturn's meridional magnetic field lines. Using a bin map of the B_ρ and B_z field components, the field lines can be traced from the equator to the inner magnetosphere. The traces reveal a magnetic field greatly compressed on the dayside and highly elongated on the nightside, which are presumably the effects of solar wind compression and viscous flow around the magnetosphere. An analytical model is proposed that accommodates this day-night asymmetry using an H parameter that is higher on the dayside and lower on the nightside. The model can be adjusted for magnetodisk warping by using a transformation that depends on solar latitude. The figure below shows traces of the meridional field, displayed in cylindrical coordinates where the z axis is the spin (magnetic) axis of Saturn. Non-dipolar field lines are those from a force-balance model. On the dayside, the model magnetopause of Pilkington et al. (*JGR, 119*, 2014, 10.1002/2014JA019774) has also been drawn as a dot-dash line. A solid line indicates the center of a warped magnetodisk, for a solar latitude of 10°, from the model of Arridge et al. (*JGR, 113*, 2008, 10.1029/2007JA012963.). Dotted lines display dipole field lines.

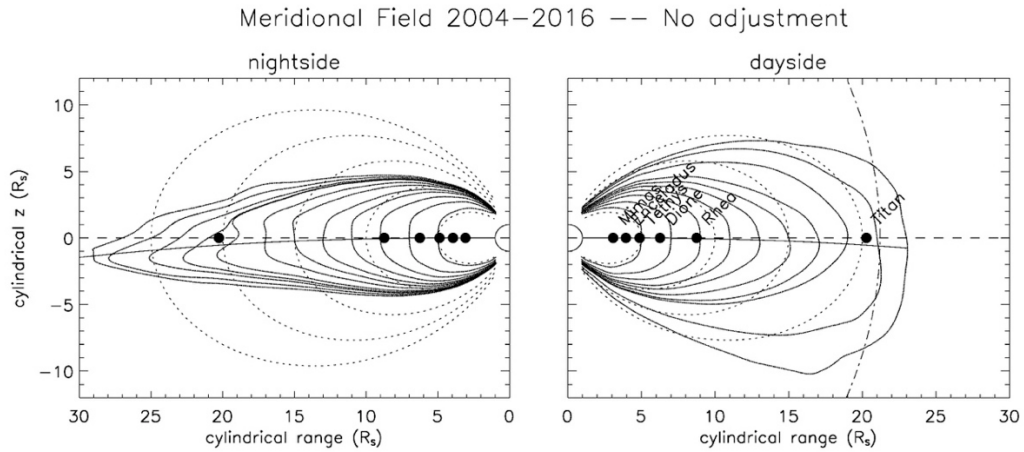

Saturn's Magnetic Field Observations from the Cassini Grand Finale

Michele K. **Dougherty** (1), H. Cao (2, 3), K. K. Khurana (4), G. Hunt (1), G. Provan (5), S. Kellock (1), M. E. Burton (6), T. A. Burk (6) and the Cassini Magnetometer Team
Physics Department, Imperial College London, SW7 2AZ, UK, +442075947757, (m.dougherty@imperial.ac.uk), Department of Earth and Planetary Sciences, Harvard University, MA 02138, USA. Division of Geological and Planetary Sciences, Caltech, CA 91125, USA. Department of Earth, Planetary and Space Sciences, UCLA, CA 90025, USA. Department of Physics and Astronomy, Leicester University, UK. Jet Propulsion Laboratory, CA 91109, USA.

During the Cassini Grand Finale orbits at Saturn the focus of the magnetometer investigation was determination of the internal planetary magnetic field as well as the rotation rate of the deep interior. The unique geometry of these orbits provided an opportunity to measure the internal magnetic field at closer distances to the planet than ever encountered before. The surprising close alignment of Saturn's magnetic axis with its spin axis (known about since the Pioneer 11 observations) has been confirmed, however external effects, observed even around periaspse are masking some of the magnetic field signals from the interior. The varying northern and southern magnetospheric planetary period oscillations and field aligned currents at both high and low latitudes are contributing to the magnetic signals observed. We report new features in the internal planetary magnetic field as well as the external planetary magnetic field, enhancing our view of the auroral current systems and including the discovery of inter-hemispheric currents flowing in the magnetospheric plasma near the inner edge of the D ring.

Saturn's ionosphere: Electron density altitude profiles and ring shadowing effects from the Cassini Grand Finale

L. Z. **Hadid**[1] and M. W. Morooka[1] and J-E. Wahlund[1] and A. M. Persoon[2] and D. J. Andrews[1] and O. Shebanits[3] and W. S. Kurth[2] and N. J. T. Edberg[1] and E. Vigren[1] and A. F. Nagy[4] and L. Moore[5] and T. E. Cravens[6] and M. M. Hedman[7] and W. M. Farrell[8], and A. I. Eriksson[1].
[1]Swedish Institute of Space Physics, Box 537, SE-751 21 Uppsala, Sweden, (lina.hadid@irfu.se), [2]Department of Physics and Astronomy, University of Iowa, Iowa City, IA 52242, USA. [3]Space and Atmospheric Physics, The Blackett Laboratory, Imperial College London, London, UK. [4]Department of Climate and Space Sciences and Engineering,University of Michigan, USA. [5]Center for Space Physics, Boston University, Boston, Massachusetts, USA, [6]Department of Physics and Astronomy, University of Kansas, Lawrence, KS 66045, USA, [7]Department of Physics, University of Idaho, Moscow ID 83844-0903, [8]NASA/Goddard Space Flight Center, Greenbelt, Maryland, USA.

Introduction: We present the electron density altitude profiles of Saturn's ionosphere at equatorial latitudes ($-15^\circ \leq \phi \leq 15^\circ$) and the ring shadowing effects from all the 23 proximal passes of Cassini's Grand Finale. The data are collected by the Langmuir probe (LP) and for some cases from the plasma wave frequency characteristics of the Radio and Plasma Wave Science (RPWS) investigation. A high degree of variability in the electron density profiles is observed. However, organizing them by consecutive altitude ranges revealed clear differences between the southern (winter) and northern (summer) hemispheres. We show a layered electron density altitude profile with evidence in the southern hemisphere of an electrodynamic type of interaction with the planets innermost D ring. Similar layers were observed during the Final Plunge of Cassini, where the main ionospheric peak is crossed at ~ 1550 km altitude.

Moreover, from the ring shadow signatures on the total ion current collected by the LP, we reproduce the A and B ring boundaries and confirm that they are optically thicker than the inner C and D rings and the Cassini Division to the solar extreme ultraviolet radiation. Furthermore, observed variations with respect to the inner edge of the B ring shadow imply a delayed response of the ionospheric H^+ because of its long lifetime and/or suggest the presence of ring-derived plasma from the C and D rings reducing the shadowing signatures.

A large seasonal variation of energetic C+ and CO+ abundances in Saturn's magnetosphere probably resulting from changing ring illumination

D.C. **Hamilton**[1], S.P. Christon[2], D.G. Mitchell[3], R. Morishima[4], R. Hodyss[5]
[1]University of Maryland, Department of Physics, College Park, MD 20742 (dch@umd.edu), [2]Focused Analysis and Research, Columbia, MD 21044, [3]Johns Hopkins University Applied Physics Laboratory, Laruel, MD, 20723, [4]UCLA/JPL, Los Angeles, CA 90095, [5]Jet Propulsion Lab, Pasadena, CA 91109

In mid-2014 the Cassini/CHEMS instrument observed a rather dramatic increase in the relative abundances of both C^+ and CO^+ (a factor of 4 for C^+ and 8 for CO^+). The enhancements then decreased during 2015 and 2016, with CO^+ decreasing much more quickly. C^+ and CO^+ (the latter mass 28 molecular ions could also include N_2^+) are trace components (<1% to 2%) of the energetic (96-220 keV) ion population in Saturn's magnetosphere, which is dominated by water group ions W^+ (O^+, OH^+, and H_2O^+ and H_30^+), H^+, and H_2^+.

We suggest that the C^+ and CO^+ enhancements are associated with CO_2, possibly from Enceladus, building up on the cold rings near equinox, but then released from the north side of the A, and possibly B, rings as they were warmed above 80K in late 2013 or early 2014 by increasing solar illumination after the 2009 equinox (Morishima et al, Icarus, 279, 2-19, 2016). Hodyss et al (Icarus, 194, 836-842, 2008) found preferential sublimation of CO_2 from a CO_2:H_2O ice mixture when it was warmed above 80K. Meteoroid bombardment could be another source of carbon in the ring ice. After release from the ice, transport, dissociation, ionization, and then acceleration in the magnetosphere would produce the observed energetic C^+ and CO^+, with the enhancements subsiding as the CO_2 and other carbon species gradually become depleted.

We will report the C^+/W^+ and CO^+/W^+ abundance ratios from Cassini SOI in 2004 through the Sept. 15, 2017 end of mission as well as somewhat smaller variations observed in the N^+/W^+ ratio.

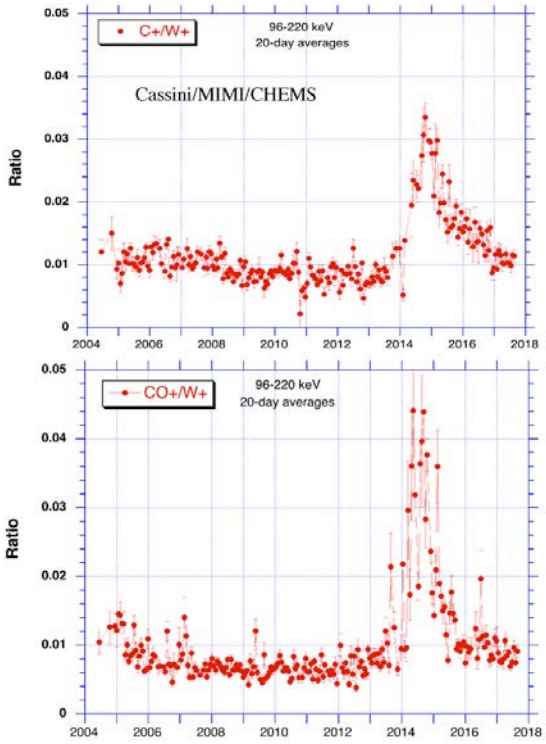

Re-examining the ordering of injection events within saturnian SLS5 longitude

G. B. **Hospodarsky**[1], S. Ye[1], T. J. Kennelly[1], W. S. Kurth[1], abd D. A. Gurnett[1]
[1]Dept. of Physics & Astronomy, Univ. of Iowa, Iowa City, IA 52241, USA (george-hospodarsky@uiowa.edu).

Introduction: Previous work by Kennelly et al. [2013] found that "young" injection events as determined by the Radio and Plasma Wave System (RPWS) instrument were strongly ordered by the SKR-derived Saturnian longitude system (SLS4), and that the ordering varied with Saturnian season. Pre-equinox, the northern hemisphere's longitude system controls the event occurrence, and post-equinox, the events were ordered by the southern hemisphere-derived longitude system. However, the number of post-equinox events in the Kennelly study were limited, and uncertainty in the post-equinox SLS4 periods increased as more data was obtained, making it unclear if the Kennelly post-equinox results still held. Recent work, using the complete Cassini data set at Saturn (over 14 years) has determined an updated longitude system (SLS5) for both the northern and southern hemispheres for the post-equinox period. We extend the Kennelly list of "young" injection events for the entire Cassini mission and compare both the original and updated list to the updated SLS5 system to re-examine for possible seasonal control.

An overview of Cassini's major findings regarding Saturn's magnetosphere

Xianzhe **Jia**[1]
[1]Department of Climate and Space Sciences and Engineering, University of Michigan, Ann Arbor, Michigan , 1433 Space Research Bldg., 2455 Hayward St., Ann Arbor, MI 48109-2143; (xzjia@umich.edu)

As the first orbiter dedicated to Saturn, Cassini completed a thirteen-year journey around the gas giant planet. The long-lived mission has collected enormous data that allow for comprehensive characterization of the structure and dynamics of Saturn's magnetosphere. The combination of equatorial and high-inclination orbits enabled the spacecraft to sample a wide range of radial distances, latitudes, and local times, thereby providing global coverage of the magnetosphere. Extensive analyses of Cassini observations conducted over the course of the mission lifetime have revolutionized our understanding of how Saturn's magnetosphere operates.

It was discovered early in the mission that Enceladus possesses active water plumes ejecting neutral gases and dust particles into space, which then become ionized providing the main plasma source for Saturn's magnetosphere. How the plasma originating from Enceladus is transported outward and eventually removed from the Saturn system is an outstanding question. With a suite of capable instruments, Cassini was able to observe plasma processes that are critical to answering this question, such as interchange-driven particle injections and plasmoid releases resulting from magnetotail reconnection. Analyses of Cassini data combined with modeling

studies have informed us of the crucial role these processes play in the transport and energization of charged particles and circulation of magnetic flux within the magnetosphere. Furthermore, Cassini's in-situ measurements together with remote observations of Saturn's aurora have provided new insights into how Saturn's magnetosphere responds to rotationally-driven and solar wind-driven processes. It is also important to realize that the time span of the mission covers almost half of a Saturn year, and is also comparable to the 11-year solar cycle. Consequently, Cassini was able to monitor long-term effects arising from seasonal variations of the magnetosphere and its response to potential solar cycle influences.

One of the most perplexing aspects of Saturn's magnetosphere revealed by Cassini is the magnetospheric periodicities. Despite the high degree of axisymmetry of Saturn's internal field, Cassini observations show that the magnetosphere exhibits ubiquitous planet-period oscillations in a wide variety of properties. Many theories and models have been put forward to explain the observed periodicities, and it seems likely that the source of the periodicities lies in the high-latitude atmosphere/ionosphere although the exact origin remains unidentified.

Throughout its mission, Cassini made a large number of close encounters with Saturn's major satellites, with Titan and Enceladus the most frequent targets. Data obtained in the vicinity of the moons reveal diverse properties in the way they interact with their surrounding plasma. In particular, Cassini's over 120 close flybys of Titan provided us with a detailed look at the interaction of the moon's induced magnetosphere with Saturn's magnetospheric plasma, and also rare opportunities to study Titan's interaction with the solar wind.

This tutorial is aimed to provide an overview of the major findings from the Cassini mission regarding Saturn's magnetosphere and its interaction with the moons. It will conclude with a discussion of open questions that may be addressed through continued analysis of the Cassini data or future missions to the Saturn system.

New insights into Saturn's inner magnetosphere during Cassini's Grand Finale: MIMI

Norbert **Krupp**[1], Elias Roussos[1], Peter Kollmann[2], Don Mitchell[2], Anna Kotova[3], Jim Carbary[2], Chris Paranicas[2], Doug Hamilton[4], Nick Sergis[5], and Michele Dougherty[6]

[1]Max-Planck-Institut für Sonnensystemforschung, Göttingen, Germany (krupp@mps.mpg.de); [2]The Johns Hopkins University Applied Physics Laboratory, Laurel, MD, USA; [3]IRAP, Université de Toulouse, CNRS, UPS, CNES, Toulouse, France; [4]University of Maryland, College Park, MD, USA; [5]Office of Space Research and Technology, Academy of Athens, Athens, Greece; [6]Imperial College London, London, UK

During the Grand Finale the Cassini spacecraft orbited Saturn in high latitude orbits between November 2016 and Sep 2017. The duration of each orbit was about a week. During the first 22 orbits Cassini's periapsis was near the F-Ring while during the final 22.5 so called proximal orbits the spacecraft approached the planet as close as 1800km above the 1bar cloud level of Saturn's atmosphere.

We will give an overview of the findings of the MIMI instrument onboard during this final year of the mission including the heliospheric conditions, the characterization of the inner radiation belt and dust in the gap between the atmosphere of Saturn and the D-Ring with in-situ and remote particle observations; the sources, sinks, transport, and the pitch angle distribution of energetic electrons in the inner magnetosphere and near the main rings, the galactic cosmic ray access, as well as the mapping and variability of the nightside plasma sheet during that time period.

The legacy of Cassini RPWS: Radio and plasma waves at Saturn

W. S. **Kurth**[1], D. A. Gurnett[1], T. F. Averkamp[1], R. Bostrom[2], P. Canu[3], B. Cecconi[4], N. Cornilleau-Wehrlin[3], W. M. Farrell[5], G. Fischer[6], P. Galopeau[7], G. Gustafsson[2], L. Hadid[2], G. B. Hospodarsky[1], L. Lamy[4], A. Lecacheux[4], P. Louarn[8], R. J. MacDowall[5], J. D. Menietti[1], R. Modolo[7], M. Morooka[2], A. Pedersen[9], A. M. Persoon[1], A. Sulaiman[1], J.-E. Wahlund[2], S. Ye[1], and P. Zarka[4].

[1]Dept. of Physics & Astronomy, Univ. of Iowa, Iowa City, IA 52241, USA (william-kurth@uiowa.edu), [2]Swedish Inst. of Space Physics, Uppsala, Sweden, [3]Plasma Physics Laboratory, Ecole Polytechnique, Paris, France, [4]LESIA, Observatoire de Paris, Meudon, France, [5]NASA Goddard Space Flight Center, Greenbelt, MD, USA, [6]Austrian Academy of Sciences, Space Research Institute, Graz, Austria, [7]LATMOS/IPSL, UVSQ, University Paris CNRS, Guyancourt, France, [8]IRAP, Toulouse, France, [9]University of Oslo, Oslo, Norway.

Introduction: The 13-year exploration of Saturn with Cassini provided enormous scientific return from the Radio and Plasma Wave Science (RPWS) investigation. While it is not possible to achieve absolute concensus on the most important results from this investigation, here we attempt to show the breadth of contributions to the study of the Saturnian system with this instrument.

Saturn Kilometric Radiation: Cassini's RPWS determined that not only does the SKR rotational modulation vary in time, there are typically two different periods in the northern and southern hemispheres. Cassini crossed the SKR source region, confirming that the cyclotron maser instability (CMI) can drive the auroral radio emissions. These are the first in situ observations of a non-terrestrial

CMI radio source. In addition, SKR was shown to be generated on field lines threading the UV auroras and diagnositic of magnetospheric dynamics imposed by solar wind compressions and tail reconnection.

Enceladus and the E ring: RPWS observations contributed to the mapping of dust from the plumes of Enceladus and the resulting E ring. The discovery of auroral hiss generated by electron beams accelerated from the moon informed our understanding of the electromagnetic interaction of the moon with the magnetosphere. Auroal hiss also provided evidence of this interaction very close to the planet on field lines threading the moon. Plasma resulting from the ionoization of material coming from Enceladus was modeled through the determination of the electron density in Saturn's inner magnetosphere. The depletion of the electron density in the plume led to the realization that charged micron-sized dust grains were a major component of a dusty plasma in the vicinity of the moon.

Lightning: High frequency radio emissions initiated in lightning strokes enabled RPWS to characterize the occurrence of lightning, hence, convective storms in Saturn's atmosphere and tracked the development of a Great White Spot storm beginning in late 2010. Coupled with amateur and ISS images, an extensive compilation of thunderstorm activity in Saturn's atmosphere was possible.

Titan's Ionosphere: The RPWS Langmuir Probe was the first instrument to confirm the existence of a substantial ionosphere at Titan. The Solar EUV dominates the ionization of the upper atmosphere of Titan, although energetic particles in Saturn's magnetosphere do contribute substantially at all Solar Zenith Angles. Observations over the orbital mission showed the effect of the vaiation of EUV over the solar cycle in the ionospheric density. One of the more intriguing discoveries was the formation of complex negative organic ions and aerosol pre-cursors in the deep ionosphere of Titan, which may have implications for how pre-biotic chemistry occurred on the early Earth. RPWS observations also helped characterize the interaction of Titan with the solar wind and the development of a compound bowshock encompassing both Titan and Saturn's magnetosphere.

Saturn's Ionosphere: An obvious result of Cassini's Grand Finale was the first in situ obervations of electron densities and temperatures in Saturn's topside ionosphere and the revelation of strong interactions between the rings and the ionosphere.

Relative fractions of water-group ions in Saturn's inner magnetosphere

Mark E. **Perry**[1], Tom E. Cravens[2], Robert Tokar[3], H. Todd Smith[1], J. Hunter Waite, Jr.[4], Ralph L. McNutt, Jr.[1]
[1]Johns Hopkins University, Applied Physics Laboratory, Laurel, MD, (Mark.Perry@jhuapl.edu); [2]University of Kansas, Lawrence, Kansas; [3]Planetary Science Institute, Santa Fe, NM; [4]Southwest Research Institute, San Antonio, TX

At two dozen times over ten years, the Cassini Ion Neutral Mass Spectrometer (INMS) measured the relative fractions of water-group ions in the inner magnetosphere of Saturn near the equatorial plane between 3.8 and 6.5 Saturn radii (R_S). Unlike energy-sorting instruments, each INMS measurement determines the abundance of a single ion, with no ambiguity in identifying the particular ion within the water group. Each INMS measurement covers a small portion of velocity space, so velocity-dependent fractions are possible if the multiple dependent parameters and temporal variations can be de-convolved. Densities and count rates are low, sometimes requiring the combining of 10,000 counts to achieve a 2-σ result. Taken together, INMS ion measurements spanned a broad range of velocity space, from the core of the distribution to multiples of the pick-up velocity.

The data show that H_2O^+ comprises the bulk of the ions near 4.0 R_S, and that the H_2O^+ fraction decreases with increasing distance from 4.0 R_S, the source of neutral water at Enceladus. At 4.0 R_S, the fraction of H_2O^+ ranges from 60% to 100%, with the water-group ions that are closest to the pick-up velocity having the highest fraction of H_2O^+. At 6.5 R_S, the three main water-group constituents, H_2O^+, OH^+, and O^+, are nearly equal. H_3O^+, which dominates the water-group ion fractions in the Enceladus plume, is 10% or less in Saturn's magnetosphere outside the plume. Other variations in the relative ion fractions do not show clear links to parameters such as velocity, density, and the orbit phase of Enceladus.

A Diffusive Equilibrium Model for the Plasma Density from 2.4 to 10 RS

A. M. **Persoon**,[1] D. A. Gurnett,[1] W. S. Kurth,[1] J. B. Faden[1], J. B. Groene[1], A. H. Sulaiman[1], S-Y. Ye[1], M. Morooka[2], and J.-E. Wahlund[2].
[1]Department of Physics and Astronomy, University of Iowa, Iowa City, Iowa, USA, (ann-persoon@uiowa.edu), [2]Swedish Institute of Physics, Uppsala, Sweden.

Electron density measurements have been obtained by the Cassini Radio and Plasma Wave Science (RPWS) instrument covering a period from 30 June 2004 to 19 April 2017. Near the F ring, densities are derived from RPWS measurements of electron plasma oscillations at high latitudes. At low latitudes, the RPWS electron densities are derived from dust impact ringing frequencies and from the Langmuir Probe (RPWS/LP) sweep data. Beyond the ring-grazing orbits, the densities are derived from RPWS measurements of the upper hybrid resonance frequency. The density measurements span latitudes up to ~35° and L values from 2.4 to 10. The electron density measurements are combined with ion anisotropy measurements from the Cassini Plasma Spectrometer (CAPS) and electron temperature measurements from the RPWS/LP to develop a diffusive equilibrium model for a two-species plasma consisting of water

group and hydrogen ions and thermal electrons in Saturn's inner magnetosphere. Density contour plots for the three plasma components are presented.

Auroral hiss emissions during Cassini's Grand Finale: Diverse electrodynamic coupling between Saturn, its rings, and Enceladus

H. **Sulaiman**,[1] W. S. Kurth,[1] G. B. Hospodarsky,[1] T. F. Averkamp,[1] A. M. Persoon,[1] S.-Y. Ye,[1] J. D. Menietti,[1] D. Píša,[2] W. M. Farrell,[3] D. A. Gurnett[1].
[1]Department of Physics and Astronomy, University of Iowa, Iowa City, Iowa, USA., [2]Institute of Atmospheric Physics CAS, Prague, Czech Republic., [3]NASA/Goddard Space Flight Center, Greenbelt, Maryland, USA. Corresponding email: (ali-sulaiman@uiowa.edu).

The Cassini Grand Finale orbits offered a new view of Saturn and its environment owing to multiple orbits of high inclination and unprecedented proximity to the planet. The Radio and Plasma Wave Science (RPWS) instrument detected striking signatures of intense auroral hiss emissions during this phase. Our results show: 1) An emission detected near the ionosphere and likely originating from an extended source region in the rings. 2) First observations of VLF saucers directly linked to Saturn's ionosphere. Both are believed to be associated with prevailing ionosphere-ring currents. And finally, 3) An emission detected near the ionosphere and directly linked to Enceladus. These detections have been afforded exclusively by the Grand Finale orbits by virtue of high-latitude and low-altitude passes. Altogether, they reveal both the greater importance and spatial extent of wave-particle processes operating between Saturn, its rings, and Enceladus. The final phase of the mission has underlined Saturn as one of the most dynamic and diverse environments in the solar system.

Dust Observation by the Radio and Plasma Wave Science instrument during the Cassini Mission

S. -Y. **Ye**[1], W. S. Kurth[1], G. B. Hospodarsky[1], A. M. Persoon[1], A. H. Sulaiman[1], D. A. Gurnett[1], M. Morooka[2], J. -E. Wahlund[2], H. -W. Hsu[3], Z. Sternovsky[3], X. Wang[3], S. Kempf[3], M. Horanyi[3], M. Seiss[4], R. Srama[5]
[1]Department of Physics and Astronomy, University of Iowa, Iowa City, IA, USA (shengyi-ye@uiowa.edu); [2] IRF-U, Uppsala, Sweden; [3] LASP, University of Colorado, Boulder, CO, USA; [4] University of Potsdam, Potsdam, Germany; [5] University of Stuttgart, Stuttgart, Germany

Wave instruments onboard spacecraft are designed to detect radio and plasma waves in space. However, when spacecraft encounter dust at tens of kilometers per second, the plasma clouds released by energetic dust impacts can couple to the electric antennas and cause either voltage pulses in waveforms or broadband noise in the spectra recorded by the receivers. The impact signals have been simulated in the lab by shooting dust particles onto a spacecraft model with electric field antennas. During the Cassini mission, such signals have been detected by the Radio and Plasma Wave Science (RPWS) instrument in the solar wind and Saturn's magnetosphere. Given the particle velocity and impact charge yield function, the size and density of the particles can be estimated from the measured signals. In various locations, RPWS measurements have been shown to be consistent with the Cosmic Dust Analyzer (CDA), the dedicated dust instrument. RPWS complemented CDA during times CDA couldn't make measurements due to pointing constraints or low dust density. RPWS carried out in-situ dust density measurement during each crossing of the Saturn's dusty rings and Enceladus plume, providing unprecedented data for these dynamic regions. A new plasma oscillation induced by dust impacts at the background plasma frequency was discovered, providing an independent measurement of local electron density in addition to the Langmuir probe and upper hybrid resonance methods. Before the end of mission, RPWS helped quantify the dust hazards posed to the spacecraft and instruments onboard during the proximal orbits, when RPWS made measurements regardless of the spacecraft attitude. The Grand Finale orbits data revealed a surprisingly low density of dust larger than 0.1 micron. Close inspection of the waveforms indicates a possible dependence of the impact signal decay time on the background plasma density.

Rings

Exogenous dust at Saturn observed by CASSINI-CDA

N. **Altobelli** [1], , S. Kempf [2], F. Postberg[3], C. Fisher[3], T. Albin[3], A. Poppe[5], R. Srama[4]
[1]ESA-ESAC (Nicolas.altobelli@sciops.esa.int), European Astronomy Center, Camino Bajo del Castillo, 28691 Villanueva de la Canada, Madrid, Spain), [2]LASP, University of Boulder, Colorado, US (sascha.kempf@lasp.colorado.edu).

The analysis of the Cassini Cosmic Dust Analyzer (CDA) subsystems data acquired since Saturn Orbit Insertion (SOI) reveals that the Saturn's System is permanently crossed by exogenous dust coming from the surrounding interplanetary space and from the interstellar medium. We report on the analysis of the full data set acquired between SOI and the end of mission.

CDA detects a population of submicron to tens of micron-sized interplanetary grains, with low relative injection speed at Saturn's Hill's boundary, and whose dynamical signature supports a collisional origin in the Edgeworth Kuiper belt or a release by Centaurs. Owing to their low speed relative to Saturn 'at infinity', their abundance is significantly enhanced by gravitational focusing inside the Saturnian System. We also observe the signature of fast, sub-micron grains of interstellar origin. Modeling suggest that dust directly released by JFC comets does not seem to be a dominant population at Saturn, while we find a possible signature of dust released by Oort cloud comets. Compositional information on the different dust populations obtained from the CDA chemical analyzer targets are also presented.

Texture classification in Cassini ISS images of Saturn's rings.

K.-M. **Aye**[1], G. R. Stewart[1], L. E. Esposito[1] and J. Colwell[2]
[1]Laboratory for Atmosphere and Space Physics, University of Colorado at Boulder, 1234 Innovation Drive, Boulder, CO 80304, USA (michael.aye@lasp.colorado.edu); [2]Dept. of Physics, University of Central Florida, Orlando FL 32816-8026

Introduction: Many observations of the Cassini mission have shown both small (meter) and mid-scale (km) sized structures in Saturn's rings. Specifically, UVIS occultation observations have shown small-scale structures (tens of meters) in their High-Speed Photometer (HSP) data, near ring spiral density waves of Inner Lindblad Resonances. At the same locations, Cassini ISS data show differences in the background texture in the rings, indicating structural changes with sizes in the 0.1-1 km scale, and ropy or straw-like signatures in the scale of 1 to 3 km.

This works focuses on applying two techniques to identify and classify differences in image texture and how the identified texture classes related to strengths of known resonances.

Methods: Both techniques are being applied after normalizing ISS images into a cylindrical map-projection centered at Saturn's center. The first technique is a simple image line based dispersion statistics, based on the premise that clumping of material increases the dispersion of the distribution of light reaching the camera. We use measures of the dispersion in the azimuthal direction to identify interesting patterns in the radial direction that repeat in their behavior close to maxima of spiral density waves. The second technique is well known in Earth-bound remote sensing data analysis called Gray-Level Co-Occurence Matrices. This method's strength lies in taking into account the 2-dimensional relationships between pixels, i.e. image texture. We will discuss the pros and cons of these two techniques, present results from their application on ISS image data, and compare them with related dispersion-based analysis of UVIS data.

Particle size and ring structure of Saturn's rings from stellar and solar occultations in the UV

T. M. **Becker**[1], J. E. Colwell[2], N. J. Cunningham[3], L. Roth[4], P. Molyneux[1], K. D. Retherford[1], R. Jerousek[2]
[1]Southwest Research Institute, 6220 Culbra Rd. San Antonio, TX, 78238, tbecker@swri.edu; [2]University of Central Florida, 4000 Central Florida Blvd., Orlando FL; [3]Nebraska Wesleyan University, 5000 Saint Paul Ave., Liconoln NE 68504; [4]KTH Royal Institute of Technology, SE-100 44 Stockholm, Sweden

Introduction: Stellar and solar occultations have proven to be critical techniques for ascertaining significant information about planetary rings, including ring structure through high spatial resolution optical depth profiles, and the particle size distributions of the

rings. Analyses of the stellar and solar occultations observed by Cassini's Ultraviolet Imaging Spectrograph (UVIS) have resulted in strong limits on the sizes of the smallest particles across the rings, the characterization of self-gravity wakes in the A and B rings, and the identification of opaque objects in the F ring. Occultations also represent a unique opportunity for continued analysis through new observations of Saturn's rings, long after the end of the Cassini mission. We will present preliminary results from a newly acquired UV-bright stellar occultation that will be observed by the Hubble Space Telescope (HST) on July 12, 2018, ~10 months after the end of the Cassini mission, as well as results derived from Cassini UVIS occultations, and a comparison between the two.

HST Stellar Occultation 2018: On July 12, 2018, the UV-bright star HD 168233 will be occulted by Saturn's rings, presenting a new opporuntity to study the structure and particle size distribution of the rings. We will observe the occultation with the HST Cosmic Origins Spectrograph (COS) G230L mode. From this occultation we hope to provide a new measurement of the particle size distribution. The size of the COS field of view, the wavelength at which it observes (165 - 320 nm), and its distance from the Saturn system will result in an optical depth profile that is different from the UVIS profiles because it will not capture all of the light from particles < 18 – 30 mm in size. Therefore, we can compare the optical depth profiles to trace the variation of the 15-30 mm particle population. We will also assess any changes to the ring structure since the end of mission, including utilizing the low elevation angle to detect and characterize self-gravity wakes, measure the number of F ring strands currently present, and observe any effects on the A ring outer edge caused by the January, 2018, Janus-Epimetheus swap.

Cassini UVIS occultations: We have utilized the detection of diffracted light in Cassini UVIS stellar and solar occultation data to constrain the ring particle size distribution across Saturn's rings. In Saturn's A ring, we have measured the unambiguous diffraction signatures detected at ring edges and determined that the minimum particle size in the A ring is ~1 mm, with the minimum particle size decreasing as a function of ring plane radius. We have used a similar technique to measure the particle size distribution of the F ring in 11 solar occultations. We compared the varying affective particle size with images from the Cassini Imaging Science Subsystem (ISS) and found that areas of the ring where disturbances (likely produced by collisions in the ring) were visible, the effective particle size is smaller than in parts of the ring where no disturbance is visible in the ISS images.

The structure of Saturn's B ring from Cassini CIRS high-resolution scans

S. M. **Brooks**[1], L. J. Spilker[1], M. R. Showalter[2], S. H. Pilorz[2] and S. G. Edgington[1]. [1]Jet Propulsion Laboratory, California Institute of Technology, Pasadena, California, United States (Shawn.M.Brooks@jpl.nasa.gov; Linda.J.Spilker@jpl.nasa.gov; Scott.G.Edgington@jpl.nasa.gov). [2]SETI Institute, Mountain View, California (mshowalter@seti.org; spilorz@seti.org)

Introduction: When Cassini flew past Titan for the 126th time on 29 November 2016, the gravity of that moon sent the spacecraft on a trajectory that would take it within 10,000 kilometers of Saturn's F ring twenty times before a subsequent encounter on 22 April 2017 would send it on ballistic trajectory carrying it between Saturn's cloud tops and the planet's D ring. The views of Saturn's rings that this trajectory provided at periapsis proved beneficial for high-resolution rings studies. This is not just because of Cassini's proximity, but also because of the spacecraft's high elevation angle above the rings, which reduces the foreshortening that degrades resolution in the ring plane.

We will report on several observations of Saturn's main rings made by Cassini's Composite Infrared Spectrometer at the high spatial resolutions enabled by the end-of-mission geometry, focusing on the B ring. CIRS' three infrared detectors cover a combined spectral range of 10 to 1400 cm^{-1} (1 mm down to 7 μm). The apodized spectral resolution of the instrument can be varied from 15 to 0.5 cm^{-1} (Flasar *et al.* 2004). We focus on data from Focal Plane 1, which detects radiation in the 10-to-600-cm^{-1} range (1 mm to 16 μm). This wavelength range includes the Wien peak of blackbody radiation at temperatures typical of Saturn's rings, making it well-suited to sensing ring thermal emission. The 3.9-mrad field of view of FP1 is broad and coarse, and the geometry at the end of the mission allowed for relatively high spatial resolution for CIRS.

Correlating temperatures from scans of that face of the rings exposed to direct solar illumination (the lit face) and the opposite (unlit) face against ring optical depth suggests differences in ring structure and/or particle transport between the lit and unlit rings across the B ring. We find that the temperature differential between the lit and unlit faces of the rings varies from 2-3 K in the most optically thin sections of the B ring's B1 region (ring radii of 92,000-99,000km) up to 20K in the optically thick portions of the B2 region of the B ring (ring radii of 99,000-104,500 km). Temperatures on the unlit side of the B ring's B3 region (ring radii of 104,500-110,000 km) vary by 5-6 K. These variations appear to be correlated with slight optical depth variations. On the other hand, lit side temperatures across the B3 region show no discernible correlations with optical depth for reasons that are not yet clear and a small, systematic (with radius) decrease of ~2 K. Ferrari and Reffet (2013) and Pilorz *et al.* (2015) published thorough analyses of the thermal throughput across this optically thick ring. We will discuss these recent CIRS rings observations and their implications in the context of such work. (B ring region definitions are taken from Colwell et al. (2009).)

This research was carried out at the Jet Propulsion Laboratory, California Institute of Technology, under contract with NASA.

Cassini's view of the faint D ring and Roche Division

R. O. **Chancia**[1] and M. M. Hedman[1], [1]Department of Physics, University of Idaho, Moscow, ID 83844-0903, USA; rchancia@uidaho.edu & mhedman@uidaho.edu

Introduction: In the last 14 years, Cassini's Imaging Science Subsystem has revealed complex structures in Saturn's dusty rings. Indeed, over the course of the Cassini mission the appearance of the D ring and Roche Division, located on either side of the main rings, have varied and evolved. Both these rings exhibit azimuthal brightness variations that appear to be tied to the rotation of the planet or its magnetosphere. We present a survey of these dusty ring regions and show that some trends can be correlated with changes in Saturn's kilometric radiation and planetary period oscillations throughout the mission.

Clues to clumping in Saturn's rings from Cassini UVIS stellar occultations

J. E. **Colwell**[1], M. R. Green[1], J. Payne-Avary[1], J. H. Cooney[1], R. G. Jerousek[1], L. W. Esposito[2], and M. C. Lewis[3], [1]Dept. of Physics, University of Central Florida, 4111 Libra Drive, Orlando FL 32816-2385, josh@ucf.edu, [2]Laboratory for Atmospheric and Space Physics, University of Colorado, 1234 Innovation Drive, Boulder CO 80303-7814, larry.esposito@lasp.colorado.edu, [3]Department of Computer Science, Trinity University, One Trinity Place, San Antonio TX 78212-7200, mlewis@trinity.edu.

Introduction: Stellar occultations by Saturn's rings observed by the Cassini Ultraviolet Imaging Spectrograph (UVIS) High Speed Photometer (HSP) spanned a range of viewing geometries providing the opportunity to probe the three-dimensional structure of the rings. Clumps of particles in the rings are generally elongated in the orbital direction or canted by ~20-25 degrees in the case of self-gravity wakes. The spacing, orientation, and aspect ratios of clumps vary across the rings. Combining the measurments of the transparency of the rings from multiple viewing geometries has enabled the average properties of self-gravity wakes to be determined throughout the A ring and in parts of the B ring where the optical depth is not too large (e.g. Colwell et al. 2006, Geophys. Res. Lett., 33, L07201; Nicholson and Hedman 2010, Icarus, 206, 410-423).

The variance in the HSP data can also be used to provide a single measure of particle or clump length scale in the rings (e.g. Colwell et al., 2018, Icarus, 300, 150-166; Showalter and Nicholson, 1990, Icarus, 87, 285-306). Additional information about the distribution and size of clumps can be gleaned by from the skewness of the HSP time series. Analysis of these higher order moments probes the structure of the rings on spatial scales comparable to or smaller than the HSP footprint size of several hundred square meters. In addition, some occultations had very high spatial resolution locally when the motion of the projection of the star in the rings nearly matched the ring particle motion. Combining these various measurements enables the average absolute sizes and three-dimensional shapes of clumps and aggregates to be determined in some ring regions.

Results: Individual self-gravity wakes can be observed in some particle-tracking occultations (where stellar footprint speed closely matches the particle motion) in the A ring. The techniques used to characterize self-gravity wakes in the A and B rings can be applied to the C ring plateaus where streaky texture has been observed in images (Tiscareno et al. 2018, Science, submitted). Comparisons of the variance and skewness of occultation data with Monte Carlo simulations of various distributions of ring particles suggest the presence small-scale gaps or holes in the C ring plateaus that may be the result of perturbations from larger particles or particle aggregates (Baillié et al. 2013, Astron. J., 145, 171). Autocorrelation analysis of the occultation data can provide the average absolute spatial scale for clumps and aggregates in some ring regions. In addition, some occultations of binary stars with small projected radial separations in the ring plane provide additional tools for measuring small scale particle clumps. The properties of clumps vary across the rings, with the A ring dominated by self-gravity wakes and evidence for larger-scale clumping or structures in some C ring plateaus. Low-optical-depth regions of the B ring can also be modeled by self-gravity wakes.

Outstanding problems in understanding Saturn's rings.

J. N. **Cuzzi**, 1Ames Research Center, NASA; Mail Stop 245-3; Jeffrey.cuzzi@nasa.gov

Introduction: Having shortened my plenary rings review to accommodate another contributed talk, I felt there might not be enough time to go into detail on a few topics perhaps of interest mostly to aficionados, regarding outstanding problems and shortcomings in current techniques. These are discussed in the poster.

1) **Nonclassical RT models**: close packing/shadowing/wakes: Salo; BEAM. On-particle shadowing, yes or no? Lab studies. Complete wavelength coverage and treatment of "grain size". Radar return and coherent Backscattering. Scattering by a layer vs by single aggregates.

2) **Impacts and Ballistic Transport:** Impact chemistry (carbon on ice); Impacts OF grains INTO grains (yields?); New Ballistic Transport models with new focussing etc; Spokes? RPWS tones?

3) **Structural and compositional puzzles:** The plateaus; Moonlet-free gaps; B Ring irregular structure; Organics? how much more can we get from CDA/INMS?

4) **Ring Origin and evolution Scenarios**: Young vs old; consistent dynamical history, rings and moons? what is a plausible time-variable meteoroid flux? The C Ring rubble belt - would it survive massive early ring? Cassini Division; giant primordial torque and clearing? Embedded moonlets: primordial or locally grown?

5) **Other**

Saturn's rings after Cassini

J. N. **Cuzzi**, Ames Research Center, NASA; Mail Stop 245-3, Moffett Field CA 94035;
Jeffrey.Cuzzi@nasa.gov

This review will provide a retrospective on Cassini's discoveries in the rings during its active data-taking phase covering the last 14 years. It will be impossible to touch on everything Cassini has seen in the rings, so the review will not be exhaustive. Instead, the intent will be to emphasize the most important discoveries in the context of unraveling the origin and evolution of the rings and the Saturn system in general. Along the way I will also introduce key evolutionary processes and combine processes and phenomena into as broad a context as possible. Major aspects of the talk will deal with ring composition and particle size (and their changes with location), embedded moonlets of all sizes and their provenance, the mostly-unexplained variety of ring structure on all scales (some of it changing before our eyes), and the emerging likelihood that the rings must actually be a recent feature of the Saturn system. Various scenarios for ring formation will be briefly introduced and compared. Cassini is not "done" of course, but will carry on for decades by virtue of the wealth of data still to be analyzed. Two more important goals of the talk will be to highlight outstanding unsolved or emerging problems and puzzles, and to suggest where existing modeling and/or analysis tools need to be refined in order to make further progress.

Saturn Ring Results from the Cassini Composite Infrared Spectrometer

L. J. Spilker[1],R. Morishima[1,2], C. Ferrari[3], E. **Deau**[1,2], Stuart Pilorz[4], M. R. Showalter[4], S. M. Brooks[1], S. G. Edgington[1]
[1]NASA Jet Propulsion Laboratory/California Institute of Technology, Pasadena, CA, 91109, USA, (Linda.J.Spilker@jpl.nasa.gov), (Ryuji.Morishima@jpl.nasa.gov), (Estelle.Deau@jpl.nasa.gov), (Shawn.M.Brooks@jpl.nasa.gov), (Scott.G.Edgington@jpl.nasa.gov), [2] University of California at Los Angeles, Los Angeles, CA 90095, USA, [3]Universite Paris-Diderot, USPC, Paris, FRANCE, (cecile.ferrari@planetcf.eu), [4]SETI Institute, Mountain View, CA 94043, USA, (spilorz@seti.org), (mshowalter@seti.org).

Introduction: The Cassini Composite Infrared Spectrometer (CIRS) measured the thermal emission of Saturn's main rings during the Ring Grazing and Grand Finale orbits. The observed thermal emission of Saturn's rings depends on multiple factors, such as the geometry of the observer and the physical characteristics of the particle. These include particle albedo, optical depth, thermal inertia, spin rate and orientation, phase angle, solar elevation angle, observer elevation angle, local hour angle, and radial location in the rings. These parameters have variable impact depending on the ring structure.

Results: During the final year of the mission, CIRS obtained some of the highest spatial resolution ring measurements of the entire mission, on both the northern lit-side and southern unlit-side of the rings. Temperatures were derived from spectra taken with focal plane 1 (FP1) between 10 and 600 cm^{-1} (17 μ m to 1 mm), at a spectral resolution of 15 cm^{-1}. The ring temperatures and scaling factors were derived from Planck fits to the FP1 spectral data. The lit-side temperatures varied from 80 to 100 K and the unlit-side temperatures varied from 70 to 90 K.

The mean temperatures of each ring anti-correlate with ring optical depth for both the lit and unlit sides. The optically thin C ring and Cassini Division are warmer than the A and B rings for both the lit and unlit sides of the ring. This anti-correlation is interpreted as a result of preferential darkening of optically thinner rings due to meteoritic bombardment, which causes the correlation between albedo and optical depth. The anti-correlation is further enhanced on the unlit side because little solar illumination reaches the unlit side of optically thick rings.

These trends, however, are not always true for fine structures in each ring. For the A ring, the unlit-side temperatures are higher at the locations of the strongest density waves (Janus 4:3, 5:4, 6:5 and Mimas 5:3) and bending waves (Mimas 5:3) than the surrounding temperatures, even though the optical depths of these resonant locations are relatively higher than those for the surrounding regions. This increase in unlit-side temperature around these features may possibly be due to enhanced vertical heat transport or particle spin rates as a result of increased stirring of the ring particles in these regions.

CIRS results from the Ring-Grazing and Grand Finale results will be discussed, along with some of the CIRS ring highlights from the mission. The research described in this paper was carried out in part at the Jet Propulsion Laboratory, California Institute of Technology, under a contract with the National Aeronautics and Space Administration. Government sponsorship is acknowledged.

Recent origin of Saturn's rings: How sure are we?

Luke **Dones**[1], [1]Southwest Research Institute, 1050 Walnut St., Suite 300, Boulder CO 80302, luke@boulder.swri.edu

The low mass reported by the radio science experiment, the purity of the water ice inferred from radiometry, and the large influx of micrometeoroids into the rings measured by the Cosmic Dust Analyzer have been said to imply a recent origin for the rings (Zhang et al. 2017; Estrada et al. 2017). However, an initially much more massive ring should evolve viscously over billions of years to have a mass comparable to the rings' current mass (Salmon et al. 2010; Charnoz et al. 2017). Thus low-mass rings do not, by themselves, indicate recent origin. In addition, formation of the rings within the past few hundred million years is statistically unlikely (Dubinski 2017). I will review the assumptions made by pollution models in order to provide robust constraints on when Saturn's rings formed.

References: Charnoz, S., et al. (2017). arXiv:1703.09741. In Planetary Ring Systems, eds. M. S. Tiscareno and C. D. Murray, Cambridge University Press. Dubinski, J. (2017). arXiv:1709.08768. Estrada, P. R., Durisen, R. H., Cuzzi, J. N. (2017). American Geophysical Union, Fall Meeting, abstract #P23B-2734. Salmon, J., Charnoz, S., Crida, A., Brahic, A. (2010). Icarus 209, 771-785. Zhang, Z., et al. (2017). Icarus 294, 14-42.

A recent origin for Saturn's rings from the collisional disruption of an icy moon

John **Dubinski**[1]
[1]Canadian Institute for Theoretical Astrophysics, University of Toronto, 60 St. George St., Toronto, ON, Canada M5S 3H8, dubinski@cita.utoronto.

Introduction: The disruption of an icy moon in a collision with an interloping comet a few hundred million years ago is a simple way to create Saturn's rings. A ring parent moon with a mass comparable to Mimas could be trapped in mean motion resonance with Enceladus and Dione in an orbit near the current outer edge of the rings just beyond the Roche zone. I present collisional N-body simulations of cometary impacts that lead to the partial disruption of a differentiated moon with a rocky core and icy mantle. The core can survive largely intact while the debris from the mantle settles into a ring of predominantly ice particles straddling the orbital radius of the parent moon.

Simulations: I have performed 3 exploratory simulations that vary the collisional direction of the comet within the plane of the parent moon orbit. The orbital radius is a=140,000 km and the velocities at impact are 11, 22 and 44 km/s for rear-end, side-on and head-on collisions. The parent moon has a mass of 2X Mimas while the comet has a mass 0.001X Mimas. I use a collisional N-body code with the parent moon and comet modelled as rubble piles consisting of 10M and 5000 particles respectively. While this method misses the details of melting and vaporization at the impact point, the energetics and phenomenology of disruption are treated adequately as revealed by the good agreement of the results of isolated impact simulations using this method to those from more sophisticated hydrodynamic methods.

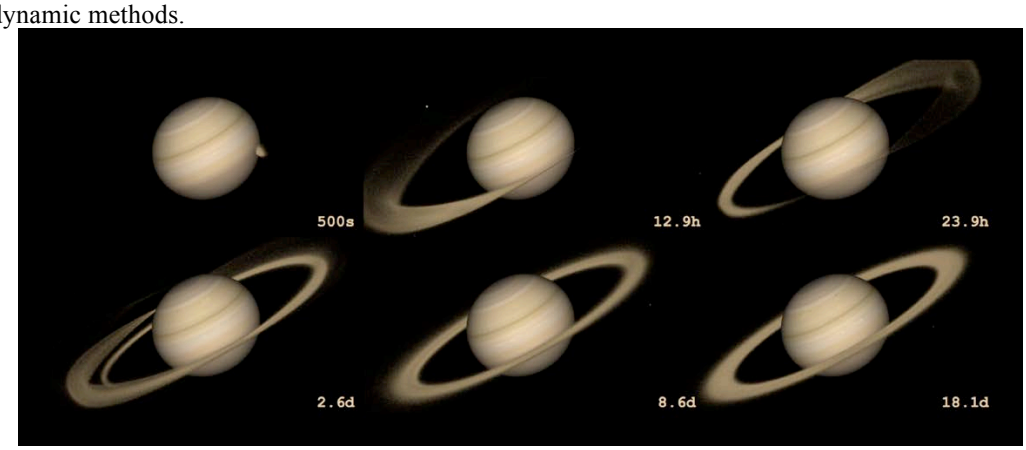

Results: This figure presents the formation of a ring from the most energetic collision. A comet of mass $M_{comet} = 3.75 \times 10^{16}$ kg collides with the moon head-on within the orbital plane with a relative velocity $v_{rel} = 44$ km/s and disrupts the moon leaving a remnant rocky core containing 8% of the original mass. The debris spreads long the orbital radius with inelastic collisions between particles leading to a thin ring in Saturn's equatorial plane within a few weeks. At the end of the simulation, the ring is composed of 91% ice with a radial width of approximately 10,000 km. View an animation here: https://youtu.be/UtVnftTd1tA.

Conclusion: The nascent ring will spread radially due to collisional viscosity while mass re-accretes onto the remnant rocky core to form a new moon that can be identified with Mimas. The icy debris that migrates into the Roche zone evolves into Saturn's ring system. Torques from tidal interaction with Saturn and resonant interactions with the rings push the newly formed Mimas outward to its current position on the same timescale of a few hundred million years. This recent collisional scenario accounts for the high ice fraction observed in Saturn's rings and explains why the ring mass is comparable to the mass of Mimas. The prior existence of a ring

parent moon in mean motion resonance results in a tidal heating rate for Enceladus in the recent past that is at least an order of magnitude larger than the current rate.

Reference: Dubinski, J. 2018, Icarus, in press, https://arxiv.org/abs/1709.08768

Modeling the bombardment of Saturn's rings and fit to Cassini UVIS spectra to estimate their age

J. P. **Elliott**[1] and L. W. Esposito[2]
[1]LASP / CU Boulder 3665 Discovery Drive, Boulder, CO 80513, (joshua.elliott@lasp.colorado.edu);
[2](larry.esposito@lasp.colorado.edu).

Introduction: Calculation of the age of the rings is dependent upon the rate of infalling meteoritic material, as well as the optical depth (and thus the filling factor) of each ring and the size and mass of the particles within the ring. We present an update to our stochastic Markov-chain based meteoritic bombardment simulation of Saturn's rings, including a correction for the collection of impact ejecta over ring particle surfaces depending on the optical depth of the ring, and the latest estimates of the meteoritic mass flux rate onto the rings from the Cassini CDA (Cosmic Dust Analyzer) presented by Kempf et al. at AGU 2017. The product of our simulation is the fractional pollution of the ring particles over time. We then perform a non-linear least-squares fit to Cassini UVIS spectra, using Hapke's 2012 model for bidirectional reflectance of an intimate mixture of regolith grains, to calculate the current fractional pollution of the ring particles. The fit is dependent upon two free parameters, the fractional pollution and surface roughness parameter, as well as upon the spectrum of the pollutant material. We examine two different pollutants, amorphous carbon, and cometary material as measured by the Rosetta Alice UV spectrometer of comet 67P/Churyumov–Gerasimenko. This value for fractional pollution is then compared to the time evolution of fractional pollution, output by our model, to determine the approximate age of the rings.

Predator-Prey analogs for Saturn ring dynamics

LW **Esposito**[1], S Madhusudhanan[1], P Madhusudhanan[1], M Rehnberg[1],
[1]LASP,University of Colorado, 3665 Discovery Dr, Boulder, CO 80303-7820. larry.esposito@lasp.colorado.edu

Introduction: Cassini observations of straw, gaps, ghosts, kittens, propellers, solitary waves and the edge disruption of the Keeler gap by Daphnis may all indicate non-linear dynamics in Saturn's rings. This dynamical behavior cycles ring material into and out of transient aggregations: We see the rings changing before our eyes! How can we understand the structures seen by Cassini and the rapid times scales? Numerical simulations cannot yet capture all the relevant physics, the multiple spatial scales or the asymptotic behavior at long time scales. An ecological analogy of a predator-prey system provides a non-linear model, including aggregation by sweep-up, disk instability and the stochastic collisions of clumps

Model: In this model, the aggregate mass is the *prey*, and the dispersion velocity is the *predator*, since the dispersion 'feeds' off the aggregates stirring the system. This, in turn, limits the growth of the 'prey'. In some cases, the system shows the dynamics of a driven pendulum or of the Duffing oscillator. For specificity, we adopt the 'two-group' model of Goldreich for proto-planetary disks, with the 'groups' being the ring particles and their aggregates. This provides a simplification of the size and velocity distributions. Our analysis gives the phase plane trajectories, the equilibrium points and the size distribution of the largest aggregates.

Forcing: Forcing at mean motion resonances creates non-linear density waves, which increase the surface mass density and decrease the relative velocity in their crests. We use Toomre's criterion to check for disk instability. This triggers aggregation, which is out of phase with the forcing, explaining the 'straw' and associated gaps seen *between* density wave crests.

Results: The largest objects have a steeper size distribution, because of the difficulty of accretion in the tidally influenced regime near the Roche limit. The knee in the size distribution of F ring 'kittens' (at about 700m) may therefore be associated with the transition from adhesive growth to collisional gravity-dominated accretion. Thus, self-gravity wakes are an equilibrium fixed point of the predator-prey model; resonant forcing creates straw; and propellers arise from accretive collisions.

Comparison to Cassini observations: The predator-prey model thus provides an intuitive description of the non-linear dynamics that leads to the structures seen in Cassini UVIS and ISS observations. It explains the phase lag, growth rate and sizes of the transient objects.

Implications of the micrometeoroid flux measured by Cassini CDA for ballistic transport in Saturn's rings

P. R. **Estrada**[1], R. H. Durisen[2] and J. N. Cuzzi[3].

[1]Carl Sagan Center, SETI Institute, 189 N. Bernardo Ave. #200, Mountain View, CA 94043, (Paul.R.Estrada@nasa.gov), [2]Astronomy Department, Indiana University, 727 East Third Street, Bloomington, IN 47405, (durisen@astro.indiana,edu), [3]NASA Ames Research Center, Mail Stop 245-3, Moffett Field, CA 94035, (Jeffrey.Cuzzi@nasa.gov).

Saturn's rings have a huge surface area-to-mass ratio which make them particularly susceptible to modification, both structurally and compositionally, due to extrinsic micrometeoroid bombardment and ballistic transport (BT) of their impact ejecta. Because the rings are predominantly water ice, the level of pollution across the rings due to this extrinsic material serves as a powerful tool for age-dating the rings if the micrometeoroid flux, the radial distribution of the fraction of non-icy material (source+pollutant) and ring mass are known. A trio of observations made by Cassini over the course of its remarkable tenure at Saturn have provided important constraints on these key dependencies that allow us to put hard numbers on the two important time scales associated with micrometeoroid bombardment – the direct deposition time scale, or the time it takes to accumulate the non-icy fraction of material, and the ballistic transport or "gross erosion" time which is the time it would take for a ring annulus of surface density σ to completely erode away if no material returned. Both of these time scales are defined by the ring mass and the micrometeroid flux at Saturn, the latter of which was measured by over a dozen years of dust collection using the Cassini Cosmic Dust Analyzer (CDA) experiment. The CDA results indicate that the range of the micrometeoroid flux at infinity for Saturn are comparable to the nominal value of the meteoroid flux value previously adopted for use in ballistic transport (BT) applications and models. Moreover, the source of the micrometeoroid flux has been associated with the Edgeworth-Kuiper Belt (EKB) and is not cometary in origin as previously assumed. A major consequence of these measurements is that the EKB flux is much more gravitationally focused, increasing the impact flux on the rings by over an order of magnitude relative to cometary, implying that the process of micrometeoroid bombardment and BT is likely even more influential in the rings' structural and compositional evolution over time than previously thought before. Also, the dynamics of this new micrometeoroid population changes the form of the distribution of the impact ejecta which has real consequences for BT and its effect on ring evolution and structure. We will demonstrate some of these consequences with updated models, and discuss remaining uncertainties regarding the CDA flux, ring mass and absolute age of the rings.

Evidence for a ring-driven current system

W. M. **Farrell**[1], D. A. Gurnett[2], W. S. Kurth[2], A. M. Persoon[2], A. Sulaiman[2], G. B. Hospodarsky[2], J. D. Menietti[2], L. Z. Hadid[3], J.-E. Wahlund[3], M. Morooka[3], R. J. MacDowall[1]
1. NASA/Goddard SFC, Grenbelt MD, 2. University of Iowa, Iowa City, IA, 3. Swedish Institue of space Physics, Uppsala, Sweden, (William.M.Farrell@nasa.gov)

Current System: During the Cassini Saturn orbit insertion (SOI) pass over the northern face of the main rings, the Radio and Plasma Wave Science (RPWS) instrument detected the presence of a whistler mode auroral hiss emission below 5 kHz located near the center of the B-ring near L ~ 1.76 R_s [Gurnett et al., 2005]. This auroral hiss also provided evidence of a low-density plasma cavity over the B-ring. Auroral hiss is commonly associated with field aligned electron beams, and it was thus concluded that an outward-propagating electron beam is generated in this region - a location also near the synchronous point [Xin et al., 2006].

From this observation, a new ring-driven current system was conceived by Xin et al. with the ring material moving in Keplerian motion creating a possible drag-like force on the co-rotating plasma, to produce radial E-fields and currents over the rings. The radial currents emanate from the field-aligned incoming current near the synchronous location where the auroral hiss was observed and close back to the ionosphere at the inner and outer edges of the rings.

Subsequent Supporting Evidence. Subsequent RPWS observations confirm the presence of the various elements of the Xin et al. current system:

- During SOI, bursts of auroral hiss emission were observed at the outer edge of the A-ring by RPWS. These events were initially reported to possibly be from impacts on the rings. However, the burst localization limited to only the very outer edge of the A-ring suggests the non-unique possibility that these auroral hiss emissions are associated with bursty field-aligned electron beams that make up the outer edge of the Xin et al. current system at L ~ 2.2.

- Farrell et al. [2005, 2008] reported on z-mode radiation emitted from active plasma 'hot spots' along the field lines connected to the outer edge of the A-ring where the rings and co-rotating magnetospheric plasma disk interact.

- Kopf et al. [2011] reported on a population of events having fine structure frequency vs time emission drifts consistent with a source from the L =2.2 field line - at the outer edge of the A-ring.

- Using the Langmuir probe, Wahlund et al. [2018] found evidence for a D-ring current system connecting the inner ring to the ionosphere during the Grand Finale orbital sequence.

-Sulaiman et al. [2018] also observed auroral hiss on field lines connected to the D-ring, which is indicative of field-aligned currents from this inner-most ring.

We also find that given the Xin et al. current system, the evolution of the enigmatic spokes, including the radial transport of material, can be more easily understood.

Objectives. We will present the evidence in support of the Xin et al. current system, and in the process, the presentation serves as a review of the truly spectacular observations collected by RPWS and other plasma instruments in the vicinity of the main rings.

rss_ringoccs: An open-source analysis package for Cassini RSS ring occultation observations

R. G. French[1], J. W. Fong[2], R. J. Maguire[3], and G. J. Steranka[4].
[1]Wellesley College, Astronomy Dept. Wellesley, MA 02481 (rfrench@wellesley.edu), [2](jfong@wellesley.edu), [3](rmaguire@wellesley.edu), [4](gsteranka@wellesley.edu).

Introduction: Over the course of the Cassini mission, the RSS Team planned, observed, and recorded dozens of ring occultation experiments at three radio wavelengths (0.9, 3.6, 13 cm, or Ka-, X-, and S-band, respectively), providing high-resolution profiles of Saturn's rings at km-scale or better. Although the raw data for these observations are available from NASA's Planetary Data System, as well as selected diffraction corrected observations of the rings at 1- and 10-km resolution, the processing steps required to convert the raw data to diffraction-corrected profiles are complex, and considerable effort is required to accomplish these tasks. For the benefit of scientists wishing to explore RSS ring occultation data on their own, and to provide a starting point for others to develop their own analysis methods, we have developed *rss_ringoccs*: a GitHub-based open-source software package written in Python 3 to process and analyze RSS ring occultation data, starting from the original raw data and ending with diffraction-corrected ring profiles. Our goal is to preserve the legacay of the Cassini RSS ring observations by ensuring that they are easily accessible to scientists for decades to come.

Our data processing methods are based on the definitive paper "Profiling Saturn's Rings by Radio Occultation" (Marouf et al., 1986 [Icarus 68, 120-166]), which describes the theory of diffraction reconstruction technique at the heart of the analysis, and the more recent and Cassini-specific "Cassini Radio Science User's Guide" that provides additional information about the steps required to produce a calibrated diffraction pattern that is the input to the Fresnel transform inversion process. Following the steps in these documents, we divide our analysis and comparisons into three distinct steps: determination of the occultation geometry, conversion of the raw radio science data to a normalized, phase-corrected diffraction pattern that is uniformly spaced in ring plane radius, and the Fresnel inversion of the diffraction profile to produce a diffraction-corrected radial optical depth profile of the rings at a requested spatial resolution.

The *rss_ringoccs* package includes extensive documentation, tutorials, and detailed installation instructions. Our emphasis has been on clarity and simplicity, and we do not claim that our methods represent the state of the art in every aspect of signal processing or numerical efficiency. Nevertheless, the intermediate products and the final diffraction-corrected radial optical depth profiles produced by *rss_ringoccs* are in excellent agreement with the reduced RSS data hosted on the PDS that were obtained by a completely independent analysis pipeline by others on the RSS Team, serving as a useful confirmation of their validity.

Cassini and the PDS ring-moon systems node

M. K. Gordon[1], M. R. Showalter[1], R. S. French[1] and M. T. Tiscareno[1].
[1]SETI Institute, 189 Bernardo Ave Suite 200, Mountain View, CA 94043. (mgordon@seti.or).

Introduction: The Ring-Moon Systems Node (RMS Node) hosts the complete sets of data submitted to the PDS by the Cassini remote sensing instruments – more than one million data products from CIRS, ISS, UVIS, and VIMS combined. We also host more than 200 ring occultation profiles (RSS, UVIS, and VIMS) from the prime mission. The last scheduled routine data delivery from Cassini will have been ingested by PDS shortly before this meeting. That will be followed in the next month or two by a substantial delivery from across Cassini as part of the End Of Mission (EOM) closeout.

OPUS Now: The RMS Node hosts OPUS – an accurate, comprehensive search tool for spacecraft remote sensing observations beyond the asteroid belt. For Cassini, OPUS currently supports ISS, UVIS, and VIMS. Search results include preview images for all products returned by a search, and calibrated images for Cassini ISS. We produce and incorporate into OPUS detailed geometric metadata for every object in the instrument field of view for all three instruments for both the Jupiter and Saturn encounters. OPUS also supports New Horizons (LORRI, MVIC), Galileo (SSI), Voyager (ISS), and several HST instruments.

OPUS Soon: We are currently working to incorporate the Cassini ring occultation data sets into OPUS. As part of a project to migrate the Cassini remote sensing datasets from PDS3 to PDS4 we will update our CIRS pipeline to reformat the data into fixed width tables (much more accessible than the current format) and then generate detailed geometric metadata for each CIRS observation and incorporate all of that into OPUS. In addition, we are nearing the completion of a project to automatically navigate most of the Cassini ISS images and generate substantially improved SPICE C-kernels. All of this will be incorporated into OPUS along with the capability to generate backplanes on demand for each of more than thirty relevant geometric parameters.

OPUS and Cassini End of Mission: RMS will receive and add to OPUS:

- RSS, UVIS, and VIMS ring occultations for the entire mission, all available at 1km resolution, and for many of the highest quality occultations also at the finest practical resolution.

- Radial profiles extracted from a subset of ISS main ring images, a false, longitudinally symmetrical 'filter' generated from each profile, and the result of subtracting that filter from the original calibrated image. The result highlights features like propellers.
- Derived spectral profile data from a subset of the VIMS ring observations.
- More than 150 radius vs. longitude, ISS F-Ring Mosaics.

Support during the meeting. I will be available all week to discuss everything PDS – navigating PDS, navigating the RMS Node website, using OPUS, finding data elsewhere in PDS, submitting data to PDS, and topics relating to using PDS4. Contact me via email to setup a meet time: mgordon@seti.org

---

Particle properties in Saturn's rings from skewness of Cassini UVIS stellar occultations

M. R. **Green**, J. Payne-Avary, J. H. Cooney, J. E. Colwell.
Dept. of Physics, University of Central Florida, 4111 Libra Drive, Orlando FL 32816-2385, (mraechelgreen@knights.ucf.edu).

Introduction: The Cassini UVIS High Speed Photometer measured stellar signals through Saturn's rings over a variety of viewing geometries, providing different line-of-sight optical depths for each location in the rings. The data are described by Poisson counting statistics, and the excess variance can be used to provide a measure of particle or clump length scale in the rings (e.g. Colwell et al., 2018, Icarus, 300, 150-166; Showalter and Nicholson, 1990, Icarus, 87, 285-306). The next higher moment of the occultation data, the skewness, has additional information about the distribution of particles and clumps on scales that are below the spatial resolution of the occultations.

Results: We carried out Monte Carlo simulations of various distributions of ring particles and simulated occultations through these simulated ring patches. We find a relationship between skewness, S, and optical depth that varies with particle size, and have also simulated the effects of isloated features in the rings such as large clumps or gaps. These affect the skewness while not necessarily providing a significant change in the excess variance. The skewness thus has the potential to reveal additional information about the ring structure. We combine our simulations with analyses of regions in the C ring and Cassini Division where the normal optical depth is low. In these regions, occultations over a wide range of incidence angles provide a range of observed optical depth for the same ring material, allowing comparison of the distribution of S with optical depth between data and our Monte Carlo simulations. The best matches to the skewness require isolated features in the rings, perhaps related to streaky texture (Tiscareno et al. 2018, Science, submitted) or the "ghosts" or small gaps hypothesized to be due to large boulders in the rings (Baillié et al. 2013, Astron. J., 145, 171). Different ring particle distributions provide the best fits to different regions in the C ring.

Still more Kronoseismology with Saturn's rings, filling in the spectrum of planetary normal modes

M. M. **Hedman**[1], P.D. Nicholson[2], R.G. French[3] M. El Moutamid[2].
[1]Physics Department, University of Idaho, 875 Perimeter Drive, MS 0903 Moscow ID 83844-0903 (mhedman@uidaho.edu), [2]Department of Astronomy, Cornell University, Ithaca NY 14850, [3]Astronomy Department, Wellesley College, 106 Central Street, Wellesley MA 02481.

Saturn's rings are an exquisitely sensitive probe of Saturn's gravitational field because oscillations and asymmetries within the planet give rise to spiral density waves in the rings. Detailed studies of these waves have already provided information about the frequencies of certain normal-mode oscillations within the planet, yielding new insights into Saturn's internal structure. However, the visible waves correspond to a fraction of the possible planetary normal modes, implying that only certain normal modes have large enough amplitudes to obviously perturb the rings. Using wavelet-based filtering techniques, we have been able to combine data from multiple stellar occultations to identify signals from previously unseen density waves. These extremely weak waves appear to be generated by additional planetary normal modes, and so provide new information about the planet's interior and the excitation spectrum of Saturn's normal modes.

Analyzing propeller gaps in Cassini NAC images

H. **Hoffmann**[1], M. Seiler[1], M. Seiß[1], and F. Spahn[1].
[1]Theoretical Physics Group, Institute of Physics and Astronomy, University of Potsdam, Karl-Liebknecht-Str. 24/25, 14469 Potsdam, Germany (holger.hoffmann@uni-potsdam.de).

Among the great discoveries of the Cassini mission are the propeller-shaped structures created by small moonlets embedded in Saturn's dense rings. These moonlets are not massive enough to counteract the viscous ring diffusion to open and maintain circumferential gaps, distinguishing them from ring-moons like Pan and Daphnis.

Partial gaps are one of the defining features of propeller structures. Until recently only the largest known propeller named Blériot was known to show well-formed partial gaps in images taken by the Narrow Angle Camera onboard the Cassini spacecraft. Since then, partial gaps were also resolved for the propellers Earhart and Santos-Dumont in high resolution images taken during Cassini's Ring Grazing Orbits. We analyze images of the sunlit side of Saturn's outer A ring which show the propellers Blériot and Santos-Dumont with clearly visible gaps. By fitting a Gaussian to radial brightness profiles at different azimuthal locations, we obtain the evolution of gap minimum and gap width downstream of the moonlets.

We report the following findings:

- Numerical simulations indicate that the radial separation of the partial propeller gaps is expected to be about 4 Hill radii (Spahn and Sremcevic, 2000, A&A; Seiß et al., 2005, GRL; Lewis and Stewart, 2009, Icarus). From the radial separation of the gaps in the analyzed images, we infer the Hill radii of Blériot's and Santos-Dumonts' moonlets to be about 420m and 230m, respectively.
- In order to estimate the ring viscosity parameter from the hydrodynamic model derived by Sremcevic et al (2002, MNRAS), we fit their analytic solution, which describes the azimuthal evolution of the surface density in the propeller gap region, to the data obtained from the image analysis of Blériot. We find viscosity values consistent with the parameterization given by Daisaka et al. (2001, Icarus) and compare these values to estimates from Tajeddine et al. (2017, ApJS).
- The high-resolution images of Santos-Dumont show clearly asymmetric gaps. We discuss relevant timescales for this asymmetry and interpret the azimuthal evolution in the context of a simple model of a librating moonlet (Seiler et al, 2017, ApJL).

Cosmic Dust Analyzer onboard Cassini collects material from Saturn's main rings

H.-W. **Hsu**[1], J. Schmidt[2], S. Kempf[1], F. Postberg[3], G. Moragas-Klostermeyer[4], M. Seiss[5], H. Hoffmann[5], M. Burton[6], S.Y. Ye[7], W. S. Kurth[7], M. Horanyi[1], N. Khawaja[3], F. Spahn[5], D. Schirdewahn[5], J. O'Donoghue[8], L. Moore[9], J. Cuzzi[10], G. H. Jones[11,12], and R. Srama[4].

[1]LASP, University of Colorado, Boulder, USA 3665 Discovery Dr., Boulder, CO 80303, (sean.hsu@lasp.colorado.edu), [2]University of Oulu, Finland, [3]University of Heidelberg, Germany, [4]University of Stuttgart, Germany, [5]University of Potsdam, Germany, [6]Jet Propulsion Laboratory, USA, [7]University of Iowa, USA, [8]Goddard Space Flight Center, USA, [9]Center for Space Physics, Boston University, USA, [10]NASA Ames Research Center, USA, [11]UCL Mullard Space Science Laboratory, UK, [12]The Centre for Planetary Sciences, UCL/Brikbeck, UK

The region inside of Saturn's D ring sampled during the Cassini's Grand Finale Mission is predominantly populated by grains 10s nm in radii, whose dynamics is consistent with impact ejecta from Saturn's main rings. Electromagnetic forces lead to a fast transport of tiny, charged ejecta grains (< hours), which comprises a ring mass loss pathway (100-1,000 kg/s). About 20% of them fall into Saturn, mainly in the equatorial region and the southern hemisphere, and lead to the observed H_3^+ ionospheric signature, i.e., the "Ring Rain" effect. Two grain composition types were identified from ~25% of recorded mass spectra - water ice and silicates, with a ice fraction decreasing from around 80-100% near the ring plane towards high latitudes. We find no indication of grains with pure organics or iron-oxide compositions.

Properties of aggregates and particle sizes in the C ring plateaus

Richard G. **Jerousek**[1], Joshua E. Colwell[2], Matthew M. Hedman[3], Richard G. French[4], Essam A. Marouf [5], Larry W. Esposito[6], Philip D. Nicholson[7],

1. Department of Physics and Florida Space Institute, University of Central Florida, Orlando FL 32816, (Rjerousek@gmail.com) 2. Department of Physics and Florida Space Institute, University of Central Florida, Orlando FL 32816, (Josh@ucf.edu) 3. Department of Physics, Univ. of Idaho, Moscow ID 83844 , (Mhedman@uidaho.com) 4. Department of Astronomy, Wellesley College, Wellesley, MA 02481, (Rfrench @welesley.edu) 5. Department of Electrical Engineering, San Jose State University, San José, CA 95192-0080, (Essam.marouf@sjsu.edu) 6. Laboratory for Atmospheric and Space Physics, Univ. of Colorado, Boulder CO 80309, (Larry.esposito@lasp.colorado.ed) 7. Department of Astronomy, Cornell University, Ithaca NY 14853, (Nicholso@cornell.edu)

Saturn's C ring contains distinct regions in which the normal optical depth is larger than the surrounding C ring by roughly an order of magnitude. These regions, called plateaus based on their appearance in optical depth profiles, have edges that are sharp on a scale of several km. Studies of density waves indicate that surface mass densities in the plateaus are similar to the background C ring suggesting that the larger optical depths are due to differences in particle size properties (Baillié et al. 2011, Icarus, 216, 292-308;

Hedman and Nicholson 2014, MNRAS, 444, 1369-1388). Baillié et al. (2013, Astron. J., 145, 171) studied high resolution occultations of the C ring plateaus and found a number of narrow holes where the unocculted star signal was measured over radial intervals of few tens of meters. During Cassini's ring grazing orbits, several images of the C ring plateaus, captured while the camera slewed at the same rate and direction as the particles Keplerian orbital motion, revealed long streaks aligned with the direction of the ring particles' orbital motion. We model these streaks as elongated regions of low optical depth using the bimodal optical depth, rectangular-slab model of Colwell et al. (2006, Geophys. Res. Lett., 33, L07201). We find that the average normal optical depths in these gaps are $\tau_{Gap} < 0.01$ and that the average gap width is about 10% of the spacing between them. We constrain the parameters of a simple power-law particle size distribution in the C ring plateaus by fitting optical depths measured by the Visual and Infrared Mapping Spectrometer (VIMS) at $\lambda = 2.9\mu$m, the Ultraviolet Imaging Spectrograph (UVIS) at $\lambda = 0.15\mu$m, and by the Radio Science Subsystem (RSS) at X band ($\lambda = 3.6$cm), S band ($\lambda = 13$cm), and Ka band ($\lambda = 9.4$ mm) wavelengths to those computed using the simple power-law size distribution where the number of particles in the radius range $[a,a+da]$ is $n(a)da = n_0(a/a_0)^{-q}da$, n_0 is the number of particles in $[a_0, a_0+da]$, and the minimum and maximum particle radii are a_{min} and a_{max}. We find $a_{min} \sim 1$ cm in the C ring plateaus, about twice as large as those in the background C ring while $a_{max} \sim 2$ m. The mean power law index in the plateaus is $q \sim 3.0$ compared with $q \sim 3.15$ in the background C ring. High resolution UVIS occultations also provide autocorrelation length scales that vary between the plateaus but range from several hundreds of meters to several km. Interpreting these length scales as the average spacing between gaps, particles in the C ring plateaus are arranged in only a few monolayers of the largest individual particles. We find that gaps are widely spaced with an average spacing of 0.5 km and are less than 100 m wide.

Physical properties of Saturn's rings from multi-wavelength multi-viewing-geometry extinction and scattering Cassini radio occultation observations

Essam A. **Marouf**[1], Richard G. French[2], Kwok K. Wong[1], Aseel Anabtawi[3], and Colleen McGhee-French[2], [1]San Jose State University, Electrical Engineering Department, San Jose, CA 95192-0084, essam.marouf@sjsu.edu, [2]Wellesley College, Astronomy Department, Wellesley, MA 02481-8203, rfrench@wellesley.edu, [3]Jet Propulsion Laboratory, California Institute of Technology, Pasadena, CA 91109, aseel.anabtawi@jpl.nasa.gov.

Cassini radio occultations of Saturn's Rings provided unprecedented opportunities to constrain/determine physical properties of Saturn's main rings using complementary approaches. Measurements of differential extinction of 0.94, 3.6, and 13 cm-wavelength (Ka, X-, and S-band, respectively) sinusoidal coherent radio signals transmitted by Cassini unambiguously identify presence of particles in the millimeters to decimeters size range. The X-band optical depth and the X/S and X/Ka differentials determine/constrain the minimum size, the absolute abundance, and the index of assumed power-law size distribution model of ring particles within local features as well as within broad regions, and variability of the parameters across the ring system.

Simultaneously observed scattering/diffraction by ring features resolved in spectrograms of the Doppler broadened near-forward scattered/diffracted signal constrain/determine the meter to ~20 meters (the maximum) particle sizes and their absolute abundance in ring regions free of gravitational wakes, such as the C Ring and the Cassini Division. In ring regions where gravitational wakes are abundant (the A and B Rings), both cylindrical and spherical diffraction components are identifiable in the observed near-forward scattered signal spectra. When experiment geometry and SNR allow, the width, strength, and frequency drift rate of the spectral signature of a resolved cylindrical component determine the mean wakes width, ring areac coverage fraction, and mean wakes canting angle. The spherical component constrains the size distribution of individual ring particles within and in the vicinity of the wakes. Measurements of feature oblique optical depth variability with Earth-relative longitude and ring opening angle (multi-viewing-geometry) provide self-consistency checks of inferred physical model parameters.

For particles large compared to the measurement wavelength, the radio occultation extinction and scattering/diffraction observations are interpreted based on the stochastic geometry of randomly blocked diffraction screen ring models. Solutions of demanding electromagnetic interaction problems are replaced with solutions of stochastic geometry problems. Under similar conditions, the diffraction screen approach yields identical results to traditional radiative transfer approach to solving the multiple scattering problem when the observation geometry is close to forward scattering, as is the case for radio occultations. However, the randomly blocked diffraction screen approach enjoys the advantages of being intuitive, computationally efficient, and capable of investigating arbitrarily packed thin or thick ring models.

We demonstrate the above using example results selected from a subset of Cassini radio occultation observations of interesting ring features/regions. The latter include the C Ring plateaus, features within regions B1and B2 of the B Ring, the band interior to the dynamic outer edge of the B Ring, the Cassini Division ramp, inner and outer subregions of the A Ring, and sample waves.

INMS compositional constraints on organics and other volatiles in Saturn ring rain

K. E. **Miller**[1], J. H. Waite, Jr.[1], R. Perryman[1], M. Perry[2], and C. R. Glein[1].

[1]Southwest Research Institute, San Antonio, TX, USA, 78238 [2]Johns Hopkins Applied Physics Laboratory, Laurel, MD, USA, 20723. (kmiller@swri.edu).

Introduction: During the final six Cassini orbits, the Ion and Neutral Mass Spectrometer (INMS) collected compositional data from altitudes within 2,000 km of Saturn's 1-bar pressure level, providing an unprecedented chemistry dataset. Earlier models suggested that the only neutrals present above INMS detection limits would be H_2, HD, He, and possibly H_2O [1, 2]. Instead, INMS measured signal across its full mass range (1 to 99u), including abundant organic species. Based on their altitude profiles, masses greater than 4u originate from Saturn's rings, most likely as nanoparticles. We will present compositional constraints for the ring particles entering Saturn's atmosphere.

Methods: Mass spectra were fit using a combination of INMS calibration data and NIST ionization-dissociation patterns. Our fitting routine follows [3] using a catalog of species compiled based on observations of comets [4, 5] and ice irradiation experiments [6, 7]. Species selected from the catalog are fit according to their most abundant peak, which is frequently the M^+ peak. Using a linear combination of peak fragments, a residual mass spectrum is calculated subsequent to the addition of each species. As such, the fits are degenerate and are dependent on the order in which compounds are added. To account for this, we generate multiple independent fits for each spectrum to constrain the range of possible compositions.

Results: The mass spectra indicate abundant C-bearing material in Saturn's exosphere. CH_4 and other organics are major contributors to masses above 4u. CO_2 is likely present, although its identification is complicated by the presence of isobaric C_3H_8. Signal at 28u is partially attributed to C_2H_4, but also appears to have contributions from CO or N_2.

Masses below ~70u are fit well by a combination of organics, water, ammonia, H_2, HD, CO_2, CO or N_2, He, and low abundances of S-bearing species such as H_2S. Above 70u, mass peaks may be due to fragments from large aromatic species, although unambiguous identification of the parent molecules is not possible.

Discussion: Our current fits for organics (excluding methane) yield bulk H/C ratios between 2 and 2.5, and O/C and N/C ratios that are consistent with chondritic and cometary complex organic material [8,9]. The S/C ratio is depleted relative to chondritic organics. Most N is attributed to NH_3, which may be either an indigenous species or a product of high-velocity impacts of organic nanoparticles with the spacecraft.

References: [1] Müller-Wodarg I. *et al.*, (2012) *Icarus, 221*, 481-494. [2] Koskinen T. *et al.*, (2015) *Icarus, 260*, 174-189. [3] Magee B. A. *et al.*, (2009) *Planetary and Space Science, 57*, 1895-1916. [4] Bockelée-Morvan D., (2011) *Proceedings of the International Astronomical Union, 7*, 261-274. [5] Altwegg K. *et al.*, (2017) *Monthly Notices of the Royal Astronomical Society,* S130-S141. [6] Materese C. K. *et al.*, (2015) *The Astrophysical Journal, 812*, 150. [7] Hudson R. *et al.* (University of Arizona Press, Tucson, 2008), pp. 507-523. [8] Alexander C. O. D. *et al.*, (2007) *Geochimica et Cosmochimica Acta, 71*, 4380-4403. [9] Bardyn A. *et al.*, (2017) *Monthly Notices of the Royal Astronomical Society, 469*, S712-S722.

Shaping Saturn's F ring

C. D. **Murray**[1], N. J. Cooper[1], N. O. Attree[2] and G. A. Williams[1].
[1]Astronomy Unit, Queen Mary University of London, Mile End Road, London E1 4NS, U.K. (C.D.Murray@qmul.ac.uk),
[2]Laboratoire d'Astrophysique de Marseille, Pôle de l'Étoile Site de Château-Gombert, 38, rue Frédéric Joliot-Curie, 13388 Marseille cedex 13, France.

Abstract: Images of the F ring obtained with the Cassini ISS cameras revealed an apparently multi-stranded, narrow ring with several unusual radial and longitudinal features. Here we present evidence that shows that the structure of the F ring has been determined by the combined effects of gravitational and collisional processes acting on a variety of timescales.

Gravitational perturbations at each Prometheus passage produce a series of regular, trailing, periodic structures in the ring's core, its strands and surrounding dust; the appearance of these "streamer-channel" structures depends on the orbital phase with "streamers" appearing when Prometheus is near its periapse and "channels" appearing when it is at its apoapse. Observations of "fan"-like structures in the dust near the core provide evidence for the localized perturbing effect of embedded objects, possibly formed near the edges of the channels where the perturbations from Prometheus cause a maximum in surface density combined with a minimum in relative velocity.

The multi-stranded nature of the F ring is a consequence of low velocity (~1–100 ms^{-1}) collisions between a population of ~100 small (estimated diameter ~5 km) objects and the F ring's core. The best evidence for this comes from observations made in late 2006 and early 2007 of one particular object, S/2004 S 6. It was tracked and observed to have multiple collisions with the core producing a series of initially radial "jets" of material. These radial features subsequently sheared to give the *appearance* of parallel strands although they were actually kinematic spirals. Numerical simulations of the collisional process suggest that such colliding objects are composed of loose clumps of material and that the jets are formed when they collide with similar clumps in the core. There is good evidence that the more spectacular jets are the result of collisions with objects that have already broken up. In 2016 and 2017 several objects, sometimes multiple in nature, were tracked and observed to collide with the core. The orbits and nature of these objects are

discussed. Observations of "mini-jets" (shorter, linear features observed close to the core) provide evidence for an additional population of smaller objects with lower collisional velocities (~1-10 ms^{-1}).

We suggest that this population of embedded and colliding objects could be formed when the gravitational effect of Prometheus at each synodic passage triggers the collapse of ring material. This same process can occur both in the F ring core and in a collisional strand. We also present new results based on the tracking of clumps detected in a strand seen to form in 2008 and discuss the nature of the strand itself as well as possible implications for the determination of a mass for the F ring.

Saturn's outer B ring

P. D. **Nicholson**[1], M. M. Hedman[2] and R. G French[3].
[1]Cornell University, Space Sciences Building, Ithaca NY 14853 (nicholso@astro.cornell.edu), [2]Physics Department, University of Idaho, 875 Perimeter Drive, MS 0903 Moscow ID 83844 (mhedman@uidaho.edu), [3]Astronomy Department, Wellesley College, 106 Central Street, Wellesley MA 02481 (rfrench@wellesley.edu).

As first noted in Voyager images, the outer edge of Saturn's B ring is strongly perturbed by the 2:1 inner Lindblad resonance with Mimas, with a radial amplitude of at least 50 km (Porco etal. 1984). Cassini imaging and occultation data have revealed a much more complex situation, where the resonantly-forced $m=2$ perturbation exhibits a large-amplitude libration with a period of ~5.4 yr (Hedman etal. 2010, Spitale & Porco 2010, Nicholson etal. 2014). In addition, the $m=2$ variations are accompanied by free modes with $m=1$, 3, 4 and 5 (Spitale & Porco 2010, Nicholson etal. 2014). Updated fits extend our occultation coverage to span ~2.5 libration periods, while hinting at an additional normal mode with $m=6$. Furthermore, optical depth profiles and images reveal that these radial distortions extend for at least 500 km interior to the ring's edge. Using a large set of stellar occultations obtained by the Cassini VIMS instrument, we have searched for wavelike structures in this region. In addition to indications of periodic perturbations with $m=1$ and a radial wavelength of ~110 km, we find what appears to be an axisymmetric (i.e., $m=0$) wave propagating inwards from the ring's outer edge. Supporting evidence for such a wave is found in mosaics assembled from several Cassini imaging sequences. Similar $m=0$ density waves are seen at two other resonantly-perturbed sharp ring edges (Hedman etal. 2018), suggesting that they may be driven by non-linear interactions between multiple edge modes.

Thermal infrared determinations of particle size properties and ring emissivity with Cassini CIRS

S. **Pilorz**[1], J. Colwell[2], M. Showalter[3], S. Edgington[4], J. Pearl[5], N. Altobelli[6].
[1]SETI Institute, 189 N. Bernardo, Ste 200, Mt. View, CA 94043, (spilorz@seti.org), [2]UCF, 4111 Libra Dr., Phys.Sci. Bldg. 434, Orlando, FL 32816, (josh@ucf.edu), [3] SETI Institute, 189 N. Bernardo, Ste 200, Mt. View, CA, 94043, (mshowalter@seti.org), [4] JPL, MS 230/205, 4800 Oak Grove Dr., Pasadena, CA 91109, (scottge@jpl.nasa.gov), [5]GSFC, Code 693, Greenbelt, MD 20771 (john.c.pearl@nasa.gov), [6]ESAC/ESA, Operations Dept., Directorate of Science, Madrid, Spain, (naltobelli@sciops.esa.int).

Introduction: During Cassini's mission, the primary use of the CIRS (Composite Infra-Red Spectrometer) instrument for ring studies was to catalogue the directional and temporal variations of thermal emission from the rings and its dependency on ring radius. Those results have been widely reported on.

Here we report on two different uses of the CIRS data that have only been exploited in the final stages of the mission. We report first on stellar occultation data taken in the mid-infrared, which extends the leverage of photometric analyses of the rings to constrain a range of particle sizes not previously observable from Voyager or Cassini. That analysis dovetails with a separate study of the radial dependence of ring emissivity, which is gleaned from fits to thermal infrared spectra.

Stellar occulations of the eta Carinae system were acquired in the mid infrared at 12 and 15um. A careful photometric study including diffraction effects supports Jerousek *et al*'s (1) recent conclusion that a sub-millimeter population of particles exists in the wake-gaps in the trans-Encke portion of the A ring; that a possible micron-size population of particles exists within gaps in the outer B ring; and that the mid-C ring shows evidence for a population of sub-centimeter sized particles as well. The study demonstrates that the mid-IR optical filling factor is similar to the optical filling factor at UV and near-IR wavelengths throughout most of the rings.

To derive emissivity, we use a database containing fits to every mid-far IR spectrum of the rings by a black-body spectrum multiplied by a scalar emissivity factor. These fits are extraordinarily good, and the emissivity factor contains contributions from the emissivity of the ring material itself, the optical filling factor of the rings as viewed by CIRS, and effects due to the distribution of different temperature emitters within the instrument field of view (FOV). Separating the contributions of these various effects has proven difficult.

Detecting spectral features in thermal infrared ring data has been difficult due to signal-to-noise (SNR) limitations, although Morishima *et al* (2) have reported on possible spectral features related to possible variations of grain size and the imaginary index of refraction of ice. Here we present a complimentary study, using the similarity of UV and IR optical filling factors of the rings described above to remove the filling factor of the rings from the fitted scalar emissivities.

The directional variations in UV optical thickness modeled by Colwell *et al* (3) using stellar occultation data are reduced to a database at 10km resolution that is convolved with the CIRS detector's response function to produce effective optical filling factors for every far-IR CIRS spectrum taken of the rings throughout the mission. Assuming a simple model for thermal emission, dividing the derived IR filling factor from each fitted emissivity allows a determination of 0.91+-0.02 for the average bulk emissivity of the rings. The mid-C ring shows either a high emissivity feature, or a higher optical thickness in the IR than the UV.

References: (1) Jerousek, R., *et al*, Small particles and self-gravity wakes in Saturn's rings from UVIS and VIMS stellar occultations, ICARUS, 279, 36-50, 2016; (2) Morishima, R., *et al*, Regolith grain sizes of Saturn's rings inferred from Cassini-CIRS far-infrared spectra, ICARUS, 221 (2), 888-899, 2012; (3) Colwell, J., *et al*, Cassini UVIS Stellar Occultation Observations of Saturn's Rings, Astron. Jou., 140, 1569-1578, 2010

Viscous spreading and the mass of Saturn's rings

J. **Salmon**[1], S. Charnoz[2], and A. Crida[3].
[1]Southwest Research Institute, 1050 Walnut Street – Suite 300, Boulder, CO 80302 (julien@boulder.swri). [2]Institut de Physique du Globe de Paris, 1, rue Jussieu - 75238 Paris cedex 05, France (charnoz@ipgp.fr). [3]Observatoire de la Cote d'Azur, 96 Boulevard de l'Observatoire, 06300 Nice, France (crida@oca.eu).

Introduction: Viscous spreading is a major evolutionary process for all astrophysical disks, and in particular dense planetary rings such as Saturn's rings, as it globally redistributes the disk's mass and angular momentum. This process also results in mass being lost by infall onto the planet through its inner edge, and for bringing material through the Roche limit where accretion becomes possible. The understanding of this process is highly dependent on the model used for the viscosity and thus to the physics responsible for angular momentum transport in the disk. Detailed N-body simulations have produced very accurate models for the viscosity of a particulate disk such as Saturn's rings, taking into account the collisions between particles but also the effects of the disk's self-gravity.

Numerical Model: Using a 1D hydrocode (Salmon et al. 2010), I will show that, using a viscosity that accounts for the disk's self-gravity (Daisaka et al. 2001), an initially massive self-gravitating narrow ring undergoes two successive evolutionary stages : (1) a transient rapid spreading while the disk is self-gravitating, with the formation of a density peak inward and an outer region marginally gravitationally stable, and with an emptying time-scale proportional to $1/M^2$ (M is the disk's initial mass), and (2) an asymptotic regime where the spreading rate continuously slows down as larger parts of the disk become non-self-gravitating due to the decrease of the surface density, until the disk becomes completely non-self-gravitating. At this point its evolution dramatically slows down, with an emptying time-scale proportional to 1/M, which significantly increases the disk's evolution timescale.

Implications for the Mass of Saturn's Rings: Because viscous spreading is an asymptotic process (the rings' evolution timescale keeps increasing as their mass decreases), we find that increasing the initial rings' mass does not affect the mass of the system after several billion years of evolution. We find that with an order of magnitude variation in the initial rings' mass, all systems have a mass ~0.37-0.41 Mimas masses after 4.5 Gyrs, strikingly close to the recent estimates obtained during the last orbits of Cassini (Figure 1). This would argue in favor of an old ring system, as it would be a remarkable coincidence that the rings were born recently with that particular mass. This is at odds with the apparent pristine ice composition of today's rings and the estimated meteoritic flux. I will discuss possible avenues to try and reconcile these conflicting results.

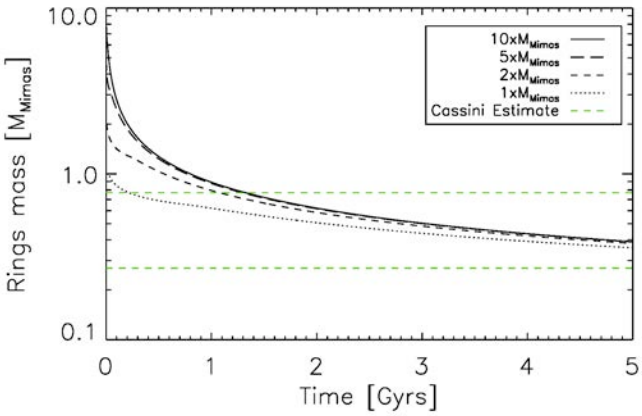

Figure 1: Evolution of the mass of Saturn's rings as a function of time due to viscous spreading, for different initial masses. After 4.5Gyrs of evolution, all systems have a similar mass of ~0.4 masses of Mimas, remarkably similar to the Cassini measurements.

Hydrodynamic simulations of asymmetric propeller structures in the Saturnian ring system

M. **Seiler**[1], M. Seiß[1], H. Hoffmann[1], and F. Spahn[1].
[1]Theoretical Physics Group, Institute of Physics and Astronomy, University of Potsdam, Karl-Liebknecht-Str. 24/25, 14476 Potsdam, Germany (michael.seiler@uni-potsdam.de)

Small sub-kilometer sized objects (called moonlets) embedded in the dense rings of Saturn cause density structures due to their gravitational interaction with the surrounding ring material which resemble a propeller, giving the structure its name in this way. The prediction of the existence of propeller structures within Saturn's rings (Spahn and Sremcevic 2000, AAP; Sremcevic et al. 2002,

MNRAS) led to their detection (Tiscareno et al. 2006, Nat; Sremcevic et al. 2007, Nat; Tiscareno et al. 2008, AJ). The recurrent observation of the large outer A ring propellers in Cassini ISS images allowed the reconstruction of their orbits. This analysis yielded that the observed propellers are deviating considerably from their expected Keplerian orbit (Tiscareno et al. 2010, ApJL; Tiscareno et al. 2018, PSG). The offset motion of the largest propeller structure –called Bleriot– can be astonishingly well composed by a three-mode harmonic fit (e.g. Seiler et al. 2017, ApJL).

The origin of this offset motion still is on debate. Two hypotheses are in discussion:

Whether the moonlet is perturbed resonantly by one or several of the large outer moons (Seiler et al. 2017, ApJL) or it is stochastically migrating (Rein & Papaloizou 2010, AAP; Pan & Chiang 2010, ApJL; Pan & Chiang 2012 ApJ; Pan et al. 2012, MNRAS; Tiscareno 2013, PLANSS).

However, the changing orbital position of the moonlet is effecting the shape of its created propeller structure. Thus, here, we perform hydrodynamic simulations to study the changes of the propeller structure due to a disk-embedded moonlet which is librating around its mean orbital position. We present results showing how the induced propeller structure changes because of the libration of the moonlet and if these changes might visible in Cassini images. Further, we apply our results to the moonlets Bleriot and Santos Dumont.

Synergy between density waves and viscous overstability in Saturn's rings

G. R. **Stewart**[1], [1]LASP, University of Colorado, 3665 Discovery Drive, Boulder, CO 80303-7820, (gstewart@lasp.colorado.edu).

Introduction: Observations of spiral density waves are the primary tool used to measure the local surface density in Saturn's rings. An outstanding puzzle is that density waves observed in the optically thick B ring imply surface densities that are comparable in magnitude to the surface densities measured in the optically thin A ring. This observation implies a nonlinear relation between ring opacity and surface density that is difficult to explain unless the interior density of ring particles in the B ring is less than a quarter of the density of solid water ice in order to prevent particles from clumping into self-gravity wakes as is observed in N-body simulations. Such high porosities would be difficult to maintain in the presence of frequent particles collisions. In Saturn's A ring, the dependence of the ring transparency on the viewing geometry as seen in stellar occultations as well as the quadrupole brightness asymmetry of reflected sunlight by the rings imply particle clumping into self-gravity wakes with a preferred pitch angle. The degree of particle clumping into self-gravity wakes in the A ring is well-matched by N-body simulations of ring particles with interior densities of about one half the density of sold water ice. So the B ring density waves seem to imply a drastic change in ring particle properties between the A and B rings. Is there an alternative explanation?

Classical Density Wave Theory: The published theory for spiral density waves in planetary rings finds that self-gravity mainly determines how the radial wavelength varies with the distance from the satellite resonance position. This conclusion rests on the assumption that pressure and viscous forces due to particle collisions in the rings are weak on the ~ 10 km scale wavelength of the density wave. However, in high optical depth rings, such as Saturn's B ring, viscous forces are known to excite overstable oscillations with wavelengths on the ~ 100 m scale due to a Hopf bifurcation in the dynamics. This scale is about one hundred times smaller than the wavelength of most density waves in Saturn's rings, so it is tempting to ignore its influence on the dispersion relation for density waves. But this reasoning is flawed. It is more accurate to think of the density wave as a large-scale modulation of the small-scale viscous overstability. The extraordinary propagation distance of the Janus 2:1 density wave in Saturn's B ring provides strong evidence that this interaction between large and small scales is important in Saturn's B ring.

Revised Density Wave Theory: We have therefore modified the Shu et al. (1985) formulation for nonlinear density waves to include nonaxisymmtric, but tightly wound viscous overstabilities. Using the multiple-scale expansion method, we have expanded the dynamics about the Hopf bifurcation point in order to study the nonlinear interactions between the small-scale overstable oscillations and the large-scale spiral density wave. Initial results of this project will be presented.

A new suite of hydrodynamical simulations of collisions between Saturn's icy mid-sized moons

L. F. **Teodoro**[1], J. N. Cuzzi[2], P. Estrada[3], M. Cuk[3], J. Kagerreis[4] and V.R. Eke[4].
[1]BAERI/NASA ARC, Moffett Field, CA 95136 (luis.f.teodoro@nasa.gov), [2]NASA ARC, Moffett Field, CA 95136 (jeffrey.cuzzi@nasa.gov), [3]SETI Institute, Mountain View, CA 94043 (paul.r.estrada@nasa.gov and mcuk@seti.org), [4]Durham University, Durham DH1 3LE, UK (jacob.kegerreis@duham.ac.uk and v.r.eke@durham.ac.uk)

At the moment, the hypothesis of a recent origin of the Saturn mid-sized satellites and its rings is under close scrutiny. Central to this discussion are the collisions between mid-sized objects (M_{body} ~ 10^{19} – 10^{21} kg) resulting from the destabilization of a previous mid-sized moon system which could potentially provide a pathway to the formation of rings and reaccreted moons ~ 100 Myr ago (Cuk et al. 2016). Exploring the latter scenario, Ryuki and Charnoz (2017) used a Smooth Particle Hydrodynamic (SPH) code to investigate the outcome of collisions between two proto-Rhea-sized bodies (M_{Rhea} ~ 10^{21} kg) at an impact velocity of 3 km s^{-1} over

several impact angles, but used only $N = 2 \times 10^5$ SPH particles, and only modeled the initial impact. Here we present our results of a new suite of SPH simulations modeling impacts between Saturn's icy mid-sized moons. This new suite of simulations utilize a new version of the parallel tree code (Warren and Salmon 1995) that has been modified to include SPH (e.g., Kagerreis et al. 2018) with the relevant Equation of State (EOS) where we track the dynamical evolution of $N = 10^6 - 10^7$ SPH particles within the simulation volumes. The initial conditions are in the frame of the target while the impactor's initial speed is set to 3 km s^{-1}. We sample the parameter space spanned by the impactor orbital angular momentum, which translates into an impact angle, and the ratio between the mass of the impactor to the mass of the target. In our suite of simulations this ratio spans from 0.055 to 1.00 which encompasses Enceladus-Rhea to Rhea-Rhea impacts. Figure 1 shows a snapshot of an impact between a Rhea- and Enceladus-like object. From these higher resolution simulations we can not only determine the number of bound objects (largest fragments) and their post-collision trajectories essential for continued modeling the dynamical evolution of the system, but also their internal states which can be used to gauge the potential for impact-driven differentiation via follow-up internal thermal evolution modeling, especially for grazing, hit-and-run-type collisions. Amongst our preliminary results, we will show for example, many more bound objects resulting from an array of collisional outcomes compared to the calculations of Ryuki and Charnoz (2017).

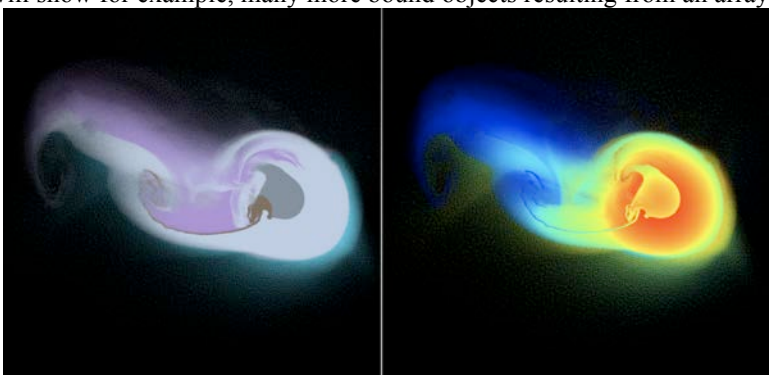

Figure 1 Snapshot of a Rhea-like object (target) and an Enceladus-like object (impactor, $M_{Enc} \sim 1.1 \times 10^{20}$ kg) a few hours after the impact. *Left panel:* provenance of the SPH particles within the simulation volume. Light and dark gray denote the Rhea-like water ice mantle and silicate core, respectively. Violet and brown represent the Enceladus-like icy mantle and silicate core, respectively. *Right panel*: logarithmic temperature field.

Radial distribution of textures in Saturn's main rings

Matthew S. **Tiscareno**[1] and the Cassini Imaging Team
[1]Carl Sagan Center for the Study of Life in the Universe, SETI Institute, 189 Bernardo Avenue #200, Mountain View CA 94043 (matt@seti.org).

During its Ring Grazing Orbits (RGO) and Grand Finale (GF), the Cassini spacecraft passed very close to the outer and inner edges (respectively) of Saturn's main rings. During these maneuvers, the Cassini ISS camera executed a series of very high-resolution images of the main rings. While hints of ring textures (clumpy, feathery, streaky, etc.) had been previously seen in some anomalously high-resolution images (e.g., [1]), the RGO/GF images constitute a complete radial survey for these structures, revealing that in many locations they occur in sharply defined radial bands that are not obviously correlated with other ring features.

In the example figure below, showing Plateau P1 and its environs in the C ring, the middle strip has been filtered by subtracting the average radial profile of the image, so that local structures and textures are more visible. The plateau itself exhibits a streaky texture, while the continuum C ring inward of the plateau exhibits a clumpy texture that is reminiscent of the troughs of spiral density waves in the A ring [1]. Between the two is a band with no discernible texture (i.e., "smooth"). Other radial texture bands, often similarly sharply defined, are seen in the
A and B rings.

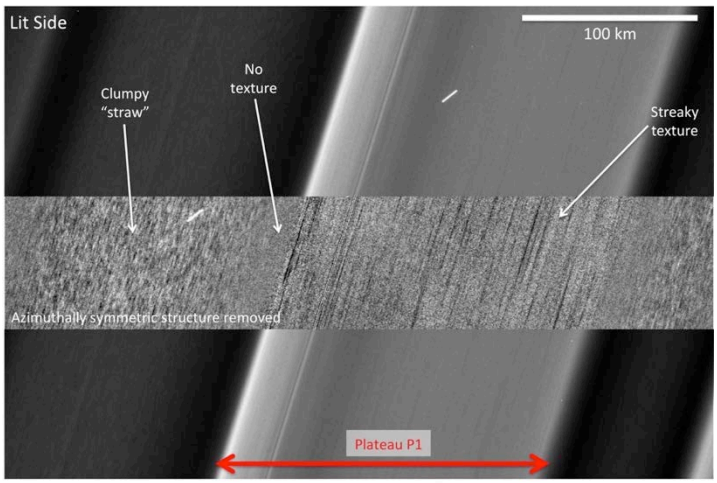

There is growing evidence that some of the more eye-catching sharply-bounded features in the main rings, such as the A ring inner edge and the C ring plateaux, are not due to changes in surface mass density (e.g., [2,3]) and thus must be due to variations in particle properties of some kind. Composition, particle size, and regolith character are candidates for various observed effects, though it is not yet clear why ring particles should be strongly sorted according to these properties. The strongly banded ring textures described here provide another window onto this process. We speculate that they may be due to different ways in which ring particles bounce off each other when they collide, and thus might be correlated to regolith character. Be that as it may, further research is greatly needed.

We will present a "geological map" of the main rings, in terms of the textures observed in the RGO/GF images, and we will discuss the implications for ring particle character and interactions.

References: [1] Porco *et al.* 2005, Science **307**, 1226. [2] Tiscareno *et al.* 2013, Icarus **224**, 201. [3] Hedman and Nicholson 2013, Astron. J. **146,** 12.

The ring atmosphere/ionosphere revisited using results from the Cassini Grand Finale Mission

Wei-Ling **Tseng**[1]; Bob Johnson[2]; O. J. Tucker[3]; Mark Perry[4]; Wing-Huen Ip[5], and Hunter Waite[6]
[1]NTNU, Taiwan; wltseng@ntnu.edu.tw; [2]UVa, USA; rej@eservices.virginia.edu; [3]NASA Goddard, USA; ojt9j1@gmail.com; [4]APL, USA; Mark.Perry@jhuapl.edu; [5]NCU, Taiwan; wingip@astro.ncu.edu.tw; [6]SwRI, USA; hwaite@swri.edu

Abstract: During the Cassini Grand Finale mission, this spacecraft, for the first time, has carried out the in-situ measurements of Saturn's upper atmosphere as well as aspects of its extended ring atmosphere. This provides critical new information for understanding the interaction between the main rings and the complete Saturnian system. The ring atmosphere has been shown to be a source of neutrals throughout the Saturn's system. This atmosphere thought to be primarily generated by the thermal desorption of the photolytic decomposition products of water ice (Johnson et al., 2006) has been shown to be a seasonal source of neutrals and plasma for Saturn's magnetosphere (Tseng et al; 2010; 2013; Christon et al., 2013; 2014). In addition, the main rings have been suggested to have a strong interaction with Saturn's atmosphere (Connerney and Waite, 1984; O'Donoghue et al., 2013; Waite et al., 2018) and ionosphere possibly through the inward diffusion of charged grains and scattered neutrals as well as by plasma exchange along field lines. The data from Cassini Grand Finale mission, now being analyzed, has already shed light on the dominant physics and chemistry in this region of Saturn's magnetosphere and exhibits surprising differences from what was seen at SOI (Elrod et al., 2012; 2014). Although recent analysis suggests that nano-sized grains were present outside the main rings (Johnson et al. 2017) at SOI, the presence of carbonaceous molecules were detected both during the proximal and F-ring orbits and have been suggested to come from the main rings (i.e., the INMS data from Waite et al., 2017; MIMI data from Mitchel et al., 2017). Using the new Cassini data as constraints we will revisit our earlier simulations of the ring atmosphere/ionosphere (Tseng et al., 2010; 2013). The goal will be to describe the temporal evolution from what was observed at SOI, an ring atmosphere dominated by O_2 and H_2, to what was seen during the Grand Finale missions, a ring atmosphere which significant sources of carbon-containing species: e.g., CO, CO_2, CH_4 (Perry et al., 2017; Waite et al., 2017; Waite et al., 2018). Of particular interest will be the relative roles of gas phase molecules and small grains in redistributing material throughout the Satunian system and into Saturn's atmosphere.

Advanced radiative transfer model for closely packed regolith surfaces

S. **Vahidinia**[1] and J. Cuzzi.[2].
[1]Bay Area Environmental Research Institute (svahidinia@yahoo.com), [2]NASA Ames Research Center (Jeffrey.Cuzzi@nasa.gov).

Introduction: We have developed a regolith radiative transfer model (RRT) for interpreting remote observations of granular surfaces applicable to microwave observations of Saturn's rings and emission spectroscopy of airless bodies. Current models make simplifying assumptions which are valid to varying, and mostly unknown degrees, and which produce results which can differ greatly in their implications about the actual surface. We will present a model that accounts for wavelength-size regolith particles which are closely packed and can be heterogeneous in composition. Intriguing results are apparent in systematic porosity variation where a volume filling factor even as small as 0.09 is "non-classical", and such effects increase with increasing filling factors.

Crater chronometers and Chronos

K. J. **Zahnle**[1], [1]NASA Ames Research Center, Moffett Field CA 94035, Kevin.J.Zahnle@NASA.gov.

Crater counts have often been pressed into service as the only available proxy clocks for Solar System worlds that have been imaged but not really understood. For outer solar sytem icy worlds the method has been problematic from the start. Under many circumstances crater counts can provide a trusty relatively chronometry, but they are only useful for absolute chronometry if the sources and historic flux of impacting bodies are known. Smith et al identified two plausible source populations, one the sun-orbiting comets (heliocentric impactors) and the other planet-orbiting (planetocentric) which are distinguished by the spatial distribution of craters they make on synchronously-rotating planets and by the size-number distribution of the craters they make. Not only are the observed craters in the Saturn system are consistent with a planetocentric source, they are inconsistent in both respects from the known population of heliocentric comets; indeed, only a few of the craters in the Saturn system can be assigned to heliocentric comets

with any degree of confidence. Planetocentric craters are useless for determining surface ages because they could have happened at any time.

A second kind of crater chronometry involves the viscous relaxation of craters. Relaxation can be used to estimate or bound the thermal gradient on a scale comparable to the depth of the crater when freshly formed. The thermal gradient maps to heat flow and hence to the thermal history of the satellite. Tethys and Dione provide an excellent case study of two extreme cases. Tethys is a true water world with negligible radioactive heating, whilst Dione has plenty of rock. Dione is also slightly bigger. The result of these contrasts is that Tethys if recently assembled would cool very quickly by conduction: it is too small to achieve the critical Rayleigh number for solid state convection, and hence the thermal inertia is small. By contrast Dione is big enough to convect upon assembly, and hence its thermal inertia encompasses all the mass of the world, and therefore it cools slowly.

Big craters on Tethys and Dione are consistent with these expectations. In particular, no big crater on Dione is unrelaxed, whilst several big craters (e.g., Penelope) on the trailing hemisphere of Tethys are extremely deep and as far as one can tell are pristinely unrelaxed. A simple model shows that it takes on the order of 100 Myrs for Tethys to cool to the point where a Penelope could form and be preserved without relaxing, which requires that Tethys be more than 100 Myrs old.

Summary: In ancient origin, the different cooling rates of Tethys and Dione was caused by radiogenic heating. Impacts are spread out over a few hundreds of millions of years. Penelope may have been a comet when impact rates were >100X what they are today. In modern origin, the difference between Tethys and Dione is solid-state convection in Dione. Penelope and other big backwards-facing craters were small moons swept up from the space between Dione and Tethys.

Saturn

Potential vorticity of Saturn's polar regions

A. **Antuñano**[1], T. del Río-Gaztelurrutia[2], A. Sánchez-Lavega[2], P.L. Read[3], and L.N. Fletcher[1]
[1] Department of Physics & Astronomy, University of Leicester, University Road, Leicester LE1 7RH, UK. (aam58@leicester.ac.uk, leigh.fletcher@leicester.ac.uk); [2] Departamento de Física Aplicada I, Escuela de Ingeniería de Bilbao, Universidad del País Vasco, Bilbao, Spain. (teresa.delrio@ehu.eus, agustin.sanchez@ehu.eus);
[3] Clarendon Laboratory, University of Oxford, Parks Road, Oxford, OX1 3PU, UK. (Peter.Read@physics.ox.ac.uk)

Introduction: Saturn's atmospheric dynamics at the upper cloud level of its polar regions (latitudes > 63º) are dominated by a fast and narrow eastward jet at 75.8º N and 70.4º S and by a strong cyclonic region at both poles. Furtheremore, Saturn's polar regions present a large variety of cloud morphologies, the most remarkable being the unique long-lived and stable Hexagon wave present at 75.8º at the north polar region . Cassini's observation of Saturn over half a saturnian year enables a detailed characterisation of the seasonal evolution of Saturn's atmosphere from the winter solstice to the summer solstice. In this work, we study of an important dynamical magnitude: the Potential Vorticity. We present zonally averaged Ertel and Quasi-geostrophic potential vorticity maps of both polar regions between 500 mbar and 1 mbar pressure for three different epochs: (i) June 2013 (early northern summer) for the north polar region, (ii) December 2008 (late southern summer) for the north and south polar regions and (iii) October 2006 (southern summer) for the south polar region. They are computed by using high resolution temperature profiles retrieved from CIRS data and wind profiles obtained from ISS data. Both potential vorticities present similar behaviours at the polar regions, displaying positive values at the north and negative in the south, indicating that the polar atmospheric dynamics is dominated by the Coriolis force at all latitudes, except at the poles where the Coriolis parameter and the relative vorticity reach the same order of magnitude. We also analyze the stability of the jets present at Saturn's polar region at the three different studied epochs by deducing meridional gradients of both potential vorticities in these regions. Finally, we compare the results of the potential vorticity and potential vorticity gradients of the different studied epochs in order to better characterize the seasonal effects on the three-dimensional atmospheric dynamics of Saturn's polar regions. An increase of the potential vorticity at the north polar region's stratosphere is observed, correlated to seasonal effects on the temperature of this region. However, no significant seasonal changes are observed at the vorticity gradients.

The eye of Saturn's north polar vortex: Surprising diversity of cloud structures observed at high spatial resolution by Cassini/VIMS during the Grand Finale

K H. Baines[1,2],L. A. Sromovsky[1], P. M. Fry[1], T. W. Momary[2], R. H. Brown[3], B. J. Buratti[2], R. N. Clark[4], P. D. Nicholson[5], and C. Sotin[2].
[1] Space Science and Engineering Center, University of Wisconsin –Madison, Madison, WI 53706; (blueskies4321@yahoo.com), (larry.sromovsky@ssec.wisc.edu), (pat.fry@ssec.wisc.edu). [2] Caltech/Jet Propulsion Laboratory, M/S 183-601, 4800 Oak Grove Drive, Pasadena CA 91109; (blueskies4321@yahoo.com), (thomas.w.momary@jpl.nasa.gov), (bonnie.j.buratti@jpl.nasa.gov). [3] Lunar and Planetary Lab and Stewart Observatory, University of Arizona, Tucson, AZ 85721; (rhb@lpl.arizona.edu). [4] Planetary Science Institute,1700 East Fort Lowell, Suite 106, Tucson, AZ; (rclark@psi.edu). [5] Cornell University, Astronomy Dept., Space Sciences Bldg., Ithaca, NY 14853; (nicholso@astro.cornell.edu).

Introduction: Near-infrared spectral maps of Saturn's north polar vortex were obtained at unprecedented spatial resolution by Cassini/VIMS under prime viewing conditions on April 26, 2017, within a month of the optimum lighting provided by the summer solstice. Two spectral images in particular, obtained from altitudes of 110,000 km and 69,600 km above the cloudtops, corresponding to VIMS pixel resolutions of 55 and 34 km, are some five times better than previous VIMS imagery. These images show small (~ 200 km across) discrete features remarkably enhanced in 3-micron absorption compared to nearby features, revealing localized ammonia clouds comprised of unusually large particles exceeding 13 microns in radius, the largest cloud particles documented during the Cassini Mission. These discrete clouds are located within the eye of the polar vortex, which otherwise is unusually clear of observable aerosols in reflected sunlight, with total 2-micron opacity < 0.04 vs > 1.0 elsewhere on the planet. The dichotomy of large-particle condensate cloud features - indicative of convective upwelling - within a large (~ 2000-km diameter) nearly aerosol-free region of downwelling characteristic of the central core of a polar vortex reveals unexpected dynamical variability not previously observed on the planet.

Polar temperature profiles of Saturn from Grand Finale UVIS stellar occultations

Z. L. **Brown**[1], T. T. Koskinen[1], R. A. West[2], A. Jouchoux[3], L. W. Esposito[3].
[1]Lunar and Planetary Laboratory, University of Arizona, 1629 E. University Blvd., Tucson, AZ 85721, USA zbrown@lpl.arizona.edu, tommi@lpl.arizona.edu, [2]Jet Propulsion Laboratory, California Institute of Technology, Pasadena, California, [3]Laboratory for Atmospheric and Space Physics, University of Colorado, Boulder, Colorado

Introduction: A global picture of Saturn's upper atmosphere is necessary to understand the dynamics of the thermosphere and surprisingly high temperatures observed there. Previous investigations of Saturn's upper atmosphere using Voyager/UVS and Cassini/UVIS data have provided insights into this region. Occultation data from these instruments are concentrated at low and mid-latitudes, with only a few observations being made poleward of 60 degrees. Additionally, secular changes in temperature and the location of the exobase make it more challenging to identify spatial trends in occultations from different points in the seasonal cycle. The 2017 Grand Finale UVIS stellar occultations overcome previous limitations and provide a vital new look at global distributions in Saturn's thermosphere. These data were taken within a six-week time period and are comprised of dozens of occultations, many of which cover polar latitudes up to 86 degrees North and South in addition to mid-latitudes. We derive temperature and density profiles from the new EUV stellar occultations with an iterative forward model approach by using the Levenberg-Marquardt technique and assuming that the atmosphere is in hydrostatic equilibrium along the local vertical direction. We report on meridional trends in temperature and density, including a first look at the polar thermosphere.

Constraints on Saturn's deep interior from seismic inversions

E. **Dederick**[1] and J. Jackiewicz[2].
[1]New Mexico State University, 1780 E University Ave, Las Cruces, NM 88003, jasonj@nmsu.edu [2]New Mexico State University, 1780 E University Ave, Las Cruces, NM 88003, ethandederick@gmail.com

Introduction: In the early 1990s it was postulated that Saturn's fundamental modes of oscillation can induce the formation of density structures within its rings. Recently, such features have been observed by Hedman & Nicholson 2013, 2014, and French et al. 2016, (and subsequent work) using optical depth data of the rings from Cassini VIMS. Each density structure corresponds to a particular mode of oscillation within Saturn. Therefore, we can use Saturn's rings as a global seismograph. Just as seismic techniques have helped constrain the interiors of the Sun and the Earth, we can utilize these techniques to constrain the interior of Saturn. We have developed the framework for performing seismic inferences of a rapidly rotating gas giant planet. Application of these seismic techniques using the ring observations allow for new constraints on both the density and sound speed of the planet's deep interior.

Saturn photochemistry and ring shadow

S. G. **Edgington**[1], S. K. Atreya[2], E. H. Wilson[3], K. H. Baines[1,6], R. A. West[2], G. J. Bjoraker[4], L. N. Fletcher[5], T. Momary[1]
[1]Jet Propulsion Laboratory, 4800 Oak Grove Drive, Mail-Stop 230-205, Pasadena, CA, 91109, (scott.g.edgington@jpl.nasa.gov), [2]University of Michigan, [3]Independent, [4]Goddard Space Flight Center, [5]University of Leicester, [6]University of Wisconsin.

Introduction: After 13 years of observing Saturn, Cassini explored for nearly a half Saturnian year. During this epoch, in addition to seasonal solar inclination changes, the ring shadow moved from covering much of the northern hemisphere to covering a large swath of the southern hemisphere. The intensity of both ultraviolet and visible sunlight penetrating through the rings varied depending on Saturn's axial tilt relative to the Sun and the optical thickness of each ring system, i.e. the rings act like semi-transparent venetian blinds. This effect magnifies the effect of axial tilt alone and acts to reduce or even turn off photochemistry and haze generation, an effect exhibited by the presence of a bluish northern atmosphere in 2004 and color change to blue in the southern hemisphere after equinox. We report on the impact of the oscillating ring shadow, seasonal axial tilt, and solar flux, on photochemistry of hydrocarbons, ammonia, and phosphine in Saturn's stratosphere and upper troposphere. The impact on the abundance of long-lived photochemical products leading to haze formation and on disequilibrium species is explored. We will also present the analysis of Cassini's CIRS, UVIS, and VIMS datasets that provide an estimate of the evolving haze content. To the above, we examine the impact of ultraviolet ring-shine (UV photons reflected by the rings) on the photochemistry of the upper atmosphere.

In parallel to the above, we will examine how the region inside Saturn's famous hexagonal jet stream evolves over time from a relatively clear atmosphere to hazy atmosphere. The hexagon jet stream acts like a barrier to transport, thus isolating Saturn's north polar region from outside influences. This will provide an addition test case of the photochemical model being applied at lower latitudes with the advantage that transport from surrounding latitudes is minimized.

The research described in this paper was carried out in part at the Jet Propulsion Laboratory, California Institute of Technology, under a contract with the National Aeronautics and Space Administration. Government sponsorship is acknowledged.

TEXES Saturn's observations in Support of the Cassini mission

T. **Fouchet**[1], T. K. Greathouse[2], S. Guerlet[3] and L. N. Fletcher[4].
[1]Observatoire de Paris, 5 Place Jules Janssen F-92195 Meudon, (thierry.fouchet@obspm.fr), [2] Southwest Research Institute, Division 15, 6220 Culebra Road, San Antonio, TX 78228, (tgreathouse@swri.edu), [3]Laboratoire de météorologie dynamique, 4 Place Jussieu, F-75005 Paris, (sandrine.guerlet@lmd.jussieu.fr), [4] University of Leicester. Department of Physics and Astronomy, University Road, Leicester LE1 7RH, UK, (leigh.fletcher@leicester.ac.uk).

Throughout the Cassini mission, the Texas Echelon Cross Echelle Spectrograph (TEXES) mounted either on the NASA InfraRed Telescope Facility (IRTF) or on the Gemini Telescope has been supporting the Cassini mission by providing exquisite spectra of Saturn with high spectral resolution (up to R~100,000) in the thermal infrared. TEXES observations especially complemented the Cassini Composite InfraRed Spectrometer (CIRS) operating in the same spectral domain. If TEXES could not compete with CIRS in terms of spatial resolution and latitudinal coverage, its higher spectral resolution (R~100,000 versus R~2,500) yielded a higher sensitivity at the thermal and compositional vertical structure as well as a higher sensitivity to trace species.

In particular, TEXES observations allowed for the first detection of propane in the atmosphere of Saturn (Greathouse et al. 2005) and the detection of the $^{15}NH_3$ isotopologue of ammonia (Fletcher et al. 2014). TEXES observations also provided a detailed picture of Saturn's thermal structure (Fouchet et al. 2016) after the onset of the encircling storm in 2010-2011, when a proeminent thermal disturbance, nick-named the beacon, completely reshaped the stratosphere in the Northern Hemisphere. The global kronian thermal structure, and some special dynamical structures, like Saturn Equaorial Oscillation, have also be followed and mapped by TEXES observations during the course of the mission, demonstrating that the community can rely on TEXES to continue the survey of Saturn's thermal structure after the end of the Cassini mission (Guerlet et al. 2017).

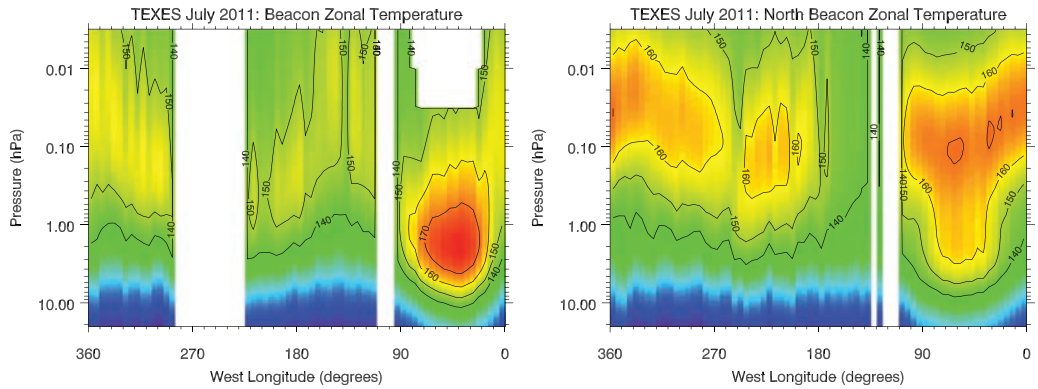

Fig. 1: Temperature cross sections retrieved for the 30–45°N meridional average (lower left), and the 40–55°N meridional average (lower right) in July 2011, when Saturn's beacon was present.

In this poster, we will present an overview of results obtained by TEXES during the Cassini mission and we will stress its importance in continuing the survey of Saturn's thermal and compositional structure.

Saturn ring seismology: Saturn's normal modes and Forcing of the slowest density waves in the C ring

A. J. **Friedson**[1], L. Cao[2], Xiaohan Xue[3], and L. Ding,[4].
[1]Jet Propulsion Laboratory/Caltech, Andrew.Friedson@jpl.nasa.gov, [2]Dept. Astronomy, Ohio State U., cao.861@osu.edu, [3]Undergraduate, California Institute of Technology, xxue@caltech.edu, [4]Dept. Physics, Massachusetts Inst. Tech., lding0410@gmail.com

Analysis of Cassini Visual and Infrared Mapping Spectrometer (VIMS) ring occultation profiles has revealed the presence of spiral density waves in Saturn's C ring that are driven by gravitational perturbations associated with the normal-mode oscillations of the planet [1, 2]. Their presence allows the C ring to serve as a sort of seismometer, since their pattern speeds reveal the frequencies of the most dominant normal modes, which are sensitive to Saturn's internal structure. The pattern speeds of a subset of these waves are observed to fall very close to that associated with the planetary rotation. The source of their excitation is unknown. Here we present

the results of a model for the source in terms of the inertial-mode and r-mode oscillations of the planet and discuss the implications of this model for the radial density stratification inside the planet. This research is supported by a grant from the NASA Solar System Workings Program. [1] Hedman, M.M. and Nicholson, P.D. 2013. AJ 146, 12. [2] Hedman, M.M. and Nicholson, P.D. 2014. MNRAS 444, 1369.

Saturn's deep atmosphere revealed by the Cassini Grand Finale gravity measurements

E. **Galanti**[1], Y. Kaspi[1] , Y. Miguel[2] , Tristan Guillot[3] , D. Durante[4] , P. Racioppa[4] , and L. Iess[4]
[1]Department of Earth and Planetary Sciences, Weizmann Institute of Science, Rehovot, Israel. (eli.galanti@weizmann.ac.il); [2]Leiden Observatory, Leiden University, The Netherlands; [3]Observatoire de la Cote d'Azur, Nice, France; [4]Dipartimento di Ingegneria Meccanica e Aerospaziale, Sapienza Università di Roma, Rome, Italy

The Cassini Grand Finale gravity measurements, performed during May-July 2017, can shed light upon a longstanding question - what is the nature of the flow beneath Saturn's clouds? Answering this question has important implications not only for the atmospheric dynamics, but also for the interpretation of the interior density structure, composition, magnetic field and core mass. Strong zonal winds exist at the observed cloud-level, forming a wide superrotating region with winds of nearly 500 m/s at the equatorial region, and smaller scale jets extending to high latitudes, but whether these are superficial atmospheric structures or whether they extend deeply into the interior is unknown.

While the low-degree even gravity harmonics, as measured by Cassini, are dominated by the shape and density structure of the planet, the higher harmonics are found to be strongly influenced by differential flow and can be used to decipher its structure. In addition, the odd harmonics can be used for this purpose as they reflect solely the flow. Using Saturn's cloud-level winds and a thermal wind balance we relate the flow to the gravity harmonics. Then an adjoint based inverse model is used to determine the flow structure that gives the best fit between the model calculated gravity harmonics and those measured by Cassini. We present a first-order estimate of the flow structure based on the Cassini measurements, and discuss its implications to the planet's interior structure.

Saturn's stratospheric dynamics and chemistry revealed by CIRS limb observations

S. **Guerlet**[1], T. Fouchet[2], M. Sylvestre[3], A. A. Simon[4], B. Hesman[4], G. Bjoraker[4], and F. M. Flasar[4].
[1]Laboratoire de météorologie dynamique. 4 Place Jussieu, F-75005 Paris, (sandrine.guerlet@lmd.jussieu.fr) [2]Observatoire de Paris, 5 Place Jules Janssen F-92195 Meudon, (thierry.fouchet@obspm.fr), [3]University of Bristol, School of Earth Sciences, Queen's Road, Bristol, BS8 1 RJ, UK, (melody.sylvestre@bristol.ac.uk), [4] NASA Goddard Space Flight Center, 8800 Greenbelt Road, Greenbelt, MD 20771, (f.m.flasar@nasa.gov).

Throughout the Cassini mission, the Cassini Composite InfraRed Spectrometer (CIRS) has acquired thousands of thermal infrared spectra in limb viewing geometry that we analyzed to map the temperature and the meridional distribution of five hydrocarbons from the lower to the upper stratosphere (10 mbar – 10 microbar). The exceptional longevity of the Cassini mission enabled us to uniquely investigate the seasonal and temporal changes over almost half a Saturn year to reveal the dynamical and chemical processes that govern Saturn's stratosphere.

In the equatorial regions, we have discovered an Equatorial Oscillation (Fouchet et al. 2008, Guerlet et al. 2011, 2018) where the mechanical forcing by upward propagating waves induces temperature anomalies of up to ±20K in the thermal structure and ±150 m/s in the zonal wind field. Our studies show that this oscillation has a temporal period of about 15 terrestrial years and resembles the terrestrial Quasi Biennal Oscillation (QBO) that affects Earth's stratosphere. Outside the equatorial regions, our survey of the thermal structure (Guerlet et al., 2009; Sylvestre et al., 2015) reveals that the seasonal warming and cooling trends observed by CIRS are, to first order, consistent with the predictions from a radiative equilibrium climate model (Guerlet et al., 2014).. One notable exception is that the region under the ring's shadow is found warmer than expected from the radiative model, both in 2005 and 2015.

We also studied the spatial distribution of hydrocarbons, by-products of the methane photochemistry, which also undergoes significant seasonal change in the upper stratosphere (Guerlet et al., 2009, 2010; Sylvestre et al., 2015). In 2005, a local maximum of hydrocarbons was observed at 20°-30°N, at odds with the low photochemical production in this region (under the ring's shadow at that time). Together with the high temperature anomaly, we had interpreted this result as the signature of a downwelling branch of the meridional circulation. In 2015, not only has this local maximum vanished, but a new maximum was building in the opposite hemisphere, at 15°-25°S. We suggest that the hydrocarbon and temperature anomalies observed in 2015 in Saturn's upper stratosphere reflects the reversal of a seasonal circulation cell.

Finally, in the Southern Polar Region we detected Stratospheric benzene and hydrocarbon aerosols, mostly likely produced by auroral chemistry (Guerlet et al. 2015). The spectral signatures of Saturn's aerosols most strikingly mimic the signatures of Titan's aerosols. We assigned the detected vibration modes to aromatic and aliphatic hydrocarbons. The aerosol mass loading was estimated to lie in the range $1-4\times10^{-5}$ g cm^{-2} , an order of magnitude less than on Jupiter, which is consistent with the order of magnitude

weaker auroral power at Saturn. Nevertheless, we demonstrated that the radiative effects of aerosols is important in the polar regions and could explain the large seasonal temperature variations observed in these regions.

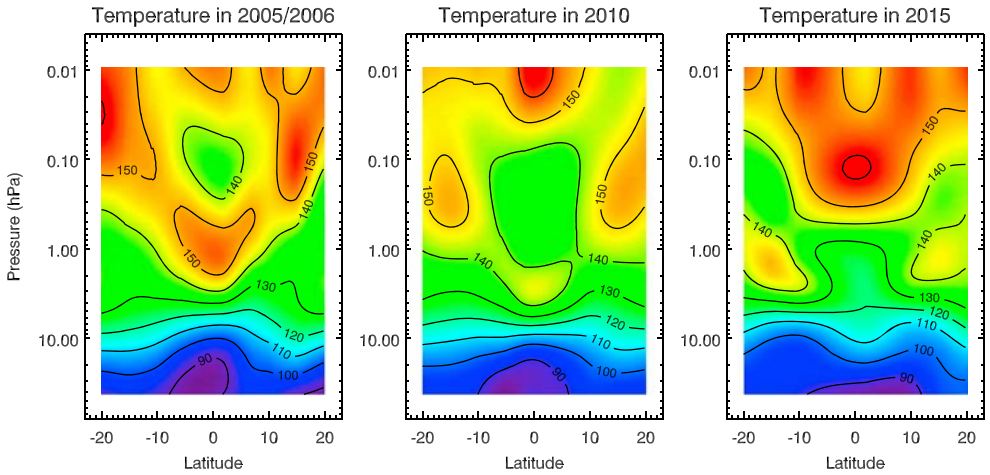

Fig. 1 Latitude-pressure cross section of the temperature (in kelvin) obtained from Cassini/CIRS limb data acquired in 2005–2006, 2010 and 2015.

A Refined Measurement of Saturn's Gravity Environment.

L. **Iess**[1] , D. Durante[1], P. Racioppa[1], and M. Mariani[1]
[1]Dipartimento di Ingegneria Meccanica e Aerospaziale, Sapienza Università di Roma, via Eudossiana 18, 00184 Rome, Italy (luciano.iess@uniroma1.it); (daniele.durante@uniroma1.it); (paolo.racioppa@uniroma1.it); (mircojunior.mariani@uniroma1.it)

Range rate measurements of Cassini acquired at the antennas of NASA's Deep Space Network and ESA's ESTRACK antennas during the Grand Finale Orbits (GFO) were successfully used to estimate the zonal field of Saturn till degree 10 and the mass of the B-ring. The gravity field determined by Cassini reveals a planet with many surprising features.

Surprisingly, and differently from what was found on Jupiter by Juno, Saturn's gravity shows residual, unexplained, accelerations (at the level of 4×10^{-7} m/s^2) that affected the motion of Cassini and were detected by the Doppler tracking system. These accelerations were absorbed using three different models: stochastic accelerations, acoustic normal modes (zonal component only), and a static tesseral field. As the nature of the unexplained accelerations is unknown at the time of this writing, the stochastic model is preferred. A tesseral field must originate from deep-seated density anomalies in the region of uniform rotation in order to be seen as a static field over the two months of the gravity measurements. This cannot be excluded, although the magnitude of the accelerations and the large degree of the required field (from 8x8 to 12x12, depending on the assumed rotation period) militates against this hypothesis. In spite of these unexpected features, the solution for the zonal field and the ring mass, relevant for interpretation, is stable and all parameters are sufficiently well determined.

We present a refined estimate of the gravity environment experienced by Cassini during the GFO, and offer the results of an extensive perturbative analysis aimed at testing the robustness of the solution.

Saturn: Cassini explores the giant planet

A. P. **Ingersoll**
Caltech mail 150-21, 1200 E. California Blvd., Pasadena, CA, USA, (api@gps.caltech.edu).

Before Cassini, we knew that Saturn had a higher proportion of heavy elements than Jupiter based partly on its bulk density and partly on the CH_4/H_2 ratio. We knew that Saturn's winds were 2-3 times stronger than Jupiter's despite its greater distance from the Sun. And we knew that Saturn's internal power was a greater fraction of its total radiated power than Jupiter's, even though Saturn should have lost its internal heat faster because of its lower mass. We thought we knew Saturn's rotation rate, and we thought we knew its atmospheric He/H ratio. These puzzling bits of information and the desire to compare the two gas giants from orbit, made the planet itself an important objective of the Cassini mission.

On approach to Saturn, Cassini took beautiful images that inadvertently illustrated seasonal change and hydrocarbon chemistry. The season was southern summer, and the southern atmosphere was smoggy - a brownish-orange color. The rings blocked most of Cassini's view of the north, but a thin crescent was visible above the rings and it was clear and blue. After orbit insertion, Cassini measured the gases in Saturn's atmosphere – the elements C, O, N, S, P, As, and Ge in combination with H, and others including CO,

C_2H_2, and C_2H_6, as well as H_2 in its two states – atoms spinning parallel and antiparallel. Most of these compounds are tracers of vertical and latitudinal motion because their chemistry is affected by temperature, pressure and exposure to sunlight.

Cassini inferred the winds from motions of the clouds and from horizontal gradients of temperature. Except at the equator, the dominant east-west winds – the zonal jets – hadn't changed since Voyager times. Cassini confirmed that the zonal jets at the equator oscillate in speed as part of a 15-year cycle that resembles the quasi-biennial oscillation on Earth. Cassini showed that eddies are pumping energy into the zonal jets. Cassini re-discovered the hexagon at 75°N, which was discovered by Voyager in 1980. Cassini discovered lightning storms, but there were only 1 or 2 on the planet at any one time. And Cassini discovered hurricane-like cyclones, but only one at each pole and none anywhere else. Finally, Cassini was lucky enough to be present during one of Saturn's giant 30-year storms, and was able to probe its inner workings and lingering effects at the surface.

Cassini narrowed the limit on misalignment between Saturn's magnetic field and its rotation axis. This probably means the field can't be used to determine the internal rotation rate, but it opens a new mystery of why the field should be so precisely aligned. Cassini discovered oscillations in the rings that matched the periods of the planet and its internal normal modes. The oscillations allow one to probe Saturn's internal structure and its rotation. Although Cassini took precise occultation measurements to determine the helium abundance, unknown winds and temperature gradients have complicated the data analysis, which has yet to yield a definitive answer.

Saturn in Lyman α: A comparison of Cassini and Voyager observations

T. T. **Koskinen**[1], R. V. Yelle[1] and G. M. Holsclaw[2].
[1]Lunar and Planetary Laboratory, University of Arizona, 1629 E University Blvd., Tucson, AZ 85721, (tommi@lpl.arizona.edu),
[2]Laboratory for Atmospheric and Space Physics, University of Colorado, 1234 Innovation Dr, Boulder, CO 80303.

Introduction: Lyman-α dayglow emissions from Saturn's atmosphere are believed to be dominated by resonant scattering of solar Lyman-α radiation by atomic hydrogen in the thermosphere. Models of this process, however, have struggled to explain the relatively high brightness values of about 3-4 kR observed by the Voyager/UVS instruments, leading to suggestions that additional sources such as electron and proton collisions contribute to the observed emissions. Alternatively, the abundance of atomic hydrogen in the upper atmosphere may have been higher than expected based on Voyager occultation results. The few published values from Cassini/UVIS observations imply lower brightness than the Voyager observations but a systematic comparison with similar observing geometries and an analysis of solar cycle variations is currently missing. We will present results on Lyman-α scans from the Cassini/UVIS archive, which contains observations that span the duration of the Cassini mission. Our results are based on the latest available calibration developed for the UVIS instrument. The observations constrain the variation of Saturn's Lyman-α brightness with solar activity, secular changes in atmospheric structure and reveal hints of the ring atmosphere that may have consequences on the influx of matter from the rings to Saturn's atmosphere.

Determination of tidal parameters at multiple frequencies within Saturn from ground and space data

V. **Lainey**[1,2], N. Cooper[2], C. Murray[2], R. Park[1] and the ENCELADE team.
[1]Jet Propulsion Laboratory, California Institute of Technology, 4800 Oak Grove Dr, Pasadena, CA 91109
(valery.j.lainey@jpl.nasa.gov; Ryan.S.Park@jpl.nasa.gov); [2]IMCCE, Paris Observatory; [3]Queen Mary University of London Affiliation, Mile End Rd, London E1 4NS, Royaume-Uni (n.cooper@*qmul*.ac.uk; *c.d.murray@qmul*.ac.uk)

Introduction: Tidal deformation and dissipation of planets and satellites are fundamental mechanisms for driving their orbital and thermal evolutions. Features like orbital resonance, intense volcanic activity and resurfacing appear to be associated with tidal dynamics. Moreover, tidal effects play a significant role in sustaining a liquid ocean inside of icy bodies over long time scale. There exist many tidal models available for giant planets today, but still poorly constrained by data. In particular, the sensitivity in frequency of tidal parameters, a critical point for characterizing tidal mechanism, is barely constrained by astrometry and satellite geodesy. In the absence of such measurements, our knowledge of the interior structure and evolving processes in gas giants remains rather limited, preventing an accurate assessment of past evolution and formation of the planetary and exoplanetary systems. Here we will provide the first results, derived from observations, on the tidal frequency sensitivity of Love numbers within Saturn. Consequences on tidal mechanisms arising in the interior of the planet, as well as an upcoming strategy to assess frequency variations of Saturn's tidal parameter *Q,* will be discussed.

Ring seismology as a probe of Saturn's rotation

C. R. **Mankovich**[1], M. S. Marley[2], J. J. Fortney[1], N. Movshovitz[1], and D. P. Thorngren[1].
[1]University of California Santa Cruz Department of Astronomy & Astrophysics, 1156 High St., Santa Cruz, CA 95064;
(cmankovich@ucsc.edu, jfortney@ucsc.edu, nmovshov@gmail.com, dpthorngren@gmail.com), [2]NASA Ames Research Center
(Moffett Blvd, Mountain View, CA 94035; (mark.s.marley@nasa.gov).

Saturn's nonradial oscillations perturb the orbits of ring particles. The C ring is fortuitous in that it spans several resonances with Saturn's fundamental acoustic (f-) modes, and its moderate optical depth allows the characterization of wave features using stellar occultations. The growing set of C-ring waves with precise pattern frequencies and azimuthal order m measured from Cassini stellar occultations (Hedman & Nicholson 2013, 2014; French et al. 2016) provides new constraints on Saturn's internal structure, with the potential to aid in resolving long-standing questions about the planet's distribution of helium and heavier elements, its means of internal energy transport, and its rotation state.

We construct Saturn interior models and calculate mode eigenfrequencies, mapping the planet mode frequencies to resonant locations in the rings to compare with the locations of observed spiral density and vertical bending waves in the C ring. While spiral density waves at low azimuthal order (m=2-3) appear strongly affected by resonant coupling between the f-modes and deep g-modes (Fuller 2014), the locations of waves with higher azimuthal order can be fit with a spectrum of pure f-modes for Saturn models with adiabatic envelopes and realistic equations of state. Notably, several newly observed density waves and bending waves (Hedman et al., in preparation) align with outer Lindblad and outer vertical resonances for non-sectoral (m!=l) Saturn f-modes of relatively high angular degree, and we present normal mode identifications for these waves. We assess the range of resonance locations in the C and D rings allowed for the spectrum of f-modes given gravity field constraints, point to other resonance locations that should experience strong forcing, and use the full set of observed waves to estimate Saturn's bulk rotation rate.

Saturn density profiles from gravity data with minimal assumptions

N. **Movshovitz**[1], J. Fortney[1], D. Thorngren[1] and C. Mankovich[1].
[1]Astronomy and Astrophysics, University of California, Santa Cruz, Santa Cruz CA. (nmovshov@gmail.com)

Abstract: The external gravity field of a planetary body is determined by the distribution of mass in its interior. Therefore, a measurement of the external field, properly interpreted, tells us about the interior density profile, $\rho(r)$, which in turn can be used to constrain the composition in the interior and thereby learn about the formation mechanism of the planet. Recently very high precision measurements of Saturn's gravity have been made by the radio science instrument on Cassini during its Grand Finale orbits.

The measured gravity coefficients come with an associated uncertainty. The process of computing gravity coefficients from a given density profile and rotation rate introduces further uncertainty, the result of unavoidable approximations and discretization. The question of how best to account for this uncertainty is not trivial. In essentially all prior work on matching models to gravity field data inferences about planetary structure have rested on assumptions regarding the imperfectly known H/He equation of state and the assumption of an adiabatic interior. Here we wish to vastly expand the phase space of such calculations.

We present a framework for describing all the possible interior density structures of a Jovian planet constrained by a given set of gravity coefficients and their associated uncertainties. Our approach is statistical. We produce a random sample of $\rho(a)$ curves drawn from the underlying (and unknown) probability distribution of all curves, where ρ is the density on an interior level surface with equatorial radius a. Since the resulting set of density curves is a random sample, that is, curves appear with frequency proportional to the likelihood of their being consistent with the measured gravity, we can compute probability distributions for any quantity that is a function of ρ, such as central pressure, oblateness, core mass and radius, etc. With the additional information from theoretical equations of state we can also derive quantities relating to composition, such as the heavy element total mass and distribution. Our approach is also Bayesian, in that it can utilize prior assumptions about the planet's interior, as necessary, without being overly constrained by them.

We apply this approach to produce a sample of Saturn interior models based on recently published gravity data from Grand Finale orbits and discuss their implications.

A survey of slowly moving thermal waves in Saturn from Cassini CIRS and ground-based thermal observations from 2003 to 2017

Glenn S **Orton**[1], Leigh N Fletcher[2], James Sinclair[3], F Michael Flasar[4], Richard K. Achterberg[5], Padma Yanamandra-Fisher[6]
1. MS183-501, Jet Propulsion Laboratory, California institute of Technology, Pasadena, CA 91109; (glenn.orton@jpl.nasa.gov), 2. S7, Physics and Astronomy Building, University of Leicester, University Road, Leicester, LE1 7RH, UK; (leigh.fletcher@le.ac.uk), 3. MS183-501, Jet Propulsion Laboratory, California institute of Technology, Pasadena, CA 91109; (james.sinclair@jpl.nasa.gov), 4. Mail Code 693, NASA Goddard Space Flight Center, Greenbelt, MD 20771; (f.m.flasar@nasa.gov), 5. University of Maryland; Mail Code 693, NASA Goddard Space Flight Center, Greenbelt, MD,; (richard.k.achterberg@nasa.gov), 6. Space Science Institute, 4750 Walnut St, #205, Boulder, CO 80301; (padmayf@gmail.com).

Hemispherical maps of Saturn's atmosphere made both by Cassini's Composite Infrared Spectrometer (CIRS, 7-1000 μm) and ground-based mid-infrared observations (7-25 μm) were surveyed for the presence and properties of zonal thermal waves and their variability in time. The most inclusive CIRS surveys, FIRMAPs (15 cm^{-1} spectral resolution), covered the planet from the equator to

either north or south pole, sweeping through the latitude range while the planet rotated beneath over its ~10-hour rotation. Additional measurements were made by ground-based observations at the Infrared Telescope Facility using the MIRSI instrument, the Very Large Telescope using VISIR and the Subaru Telescope using COMICS. We sampled spectral ranges dominated both by upper-tropospheric emission (80-200 mbar) and by stratospheric emission (0.5-3 mbar). We examined data that were taken from 2003 through the end of the Cassini mission in 2017.

Several types of slowly moving zonal thermal waves were detected: (1) meridionally broad wavenumber-1 through -3 oscillations, (2) equatorial waves, some of which extend northward to mid-latitudes, (3) prominent wavenumber-12 oscillations in the southern hemisphere, which also have components of wavenumbers 1 through 3 and extend over 15°-35°S latitude, (4) mid-latitude wavenumber > 2 oscillations in both hemispheres with variable time dependence and morphology, and (5) discrete low-latitude tropospheric features. The prominent southern-hemisphere waves appear to have distinct periods of maximum intensity around 2003-2004 from ground-based observations and 2008-2009 from CIRS FIRMAPs. They appear in long "trains" that never covered more than 180° in longitude, unlike slowly moving waves in Jupiter. These waves are easily detectable in both the stratosphere, where the other types of waves are prominent, but also in the troposphere with no detectable phase shift in longitude. These waves were also sufficiently coherent to track a mean phase speed, which is about 0.5° per day, retrograde. After 2009, wavenumber-1 oscillations in the northern hemisphere are joined by higher-wavenumber oscillations. A local temperature maximum is seen around 2010-2011, then another in 2016-2017. Further ground-based observations are required to determine whether the amplitude of northern-hemisphere waves is influenced by seasonally dependent insolation.

Monitoring Saturn's upper atmosphere density variations and determination of the Saturnian He mixing ratio using helium 584 Å airglow

C. D. **Parkinson**[1], T. Koskinen[2], and L. W. Esposito[3]
[1]CLaSP, University of Michigan, 2455 Hayward St., Ann Arbor, MI, 48109 (theshire@umich.edu)
2LPL/University of Arizona, Kuiper 413, 1629 E University Blvd, Tucson, AZ, 85721 (tommi@lpl.arizona.edu)
[3]LASP/University of Colorado, 3665 Discovery Drive, Boulder, CO, 80303 (Larry.Esposito@lasp.colorado.edu)

The atmosphere of Saturn is mainly composed of H_2 and neutral atomic helium. The study of He 584 Å brightnesses is interesting as the EUV (Extreme UltraViolet) planetary airglow have the potential to yield useful information about mixing and other important parameters in its thermosphere. Resonance scattering of sunlight by He atoms is the principal source of the planetary emission of He 585 Å. The helium is embedded in an absorbing atmosphere of H_2 and since it is heavier than the background atmosphere, it's concentration falls off rapidly above the homopause. The scattering region (i.e. where the absorption optical depth in H_2 is less than 1) generally lies well above the homopause. As the eddy diffusion coefficient, K_z, increases in the middle atmosphere, more helium is mixed into the scattering region and thus the reflected intensity increases.

Specifically, He emissions come from above the homopause where optical depth τ=1 in H_2 and therefore the interpretation depends mainly on two parameters: He mixing ratio of the lower atmosphere and eddy mixing profile, K_z. The occultations of Koskinen et al. (2015) give K_z with an accuracy that has never been possible before and the combination of these occultations and airglow analyses can therefore can provide estimates of the mixing ratio in the lower atmosphere.

Using Cassini UVIS data and powerful modeling and analysis techniques, we can address longstanding questions regarding the He mixing ratio in Saturn's atmosphere and upper atmosphere density variations using the observed He 584Å airglow. We discuss results of work to determine the Saturnian mixing ratio of He and constrain dynamics in the upper atmosphere of Saturn with particular attention to the Grand Finale end of mission analyses.

Characteristics of the neutral influx from Saturn's rings

M. E. **Perry**[1], J. H. Waite, Jr.[2], D. G. Mitchell[1], K. E. Miller[2], T. E. Cravens[3], R. S. Perryman[2], L. Moore[4], R. V. Yelle[5], H.-W. Hsu[6], M. M. Hedman[7], J. N. Cuzzi[8], D. F. Strobel[9], O. Q. Hamil[3], L. J. Paxton[1], B. D. Teolis[2], R. L. McNutt, Jr.[1]
[1]Johns Hopkins Applied Physics Laboratory, 11100 Johns Hopkins Road, Laurel, MD. (Mark.Perry@jhuapl.edu). [2]Southwest Research Institute, San Antonio, TX. [3]Department of Physics and Astronomy, University of Kansas, Lawrence, KS. [4]Center for Space Physics, Boston University, Boston, MA. [5]Department of Planetary Sciences, University of Arizona, Tucson, AZ. [6]LASP, University of Colorado Boulder, CO. [7]University of Idaho, Moscow ID.
[8]Ames Research Center, NASA. [9]Johns Hopkins University, Baltimore, MD.

Introduction: Although nanoparticles may be ubiquitous throughout Saturn's rings, they have not been studied with the thoroughness of their larger siblings. These particles, ranging from clusters of a few molecules to radii of 5 nanometers and masses of 10^5 u, are smaller than the wavelength of a UV photon and are not detected using remote observations. During Cassini's final months,

three of Cassini's *in situ* instruments made the first measurements of nanoparticles in the region between Saturn and its inner ring. Here, we describe material measured by Cassini's Ion and Neutral Mass Spectrometer (INMS) in three different altitude bands, from 1,300 to 4,000 km. The INMS data are sufficient to characterize the altitude and latitudinal distributions in the vicinity of Saturn's equator. The densities, latitude distributions, and variations describe a global-integrated flux of $(2\text{-}20)\times10^4$ kg/s that is dominated by material $<10^4$ u with radii <2 nm. The influx is a mixture of molecules and particles, with a source that is likely linked to the D68 ringlet on the inner edge of the D ring. The enormity of the mass flux denotes its temporary nature and—combined with the observed variability—suggests that the vast majority of this flux is due to a recent event, possibly the density concentration that appeared in the D68 ringlet in 2015. The predominance of hydrocarbons is unexpected and awaits a comprehensive explanation. INMS data do not eliminate silicates and ferrous components of the influx material, but their presence would further increase the mass loss of the rings.

The composition of Saturn's upper atmosphere from Cassini/INMS measurements

J. **Serigano**[1], R.V. Yelle[2], T.T. Koskinen[2], S.M. Hörst[1] , the INMS team.
[1]Department of Earth and Planetary Sciences, Johns Hopkins University, 3400 N. Charles Street, Baltimore, MD 21218 (jserigano4@jhu.edu), [2]Lunar and Planetary Laboratory, University of Arizona, 1629 E University Blvd, Tucson, AZ 85721.

Introduction: In September 2017, the Cassini spacecraft entered Saturn's atmosphere, providing new insights into the composition and structure of the planet's upper atmosphere. Prior to atmospheric entry, Cassini executed a series of 22 highly inclined orbits through the previously unexplored region between Saturn and its rings, yielding the first ever direct sampling of Saturn's atmosphere. Data returned from the Ion and Neutral Mass Spectrometer (INMS) aboard Cassini have already revealed surprising results, including an unexpected contribution of molecules into Saturn's upper atmosphere from the ring system and the presence of complex hydrocarbons in Saturn's atmosphere. We present here preliminary results of the composition of Saturn's upper atmosphere from INMS measurements during Cassini's final orbits. The upper atmospheric density and the relative abundances of Saturn's major constituents, as well as the unexpected complexities of Saturn's mass spectrum, will be discussed.

A concept for a future entry probe mission to Saturn – The Saturn PRobe Interior and aTmosphere Explorer (SPRITE)

Amy **Simon**[1], Don Banfield[2], David H Atkinson[3]
[1]NASA Goddard Space Flight Center, 8800 Greenbelt Rd, code 690 Greenbelt, MD 20771, (amy.simon@nasa.gov), [2]Department of Astronomy, 420 Space Sciences Building, Cornell University, Ithaca, NY 14853, (banfield@astro.cornell.edu), [3]Jet Propulsion Laboratory, California Institute of Technology, 4800 Oak Grove Drive
Pasadena, CA 91109, (David.H.Atkinson@jpl.nasa.gov).

Introduction: To improve models of Solar System formation, as well as to provide an improved context for exoplanet systems, measurements of the atmospheric composition and structure, and processes within the atmospheres of the giant planets are needed. In particular, measurements of the abundances of noble gases and isotope ratios of hydrogen, carbon, oxygen, and nitrogen, as well as the thermal profile, cloud structure, and dynamics of Saturn are necessary. The SPRITE (Saturn PRobe Interior and aTmosphere Explorer) entry probe mission concept addresses these important science priorities and would provide ground truth for remote sensing to improve understanding of Saturn's interior structure and composition, and (by proxy) those of extrasolar giant planets.

The SPRITE Mission concept consists of a Carrier Relay Spacecraft (CRSC) and an entry probe descending to at least ten bars in about 90 minutes. The primary scientific instrument payload of the SPRITE probe would comprise two spectrometers – a Quadrupole Mass Spectrometer and a Tunable Laser Spectrometer, and an Atmosphere Structure Instrument including a simple nephelometer and a Doppler Wind Experiment for measuring and characterizing the thermal, cloud, and dynamical structure of Saturn's troposphere. The Atmospheric Structure Instrument also includes accelerometers to measure entry accelerations from which the probe entry trajectory and descent location would be reconstructed and from which the thermal structure of the upper atmosphere would be characterized. The solar powered CRSC carries a Multi-Channel Imager for pre-entry imaging of the probe entry location, and to provide local and global context imaging for the probe measurements.

SPRITE would follow an Earth-Venus-Earth-Earth gravity assist trajectory to reach Saturn in ten years. The SPRITE probe would enter Saturn's atmosphere at a relative velocity of ~27 km/s, experiencing a peak heat flux near 3000 W/cm^2 and a peak deceleration up to 45 g's. The aeroshell would be released above the tropopause, initiating the descent science sequence and permitting up to 2 hours for the probe to reach and pass through 10 bars. To ensure low risk data return, the descent probe design is fully-redundant with a dual-channel telecommunication system powered by primary batteries. After the probe science data is collected by the flyby Carrier Relay Spacecraft, the probe data and Carrier imaging data would be downlinked to Earth multiple times through the Deep Space Network

In the context of giant planet science provided by the Galileo, Juno, and Cassini missions to Jupiter and Saturn, a small, relatively shallow Saturn probe would serve to test competing theories of solar system and giant planet origin, and chemical and dynamical evolution. The SPRITE mission would measure abundances and isotopic ratios of key atmospheric constituents, and atmospheric structure including pressures, temperatures, dynamics, and cloud locations and properties not accessible by remote sensing, also placing the data from those missions into better context.

Additional Information: Predecisional information, for planning and discussion only.

Saturn's south polar cloud structure inferred from 2006 Cassini VIMS spectra

L. A. **Sromovsky**[1], K. H. Baines[2], and P. M. Fry[3]
[1]Space Science and Engineering Center, University of Wisconsin – Madison, Madison, WI 53706,
[1](larry.sromovsky@ssec.wisc.edu), [2](blueskies4321@yahoo.com), [3](pat.fry@ssec.wisc.edu).

Introduction: According to the equilibrium cloud condensation model of Weidenschilling and Lewis (1973, Icarus 20, 4654-476) the top condensation cloud on Saturn should be composed of ammonia ice particles and extend upward from a cloud base near 1.7 bars (Atreya and Wong 2005, Space Sci. Rev. 116, 121-136). However, this NH_3 cloud layer is almost never observed from above because most of Saturn is covered by an overlying thick cloud layer of unknown composition and substantial optical depth, which is typically around 6 at a wavelength of 2 μm, and 3-4 even in the "cleared" wake region of the Great Storm of 2010-2011 (Sromovsky et al. 2016, Icarus 276, 141-162). Spectroscopic evidence of the underlying ammonia ice cloud (its strong 3-μm absorption signature) had so far been seen on Saturn only in association with lightning storms, including the Great Storm of 2010-2011 (Sromovsky et al. 2013, Icarus 226, 402-418), near 35°N planetocentric latitude, and much smaller storms located near 36°S, in the Storm Alley region (Baines et al. 2009, Planet. & Space Sci. 57, 1650-1658), presumably because these storms convected the ammonia ice to high altitudes. The ammonia signature was dramatic in the head of the Great Storm, but more subdued in the Storm Alley clouds, which is consistent with ammonia ice reaching into but not fully penetrating the upper cloud in the latter case (Sromovsky et al. 2018, Icarus 302, 360-385).

South Polar Results: In 2006, Visual and Infrared Mapping Spectrometer 0.8-5.1 μm spectral imaging observations revealed bright clouds with 3-μm absorption features in the south polar region, a surprising result because there is no associated lighting that would indicate deep convection in that region. Our radiation transfer modeling of the spectra of these features yields good fits with a stacked structure consisting of a thin stratospheric haze, a physically thin and optically thin ($\tau \approx 0.1$ - 0.2 at 2 μm) layer of non-absorbing particles near 160 mbar, a layer near 470 mbar of ammonia ice particles ($r \approx 1$-1.3 μm, $\tau \approx 2$), then a clear region down to 1.3-2 bars, where a very optically thick layer of particles (likely composed of NH_4SH) provides a needed strong reduction in thermal emission in the 5-μm window. The background clouds differ dramatically in the NH_4SH layer, which has that cloud top 1 bar or more deeper. But the ammonia layer is the main modulator of pseudo continuum I/F in reflected sunlight. That layer has an optical depth of $\tau \approx 1.3$ in background clouds, but almost double that in the bright 3-μm absorbing clouds. What makes the 3-μm absorption unexpectedly apparent in these polar clouds is the reduced optical depth of the upper cloud layer, which is an order of magnitude smaller than in other regions on Saturn, perhaps because of polar downwelling. Ammonia ice features have also been found in the north polar region (Baines et al. 2018, GRL, submitted).

Acknowledgement: This work was supported by NASA grant NNX15AL10G.

Exploring low-latitude electrodynamics in Saturn's thermosphere

J. W. **Vriesema**[1], T. T. Koskinen[2] and R. V. Yelle[3].
[1]Lunar and Planetary Laboratory (1629 E University Blvd, Tucson, Arizona, 85721 (vriesema@lpl.arizona.edu),
[2](koskinen@lpl.arizona.edu), [3](yelle@lpl.arizona.edu).

Introduction: Saturn's magnetosphere is known to be electrodynamically coupled to its thermosphere, especially in auroral regions, but less is known about the electrodynamics of the thermosphere at low latitudes. Toward the goal of developing a more complete understanding of electrodynamics in Saturn's upper atmosphere, we investigate the effect of equatorial winds on Saturn's ionospheric wind dynamo at lower and middle latitudes using an axisymmetric, steady-state model. As inputs for our model, we calculate a one-dimensional conductivity profile and construct a two-dimensional model wind profile based on results from a general circulation model but with the addition of an equatorial jet, which we assume persists up to the lower thermosphere from the troposphere. This model predicts current densities of the order 10^{-9} to 10^{-7} A m^{-2}. Our model also predicts substantial resistive (Joule) heating and ion drag, which have the potential to significantly alter the energetics and circulation balance of the upper atmosphere.

Cassini UV reflection spectra of Saturn: Acetylene and haze

R. A. **West**[1], J. Hu[1], T. Koskinen[2] and W. Pryor[3].
[1]Jet Propulsion Lab, Caltech, JPL MS 183-501, 4800 Oak Grove Drive, Pasadena, CA, 91109, (Robert.A.West@jpl.nasa.gov), (Juliette.Hu@jpl.nasa.gov); [2]Lunar and Planetary Laboratory, University of Arizona, 1629 E. Universoty Blvd., Tucson, AZ 85721, (tommi@lpl.arizona.edu); [3]Central Arizona College, 8470 N. Overfield Road, Coolidge, AZ 85228-9778, (Wayne.Pryor@centralaz.edu)

Introduction: During Cassini's tour of the Saturn system from 2004 to 2017 the Ultraviolet Imaging Spectrograph (UVIS) acquired thousands of spectral image 'cubes' of Saturn, as well as numerous solar and stellar occultations and limb scans. Here we focus on some 18,000 spectra associated with twelve long-dwell observations obtained in association with compositional observations (so-called COMPSIT) at fixed pointing (not scanning) designed by the Cassini Infrared Spectrometer (CIRS) team. The UVIS altitude coverage overlaps that of CIRS, but samples higher in the atmosphere.

Data Reduction: We include in this data set only those UVIS spatial samples on the dayside and far enough from the bright limb and terminator to be useful for analysis with a plane-parallel scattering code. These pixels satisfy the criteria $\mu > 0.1$ and $\mu_0 > 0.1$, where μ is the cosine of the emission angle and μ_0 is the cosine of the solar flux indicence angle. We used a team-constructed calibration code that converts data number to intensity, and we divided this by F where πF is the incident solar flux. In this work we are concerned with reflected sunlight between about 160 and 190 nm where signatures of acetylene and hydrocarbon haze are strong.

Analysis: In order to transform information from a large spectral data set to a comprehensible result, we tried an unconventional approach to spectral fitting. We derived eigenvectors in the spectral domain for the ~18,000 spectra using a singular value decomposition routine. We found that the first two eigenvectors contain obvious signatures of acetylene absorption. The third contains a signature of variations of instrumental origin that we had previously not suspected but in retrospect are related to well-known detector irregularities which we had previously identified. The remaining eigenvectors are mostly noise. A more careful analysis of eigenvectors 4-8 may reveal signtures of other hydrocarbons, but these are not apparent so far. The rest we can discard as noise, resulting in data compression by a factor of about 2000. We examined the behavior of the first two eigenvectors as functions of viewing and illumination geometry, latitude, and time. Correlations with solar incident angle are apparent. The next step in this process will be to construct model results from multiple scattering simulations with the goal to be able to map acetylene and haze distributions as functions of latitude and time during the mission. This will require us to discover what features of the model (column abundance, vertical distribution, etc) reproduce the first two eigenvectors that emerge from the data. We will also fold in results derived by others from occultations which have limited spatial and temporal coverage but much better vertical sampling. Ultimately these results can be combined with results from CIRS for acetylene and other hydrocarbons to produce a fuller picture of Saturn's upper atmosphere.

Titan

Seasonal variations of Titan's stratospheric temperatures and winds from Cassini/CIRS observations

R. K. Achterberg[1,3], P. J. Gierasch[2], F. M. Flasar[3] and C. A. Nixon[3].
[1]Department of Astronomy, University of Maryland, College Park, MD 20742 (Richard.K.Achterberg@nasa.gov), [2]Department of Astronomy, Cornell University, Ithaca, NY. [3]Planetary Systems Laboratory, NASA Goddard Space Flight Center, Greenbelt, MD 20771.

Introduction: The Cassini mission allowed monitoring of Titan's atmosphere for slightly under two Titan seasons, from northern mid-winter (L_S=293°) through northern summer solstice (L_S=93°). During the majority of Titan flybys, the Composite Infrared Spectrometer (CIRS) performed a nadir mapping sequence, designed for mapping temperatures between roughly 0.5 mbar and 5 mbar, in the middle stratosphere, over one hemisphere of Titan with a spatial resolution of approximately 2.5° of arc. These observations allowed us to monitor the temporal variation of Titan's mid-stratospheric temperatures over nearly two seasons.

Temperatures: From northern mid-winter through northern spring equinox, strong meridional temperature gradients were restricted to the winter hemisphere; north polar temperatures in the mid-stratosphere were about 25 K colder than the equator, while the south pole was less than 5K colder than the equator. After equinox, the southern stratosphere began cooling, as the northern stratosphere continued to slowly warm, with the temperatures at low- to mid-latitudes becoming roughly symmetric about two Earth years after equinox. Through the first half of southern autumn, middle stratospheric temperatures at the south pole dropped to ~115K, almost 30K colder than the north pole in northern mid-winter and were nearly isothermal in altitude between 0.5 and 8 mbar. After L_S=50°, south polar temperature levelled off and began to slowly increase. Three years after equinox, near equatorial temperatures began decreasing, dropping by about 4K over 5 years. This drop in equatorial temperatures can be explained by radiative cooling as Titan moves farther from the sun [1]. A plot of zonal mean temperatures at 1 mbar throughout the Cassini mission is shown in Fig. 1.

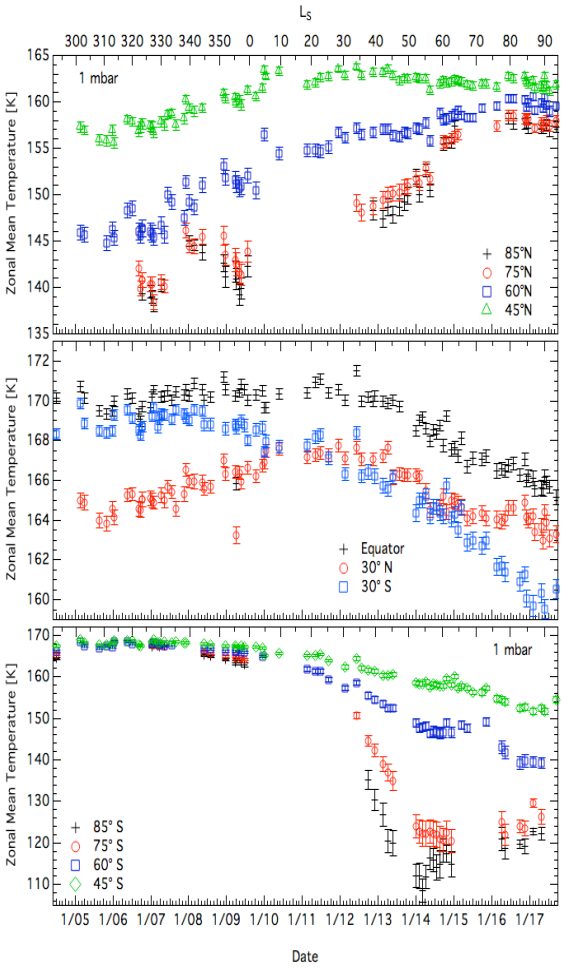

Winds: From the observed zonal mean temperatures, the zonal mean winds can be estimated from the gradient wind approximation as described in [2]. In northern mid-winter, the calculated stratospheric winds showed a strong prograde jet of about 200 m s^{-1} at northern midlatitudes, with much weaker winds, less than 90 m s^{-1}, in the southern hemisphere. During the 4 years after northern spring equinox, the winds in the northern stratosphere decelerated to just over 100 m s^{-1}, while the southern hemisphere winds accelerated, reaching over 200 m s^{-1}. The southern jet was initially located near 70°S, but during 2015 to 2016 the jet moved equatorward. At southern winter solstice the jet was at southern mid-latitudes, and the stratospheric winds were roughly symmetric to those observed in northern mid-winter.

Figure 1: Zonal mean temperatures, averaged in 5° latitude bins, as a function of time at 1 mbar at a selection of latitudes.

References: [1] Bezard, B. et al. (2018) *Icarus*, **302**, 437-450; [2] Flasar, F. M. et al. (2005) *Science,* **308**, 975-978.

Cassini UVIS observations of Titan airglow

Joseph M. Ajello[1], Emilie M. Royer[2], J. Scott Evans, Victoir Veibell, Michael Stevens, Larry W. Esposito, Charles P. Malone, Greg M. Holsclaw, William E. McClintock, Robert A. West, Jean-Claude Gérard, Thomas E. Cravens.
Laboratory for Atmospheric and Space Physics, University of Colorado, 3665 Discovery Drive, Boulder, CO, 80303-7814, [1] (Joe.Ajello@lasp.colorado.edu, [2] Emilie.Royer@lasp.colorado.edu)

To accomplish the Cassini science objective of reaching a deeper understanding of the Saturn-Titan system, it is important to measure the spectral composition of both the EUV (56.1–118.2 nm) and FUV (111.5–191.3 nm) spectra from **simultaneous** observations by the two Ultraviolet Imaging Spectrograph (UVIS) spectral channels. The complex UV airglow signature of N_2 and its dissociation products from the thermosphere and to the exobase of Titan is the principal means of studying the solar and magnetospheric energy inputs. UV nightglow emissions observed from Titan by the Cassini UVIS and by the Imaging Subsystem during eclipse of Titan by Saturn, have led to identifying that energetic Saturnian magnetosphere-plasma interactions with Titan's ambient neutral species (e.g., nitrogen) are a significant source of UV nightglow emissions [Ajello *et al.*, 2012, West *et al.*, 2012; Lavvas *et al.*, 2014]. Magnetospheric particle interactions, particularly the particles H^+ and O^+, along with secondary electrons, produce a nightglow spectrum over an extended altitude range (~200–2000 km). Dayglow emissions are *at least* a factor of ten brighter than the nightglow and are predominantly excited by photoelectrons [Stevens *et al.*, 2011]. The UVIS observed photon emissions of Titan's day and night limb-airglow on more than 1000 occasions by drifting or stepping across the full disk of Titan. Cassini UVIS viewed the entirety of Titan's dayside, nightside, or some combination of both, bracketing the terminator as shown in Fig. 1 for the dayglow and nightglow image for NI (149.3 nm) from dissociative excitation of N_2. Dissociation of N_2 has led to ~20% atmospheric loss over geologic time through creation of nitriles and deposition of organics [Ajello et al., 2008]. Upward moving atomic N, formed high in the thermosphere, can escape the exobase (~1300 km) into the Saturn magnetosphere. Unlike observations during the Voyager missions, this extended monitoring period between 2004 and 2017 has provided greater insight into the distribution and temporal variability of emissions from Titan, in particular those of the N_2 Lyman-Birge-Hopfield (LBH) bands. Not only does the UVIS instrument provide finer spatial and spectral resolution, but the observations spread over a full solar cycle during the length of the mission have provided the opportunity to examine the role of Saturn's magnetosphere on the distribution and intensity of Titan's nitrogen emissions as Titan has been observed at a variety of locations within the magnetosphere. All of these more than 1000 Planetary Data System (PDS) datasets, with separate geometry and UVIS spectra, have been organized into a single 3-dimensional data-array, referred to as a 'data-cube,' containing all of the Titan geometry, spacecraft pointing, and both calibrated and raw spectral data for both UVIS spectral channels. These data-cubes are a fundamental piece of the Titan UVIS library, with compiled UVIS observations of Titan from the entire Cassini mission [Royer *et al.*, 2016].

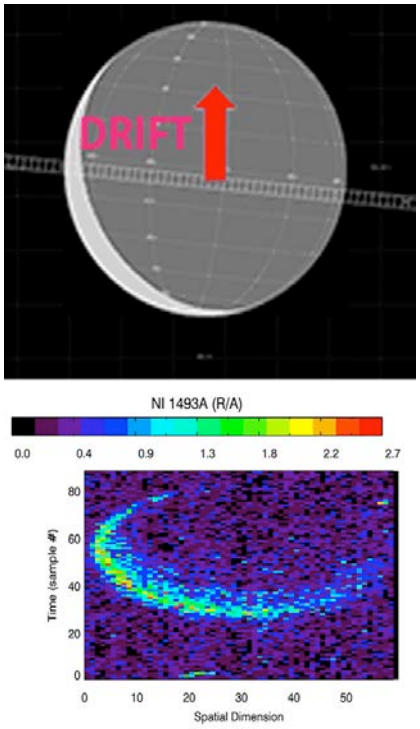

Fig. 1a). UVIS scan of Titan disk on day 2005-360:21:45, b) FUV

References: Ajello, J. M., J. Gustin, I. Stewart, K. Larsen, L. Esposito, W. Pryor, W. McClintock, M. H. Stevens, C. P. Malone, and D. Dziczek, "Titan Airglow Spectra from Cassini Ultraviolet Imaging Spectrograph (UVIS): FUV Disk Analysis", *Geophys. Res. Lett.*, 35, (2008); Ajello, J. M., R. West, M. Stevens, K. Larsen, A. I. Stewart, L. W. Esposito, W. E. McClintock, G. M. Holsclaw, and E. T. Bradley, "Cassini UVIS Observations of Titan Nightglow Spectra," *J. Geophys. Res.*, **117**, A12315 (2012); Royer, E., J. M. Ajello, R. West, G. M. Holsclaw, L. W. Esposito, and E. T. Bradley, "Cassini UVIS Observations of Titan EUV Airglow Intensity with Solar Zenith Angle," *Geophys. Res. Lett.*, **43**, (2016); Stevens, M., J. Gustin, J. M. Ajello, J. S. Evans, R. R. Meier, A. J. Kochenash, A. W. Stephan, A. I. Stewart, K. Larsen, L. W. Esposito, W. E. McClintock, G. M. Holsclaw, B. R. Lewis, and A. N. Heays, "The Production of Titan's Ultraviolet Nitrogen Airglow," *J. Geophys. Res.*, **116**, A05304, (2011); West, R. A., J. M. Ajello, M. H. Stevens, D. F. Strobel, G. R. Gladstone, and J. S. Evans, "Titan Airglow During Eclipse," *Geophys. Res. Lett.*, **39**, L18204, (2012); Lavvas, P., R. A. West, G. Gronoff, and P. Rannou, "Titan's Emission Processes during Eclipse," *Icarus*, **241**, 397-408 (2014).

Evolution of aerosols in Titan's ionospheric plasma: An experimental simulation

A. **Chatain**[1,2], O. Guaitella[2], N. Carrasco[1], N. Ruscassier[3].
[1]LATMOS, CNRS, Université Versailles St-Quentin, Sorbonne Universités, 11 Blvd D'Alembert 78280 Guyancourt France (audrey.chatain@latmos.ipsl.fr, nathalie.carrasco@latmos.ipsl.fr), [2]LPP, CNRS, Ecole Polytechnique, Sorbonne Universités, Université Paris XI, Route de Saclay 91128 Palaiseau France (olivier.guaitella@lpp.polytechnique.fr), [3]LGPM, Ecole Centrale-Supélec, 3 Rue Joliot Curie 91190 Gif-sur-Yvette France (nathalie.ruscassier@ecp.fr).

Introduction: Observations by the space mission Cassini have revealed the formation of complex organic molecules in Titan's ionosphere. To better understand this complex chemistry, several experiments were conducted to reproduce analogs of Titan's aerosols in laboratories, named 'tholins'. These tholins appear to be polymeric and nitrogenous molecules.

Aerosols stay many years in Titan's upper atmosphere, a dusty plasma where molecules are continuously bombarded by charged molecules. Consequently, they are likely to evolve during their stay. Here we address this question by experimental simulation: we analyze the effect of harsh plasma environment on tholins already formed.

Experimental simulation: To separate the processes of formation and evolution, aerosols samples used are first formed with the experiment PAMPRE at LATMOS [T Gautier *Icarus* 2016]. Then tholins are prepared in the shape of thin pellets and positioned at the center of a plasma reactor, where they are exposed during several hours in a DC N_2-H_2 glow discharge, partially representative of Titan's ionosphere. Methane is purposefully removed from this second phase to prevent the formation of new aerosols.

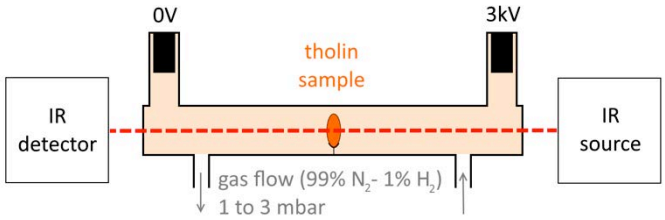

Figure 1: Experimental setup

Results: *Morphological changes.* Pellets become rougher during the exposure. Surface structure is observed through a Scanning Electron Microscope before and after an exposure of four hours. It shows that plasma sputtering attacks the surface and removes some material.

Chemical modifications. We perform in situ infrared transmission spectroscopy during the exposure. Characteristic absorption bands of tholins are distorted, witnessing changes in the samples chemical structure. Especially, we suspect C-H bond environment to be complexed. Nitrile functions are also modified.

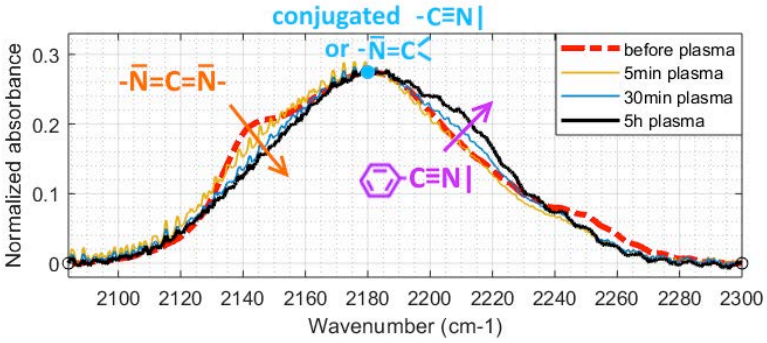

Figure 2 : IR absorption spectra of a tholin pellet during exposure.
Zoom on the nitrile part and guess of attributions to chemical functions.

Acknowledgements: NC acknowledges the financial support of the European Research Council (ERC Starting Grant PRIMCHEM, Grant agreement no. 636829). AC acknowledges ENS Paris-Saclay Doctoral Program.

Key positive ion precursors to tholin formation

D. **Dubois**[1], N. Carrasco[1,2], L. Jovanovic[1], J. Westlake[3], L. Vettier[1], T. Gautier[1].
[1]LATMOS, Université Versailles St-Quentin, UPMC Univ. Paris 06, CNRS, 11 blvd d'Alembre, 78280 Guyancourt, France (david.dubois@latmos.ipsl.fr), [2]Institut Universitaire de France, 103 bd Saint-Michel, 75005 Paris, France, [3]Johns Hopkins University Applied Physics Laboratory, Laurel, Maryland, USA.

Introduction: In Titan's upper atmosphere, Cassini detected mass signatures compatible with the presence of heavily charged molecules which are volatile precursors to the solid core of the aerosols. INMS measurements revealed molecular groupings of masses below 100 amu, while CAPS-IBS saw positive ions up to ~350 amu, well beyond the INMS detection limit. Photochemical processes are also influenced by dayside vs. nightside conditions, with photoionization dominating the dayside. From a dynamical and transport viewpoint, the ion densities were also found to be sensitive to modeled turbulent neutral transport. A previous laboratory study has also explored the influence of trace species on the first and intermediate steps of the neutral and positive ion chemistry, in hydrocarbon-enriched mixtures. Furthermore, models have indicated that primary production processes and ion-molecule reactions mainly control the production of the lighter and subsequent heavier positive ions. These reactions rely on the large abundancies of hydrocarbon building blocks (e.g. C_2H_2 and C_2H_4). These observations indicate that ion chemistry has an important role for organic growth in the upper atmosphere. However, the processes coupling ion chemistry and the formation of larger tholins have yet to be further explored. In this study, we investigate the positive ion chemistry in the laboratory, responsible for the efficient organic growth

producing tholins, simulated in the PAMPRE plasma reactor. We use a RF-generated plasma at 1 mbar pressure, coupled with an ion mass spectrometer, probing the gas phase volatiles *in situ*. We study N_2:CH_4 mixtures with 1-10% CH_4 mixing ratios, and investigate the impact of light ions on the larger ones. We further compare our results to Cassini Ion and Neutral Mass Spectrometer (INMS) measurements taken during the T40 flyby.

Acknowledgements: We are grateful to the European Research Council Starting Grant PrimChem for funding this work (grant agreement no. 636829), and data provided by the Cassini INMS instrument available through the PDS.

Photochemical activity of HCN-C4H2 ices in Titan's lower atmosphere

D. **Dubois**[1,2], M. S. Gudipati[1], N. Carrasco[2,3].
[1]Jet Propulsion Laboratory, California Institute of Technology, Pasadena, CA 91109, USA, [2]LATMOS, Université Versailles St-Quentin, UPMC Univ. Paris 06, CNRS, 11 blvd d'Alembre, 78280 Guyancourt, France (david.dubois@latmos.ipsl.fr), [3]Institut Universitaire de France, 103 bd Saint-Michel, 75005 Paris, France.

Abstract: Revealed by the Cassini and Voyager Missions, a plethora of volatile species are formed in Titan's upper atmosphere from the initial N_2/CH_4 (~98/2%) composition. As they precipitate, most of the volatiles condense in the colder lower atmosphere where they can form icy clouds (e.g. C_4N_2, HCN, C_2H_6) which have been detected above the poles. HCN is the most abundant nitrile in Titan's atmosphere and suspected to condensate in Titan's lower stratosphere (typically <100 km). Micron-sized HCN ice particles were also observed above the south pole at high altitudes (300 km). This cloud is thought to have been formed in the post-equinox winter polar vortex. In the north polar regions, HCN is also a likely prominent contributor to the *haystack* spectral signature seen at 221 cm^{-1}. These stratospheric ices may contribute as condensation nuclei for ices deeper down in the troposphere. Furthermore, C_4H_2, a simple alkyne formed by the chemistry and relatively abundant in the stratosphere, condenses near 75 km, lower than HCN. C_4H_2 can also absorb the lesser energetic photos at these low altitudes, forming the radical C_4H which then reacts with CH_4, causing the consumption of methane. Consequently, the loss mechanism for C_4H_2 is photochemistry. As soon as C_4H_2 condenses, small molecule and complex accretion with HCN may occur. The reactive state that these ices may undergo with long-UV radiation after they form is still largely unknown. We explore these conditions by stuying HCN-C_4H_2 ice mixtures in the laboratory, by using the Titan Organic Aerosol Spectroscopy and chemisTry (TOAST) setup at JPL's Ice Spectroscopy Laboratory (ISL). These ices are then irradiated at long-UV wavelengths pertaining to these low-altitude regions at low-controlled temperatures. The residue is analyzed using long-IR absorption. Our results show a solid-state HCN consumption due to irradiation, to which C_4H_2 acts as a catalyst, indicating HCN ice particle ageing in the troposphere may be facilitated by more complex condensed nuclei.

Acknowledgments: This work is partly funded by NASA Solar System Workings Funding to Murthy Gudipati and the part of the work carried out at the Jet Propulsion Laboratory, California Institute of Technology, under a contract with the National Aeronautics and Space Administration. We are also grateful to the European Research Council Starting Grant PrimChem for funding (grant agreement no. 636829).

Titan's zonal winds from Cassini radio-occultation soundings

F. M. **Flasar**[1], P. J. Schinder[2], and R. K. Achterberg[3].
[1]NASA Goddard Space Flight Center, Planetary Systems Laboratory, Code 693, Greenbelt, MD 20771, (f.m.flasar@nasa.gov),
[2]Cornell Center for Astrophysics and Planetary Science, Cornell University, Ithaca, NY 14853 USA, (schinder@astro.cornell.edu),
[3]Department of Astronomy, University of Maryland, College Park, MD 20742 USA, (richard.k.achterberg@nasa.gov).

The Voyager 1 flyby though the Saturn system gave the first indication that Titan's atmosphere globally rotates well in excess of its equatorial surface rotation rate. Available temperature data from the Voyager infrared spectrometer and central-flash data from stellar occultations suggested that the zonal winds increased with altitude from the surface to the upper stratosphere [1]. Although the Huygens Probe Doppler Wind Experiment (DWE) sounding at 10° S generally supported this picture [2], a glaring exception was the deep minimum in the measured zonal wind profile near 80 km altitude (20 mbar). Cassini radio-occultation soundings provide a means of determining the zonal winds globally, through application of the gradient wind relation to the retrieved altitude-pressure profiles. They show that the minimum near 20 mbar is global, and this structure seems to have persisted through the mission. The cause of this peculiar behavior is not known for sure, but the deceleration of the zonal winds observed in the lower stratosphere may be associated with the radiative damping of vertically propagating gravity waves that are quasi-stationary. The 20-mbar level marks the transition between the lower atmosphere, where radiative time scales are large and seasonal effects are muted, and higher altitudes, where the time scales are much smaller and large seasonal variations in temperatures and winds are observed. At this level, the damping time decreases rapidly with altitude, and the static stability becomes very large. These effects can lead to the enhanced radiative damping of an upwardly propagating wave, because both the vertical wavelength and group velocity become smaller.

Indeed, as the stationary wave encounters the level of low zonal winds, both approach zero. Here the wave drag on the mean flow can become quite pronounced.

References: [1] Flasar, F. M., M. D. Allison, and J. I. Lunine, Titan zonal wind model. In *Huygens, Science, Pyload, and Mission,* pp. 287-298, J.-P. Lebreton, ed., ESA SP-1177 (1997); [2] Bird, M. K. et al., The vertical profile of winds on Titan. *Nature* **438**, 800-802 (2005).

Trace organic volatiles in Titan lower atmosphere: Re-interpretation of Huygens/GCMS data

T. **Gautier**[1], J. Serigano[2], S. M. Hörst[2] and M.G. Trainer[3].
[1]LATMOS/IPSL, CNRS, UVSQ Université Paris-Saclay, Sorbonne Université, 11 bvd d'Alembert Guyancourt 78280, France, (Thomas.gautier@latmos.ipsl.Fr), [2]Department of Earth and Planetary Sciences, Johns Hopkins University, Baltimore, MD, USA, [3]NASA Goddard Space Flight Center, Planetary Environment Laboratory, Greenbelt, MD, USA.

Introduction: Cassini-Huygens employed an array of observational methods at Titan including remote sensing techniques, upper atmosphere in situ sampling, and the descent of the Huygens probe directly through the atmosphere to the surface (Owen et al. 2005). More than a decade later, the data acquired by the instruments on the Huygens Probe remain the only in situ measurements in Titan's deep atmosphere. In particular, the Gas Chromatograph Mass Spectrometer (GCMS) experiment on Huygens performed hundreds of mass spectra analyses below 150 km (Niemann et al. 2005). However, there has not yet been a comprehensive attempt to extract the identity and abundances of many minor components of the GCMS spectra. For example, ethane, the most abundant hydrocarbon produced by methane photolysis and retrieved by both remote observations of the lower stratosphere by CIRS (Bezard et al. 2014, Vinatier et al. 2007) and by numerical models (e.g., Lavvas et al. 2011), is strikingly absent from GCMS measurements during its descent. The absence of ethane in GCMS data near the surface can be explained by ethane condensation, but its non-detection in the first GCMS measurements above 100 km remains one of the major discrepancies in our understanding of Titan. In addition to ethane, many trace organics predicted both by models and measurements at higher altitude remain unquantified in GCMS.

Methods and Results: We present a re-analysis of the GCMS data collected during Huygens' descent, leveraging recent advances in both knowledge of Titan's atmosphere and mass spectral deconvolution for organic species in the frame of the Rosetta mission, to identify and quantify the trace species in Titan's troposphere. We will present how we deconvolve the mass spectra acquired by GCMS using the fragmentation pattern of the molecules detected and retrieve the vertical profiles for trace species encountered throughout the lower atmosphere. We will also discuss our first results on the mixing ratios of minor species in Titan's troposphere.

References: Bezard et al. 2014 Titan: Surface, Atmosphere and Magnetosphere Chap. 6, Cambridge University Press, 2014; Lavvas et al. 2011, Icarus 215 (2): 732-750**;** Niemann et al. 2005, Nature 438 (7069) : 779-784**;** Owen et al. 2005, Nature 438 (7069) : 756-757**;** Vinatier et al. 2007, Icarus 188(1) : 120-138.

Radiolysis in Titan's subsurface ocean provides a new source of deep energy for possible life

C. R. **Glein**[1*], C. Ray[2,1], J. H. Waite[1,2].
[1]Space Science and Engineering Division, Southwest Research Institute, San Antonio, TX 78228, [2]Department of Physics and Astronomy, University of Texas at San Antonio, San Antonio, TX 78249, (cglein@swri.edu).

Introduction: Saturn's largest moon, Titan, is one of the ocean worlds in the solar system, as revealed by data from the Cassini-Huygens mission [1,2]. The likely presence of liquid water in the subsurface helps to make Titan habitable for life as we know it. However, the conventional model for the internal structure of Titan has an ocean sandwiched between a crust of hexagonal ice, and a layer of denser high-pressure phases of ice overlying a rocky core. This has led to the idea that Titan may be substantially less habitable than Europa or Enceladus, because there may be a lack of energy sources to support life in an ocean that is not in direct contact with rock. Here, we present the case for the generation of a continuous source of chemical energy in Titan's ocean based on the radiolytic decomposition of water molecules. This process produces molecular hydrogen (H_2), a key redox species for a diverse assortment of known microbial metabolisms [3,4].

Modeling framework: Our geochemical model assumes that there is a significant amount of radioactive ^{40}K dissolved in Titan's subsurface ocean. This is supported by the presence of ^{40}Ar in Titan's atmosphere [5,6], and by the inference that some ^{40}K must be leached into the ocean to explain the predominance of hydrated silicates in the core [7]. For a CI chondrite abundance of K in accreted rock, our model suggests that there could be $\sim 4\times10^{16}$ moles of ^{40}K in Titan's ocean at present. Decaying ^{40}K atoms emit energetic electrons and gamma rays that can break apart surrounding H_2O molecules into H_2 and a ½ O_2 equivalent.

Results and discussion: Using the parameterized model of radiolysis presented by [8], we calculate a present rate of H_2 production from radiolysis in Titan's ocean of $\sim 6\times10^{10}$ mol/yr. For comparison, the H_2 production rate attributed to water-rock reactions at Enceladus is $(1\text{-}5)\times10^{9}$ mol/yr [9]. If we normalize these numbers to the surface area of the respective body, we obtain

~700 mol yr^{-1} km^{-2} (Titan) and 1000-6000 mol yr^{-1} km^{-2} (Enceladus). These comparisons demonstrate that radiolysis is likely to be an important source of redox species in Titan's ocean, which must now be considered in assessments of its habitability. Ongoing work is aimed at understanding the corresponding oxidant budget, and providing quantitative constraints for metabolic energy availability from radiolysis in the subsurface ocean of Titan.

Acknowledgments: This research is supported by the Cassini project (NASA contract NAS703001TONMO711123, JPL subcontract 1405853).

References: [1] Béghin et al. (2012), *Icarus* 218, 1028-1042. [2] Mitri et al. (2014), *Icarus* 236, 169-177. [3] Lin et al. (2006), *Science* 314, 479-482. [4] D'Hondt et al. (2009), *PNAS* 106, 11651-11656. [5] Waite et al. (2005), *Science* 308, 982-986. [6] Niemann et al. (2010), *JGR-Planets* 115, E12006. [7] Castillo-Rogez and Lunine (2010), *GRL* 37, L20205. [8] Ray et al. (2017), AGU Fall Meeting, P51F-08. [9] Waite et al. (2017), *Science* 356, 155-159.

Enhancement of the Huygens DISR dataset

B. **Grieger**[1] and P. Caballo-Peruchar[2].
[1]ESAC, Camino Bajo del Castillo s/n, Urb. Villafranca del Castillo, E-28692 Villanueva de la Cañada, Madrid, Spain, (bjoern.grieger@esa.int), [2]JOANNEUM RESEARCH Forschungsgesellschaft mbH, Leonhardstraße 59, 8010 Graz, Austria, (piluca.caballo-perucha@joanneum.at).

Introduction: During the descent of the Huygens probe through Titan's atmosphere, the three panchromatic cameras of the Descent Imager/Spectral Radiometer (DISR) acquired about 1200 images. Of these, 606 images were successfully transmitted to the Cassini spacecraft and relayed to Earth. The images were published within the DISR dataset by NASA's Planetary Data System (PDS) and ESA's Planetary Science Archive (PSA).

Data analysis and archiving efforts: The DISR data acquisition from the rotating probe was planned at well defined directions with respect to the Sun. Because the probe was — for still unknown reasons — rotating in the wrong direction, the Sun sensor did not work and observations were rather acquired at random directions. Because of this, the data analysis was much more complicated than expected and took significantly longer. Therefore, towards the end of the funding period, the archiving was conducted somewhat in a hurry and not everything went completely well.

"Lossy decompression" of images: The onboard compression comprised two steps: First, the original 12 bit data of the CCD was reduced to 8 bit (as the hardware compressor could only work on 8 bit data) by kind of a square rooting. Second, the image was compressed using a JPEG-like Digital Cosine Transform (DCT) algorithm.

On ground, the image was decompressed by the respective inverse DCT. While the original pixel value was an 8 bit integer, the reconstructed value deviates from it because of the lossy DCT compression, and thus it is in general a float. For the current archive version of the images, the float pixel values were rounded to the nearest 8 bit integer before transforming them back to 12 bit values. This was an additional, unnecessary destruction of information. It does not only reduce the image fidelity, cf. Fig. 1, but makes it also impossible to recover the original DCT coefficients.

New (old) high fidelity images: We are updating the DISR archive dataset by replacing the "lossy decompressed" images with a version that preserves the full fidelity of the original data. We are also providing the complete information which is needed to recover the DCT coefficients and to revert the onboard processing in order to constrain the pixel values of the original onboard images.

Mosaic: A full mosaic of the landing side employing all images was created by Erich Karkoschka. The current archive dataset contains renderings of this mosaic for different widths and resolutions. We now provide also the underlying data which is represented on a circular exponential grid.

Digital elevation models: Digital elevation models (DEMs) of a few selected areas had been created by the United States Geological Survey (USGS), but they were not included in the archive. We report on an attempt to create a full DEM by simultaneously employing the complete set of images.

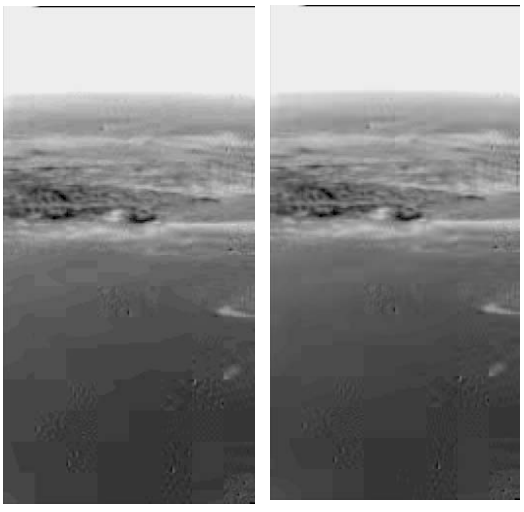

Figure 1: Comparison of an image which has been rounded to the nearest 8 bit integer after decompression and before inverse square rooting as it is currently in the archive (left) and the same image without such rounding (right), both shown with a gamma stretch of 4.

Taking the long view: High resolution MM/SubMM spectral imaging of Titan's atmosphere with ALMA

M. **Gurwell**[1], E. Lellouch[2], R. Moreno[3], B.J. Butler[4], S. Vinatier[5], A. Moullet[6], E. Villard[7], T. Hidayat[8], L. Lara[9]
[1]Harvard-Smithsonian Center for Astrophysics, MS 42, 60 Garden St, Cambridge, MA 02138; (mgurwell@cfa.harvard.edu), [2]Observatoire de Paris, LESIA/CNRS, 5 place J. Janssen, 92195 Meudon, France; (emmanuel.lellouch@obspm.fr), [3](raphael.moreno@obspm.fr), [5](sandrine.vinatier@obspm.fr), [4]National Radio Astronomy Observatory, PO Box O, 1003 Lopezville Road, Socorro, NM 87801; (bbutler@nrao.edu), [6]National Radio Astronomy Observatory, 520 Edgemont Road, Charlottesville, VA 22903; (amoullet@nrao.edu), [7]ALMA/ESO, Alonso de Córdova 3107, Vitacura, Santiago, Chile; (evillard@alma.cl), [8]Bosscha Observatory & Deparment of Astronomy, Institut Teknologi Bandung, Ganesha 10, 40132, Bandung, West Java, Indonesia; (taufiq@as.itb.ac.id), [9]IAA-CSIC, C/ Glorieta de la Astronomia s/n 18008 Granada, Spain; (lara@iaa.csic.es)

Introduction: Flybys of Titan by the Cassini spacecraft demonstrated the importance of characterizing and monitoring the vertical and spatial distributions of molecular species, providing insight into the variability of chemistry and atmospheric circulation which exhibit significant, global changes occurring over relatively short time periods as well as seasonally. Observations of Titan's upper atmosphere by Cassini instruments, including CIRS and INMS, can only be described as spectacularly successful from the 127 flybys covering a half-Titan year. These results show that Titan is incredibly dynamic on seasonal timescales, and that continuing study of Titan through at least one full year is important. Fortunately, the unique sensitivity, access to many submillimeter spectral lines, and high resolution capabilities of the Atacama Large Millimeter/submillimeter Array (ALMA) will allow for extended, detailed exploration of many photochemically important species in, and atmospheric dynamics of, Titan's stratosphere and mesosphere.

ALMA: ALMA is a large mm/submm interferometer located in the Atacama region of northern Chile, at roughly 5000m altitude. Up to 50 12-m antennas can be used together to provide extremely sensitive imaging of astronomical targets, with spatial resolution as fine as 20 milliarcseconds in the 870 μm window of Earth's atmosphere. While nearly insensitive to non-polar molecules (such as the primary atmospheric constituents N_2 and CH_4), ALMA is adept at observing many of the trace species in Titan's stratosphere and mesosphere. We utilized ALMA to obtain a comprehensive view of Titan's stratosphere in mid-2016 using three tunings covering rich portions of the 870 micron atmospheric window. Observations on July 22 and August 19 provided high spectral and spatial resolution imaging of many important species in Titan's atmosphere, including CO (plus ^{13}CO and $C^{18}O$), HCN (plus DCN, $H^{13}CN$, and $HC^{15}N$), HNC, CH_3CN, CH_3CCH, C_2H_5CN, and HC_3N, while covering lines of other species and their isotopomers. The resolution achieved was ~0.16" in the N-S direction, equivalent to ~1100 km linear resolution at the distance of Titan, and finer than the height of the atmosphere from surface to exobase. Selected species were observed with extremely high spectral resolution (61 kHz, or R~6 million, for CH_3CN, HCN, HNC, DCN, and HC_3N) allowing for direct measure of global circulation at different altitudes.

Our preliminary results show that many molecules show spectacular gradients as a function of latitude, and they vary by species. For example, CH_3CN shows very strong emission in the high northern latitudes, CH_3CCH shows peaks at both high northern and southern latitudes (with preference to the north), while HC_3N peaks at high southern latitudes. Winds show zonal speeds from 175 m/s (from CH_3CN/CH_3CCH) up to 300 m/s (HCN, HNC, and HC_3N); the HCN/HNC and HC_3N line cores probe higher altitudes than CH_3CN/ CH_3CCH, suggesting increasingly strong zonal winds with altitude.

Future: While presenting highlights of these initial high resolution ALMA observations, we will also explore how this study, conducted while Cassini was still in operation, will allow for detailed comparison/validation of results, and point toward future observations with ALMA at even higher resolution, extending the observational 'reach' of Cassini for decades.

Titan Surface Temperatures Through the Cassini Mission

D. E. **Jennings**[1], V. Cottini[1,2], C. A. Nixon[1], A. Coustenis[3] and T. Tokano[4]
[1]Goddard Space Flight Center, Greenbelt, MD 20771, USA (donald.e.jennings@nasa.gov, conor.a.nixon@nasa.gov), [2]Department of Astronomy, University of Maryland, College Park, MD 20742, USA (valeria.cottini@nasa.gov), [3]LESIA, Observatoire de Paris, CNRS, Paris Science Let. Res. Univ, Univ. Paris-Diderot, 5, place Jules Janssen, F-92195 Meudon Cedex, France (Athena.Coustenis@obspm.fr), [4]Institut für Geophysik und Meteorologie, Universität zu Köln, Albertus-Magnus-Platz, Köln 50923, Germany (tokano@geo.uni-koeln.de).

The Composite Infrared Spectrometer (CIRS) on *Cassini* measured surface brightness temperatures on Titan from 2004 to 2017, exploiting an atmospheric spectral window at 19 microns where radiation is transmitted from the surface to space (Jennings *et al.* 2016; Cottini *et al.* 2012). Surface temperatures were mapped in six 2-year time segments and one final 7-month segment. Mapping was performed using zonal averages in 10-degree latitude bins. Seasonal advancement of the pole-to-pole temperature distribution was tracked as winter in the north gave way to winter in the south. The maximum temperature was always in the vicinity of the equator, but during the course of the mission the latitude of the center of north-south symmetry of the temperature distribution moved from 12 S to 25 N. The center of symmetry, which generally followed the subsolar latitude, crossed the equator in mid-2010, corresponding to a 0.8 year (0.35 Titan month) seasonal lag. This seasonal lag was consistent with Voyager results from 1980, one Titan year earlier. Near the beginning of the mission the North Pole was at a temperature of 90.5 K while the South Pole was at 91.5 K. By late in the mission the pattern had reversed, with 91.5 K in the north and 89.5 K in the south. As the latitude distribution shifted northward the maximum temperature decreased, from 93.8 K at the beginning of the mission to 93.0 K near the end. Lower temperatures later in the mission could not have been caused entirely by the increasing solar distance. A comparison with the predictions of Tokano (2005),

which took account of the decreasing solar irradiance, showed agreement during the first portion of the mission up to about 2012. But late in the mission the observed temperatures in the north fell below the model by about 1 K. Surface temperatures in the north may have been depressed by evaporation from lakes and wet ground. Our results, echoing findings in Titan's lower stratosphere (Coustenis et al., 2018), exemplify the north-south seasonal asymmetry on Titan.

References: Jennings, D.E. *et al.*, ApJ Lett. 816, L17 (2016); Cottini, V. *et al.*, 2012. Planet. Space Sci. 60, 62 (2012); Coustenis, A., *et al.*, 2018. *Astroph. J.*, *Lett.*, **854**, no2; Tokano, T., Icarus 173, 222 (2005)

Infrared spectroscopy support for the Cassini mission

A. **Jolly**[1], Y. Benilan[1], M. Faye[1], L. Manceron[2], C. A. Nixon[3] , N. A. Lombardo[3], D. E. Jennings[3].
[1]LISA, UMR 7583 du CNRS, Universités Paris Diderot et Paris-Est Créteil, France (jolly@lisa.u-pec.fr), [2]Synchrotron SOLEIL, L'orme des Merisiers, Saint-Aubin-BP 48, 91192 Gif-sur-Yvette Cedex and MONARIS, CNRS-Sorbonne Université UMR 8233., 4, place Jussieu 75005, France [3]NASA Goddard Space Flight Center, Greenbelt, MD, 20771

Introduction: The Composite Infrared Spectrometer (CIRS) on-board Cassini has recorded spectra in the far and mid-infrared from 2004 to 2017 with a spectral resolution of up to 0.5 cm-1. One of the goals of the instrument was to detect minor species in Titan's atmosphere. Despite tremendous efforts from the spectroscopic community, a lack of spectroscopic knowledge still prevents us from a complete interpretation of the observations. During the mission we carried out many spectroscopic experiments, sometimes at low temperature to mimic Titan's environment, and sometimes at high resolution to reach the rotational structure. We have used different apparatus including a synchrotron source to reach the far infrared. Molecular samples have been synthesized and purified to obtain absolute intensity values that are necessary to determine precise abundances. Also, we have initiated a collaboration with André Fayt on the theoretical aspects which helped us to solve the complex problem of hot band contributions for linear molecules. Finally we used sophisticated spectroscopic models to calculate extensive line lists which have been made available to the CIRS team and most are now included in the HITRAN and GEISA databases.

Presentation: In the presentation, we show how spectroscopic studies could sometimes lead to detections of minor species or new interpretations of CIRS observations. In the case of C_2HD, precise intensity measurements and the first line lists where produced to ensure the quantification of a new deuterated molecule in Titan (Coustenis, 2008). For HC_3N and C_4H_2, high resolution spectra were reanalyzed with the help of a global model to obtain new extensive line lists including missing hot band contributions. With the help of the new spectroscopic parameters, CIRS observations could be precisely reproduced, with the exception of small features which turned out to be due to ^{13}C isotopologues of HC_3N *(Jennings 2008)* and C_4H_2 *(Jolly 2010)*. For C_4H_2, we also revised band intensities, in particular in the far infrared domain, measuring new values at the SOLEIL synchrotron facility *(Jolly 2014)*. In the meantime, new high resolution spectra were recorded at SOLEIL for C_2N_2 including the contribution of the ^{15}N isotopologues *(Fayt 2012)*. This time, the small separation between the specral features prevented us from detecting a new isotopic species. We also studied the longer carbon chains such as HC_5N, C_6H_2 and C_4N_2. Band intensity measurements were carried out for all three molecules and for C_4N_2 a careful analysis of high resolution data has led to the first line lists. No detection of this molecule was possible but a precise abundance upper limit of C_4N_2 in the gas phase in Titan's atmosphere was determined *(Jolly 2015)*. Photochemical models of Titan's atmosphere predict significant amounts of allene (CH_2CCH_2) and butane (C_4H_{10}) but they could not be detected by CIRS. Low temperature spectra of those molecules were recorded down to 150 K in the mid and far infrared. Line lists have been compiled for the first time for allene which led a precise abundance upper limit *(Lombardo 2018)*.

Conclusion: Many spectral features are still unidentified in CIRS spectra that could be due to new molecules or to imperfection in spectroscopic data. The need for better spectroscopic parameters is still high and will grow even more with future higher resolution observations.

Visualization and Analytics of Saturnian Moons Data

E. S. **Law**[1], B. Mitchell[1], K. L. Mitchell[1] and T. L. Ray[1], Solar System Treks Team[1],[1]Jet Propulsion Laboratory, 4800 Oak Grove Dr, MS 168-200, Pasadena, CA 91109, Emily.Law@jpl.nasa.gov.

Introduction: The Cassini mission conducted multi-instrument investigations of the Saturn system. It brought back a valuable collection of data about those worlds. At NASA's Jet Propulsion Laboratory, we are developing a suite of online portals and value added geospatial data products that will allow scientists to conduct detailed studies.

As web-based toolsets, the Titan Trek and Icy Moons Trek portals do not require user to install any software beyond current web browsers. They provide analysis tools that facilitate measurement and study of terrain including distance, height, and depth of surface features. They allow users to easily find and access the geospatial products that are available. Data include imagery from the VIMS and ISS cameras, as well as the RADAR synthetic aperture images, topography, derived physical parameters and community-sourced geological and hydrological mapping products.

Users have the ability to drill down to find the PDS data used to produce the geospatial products. Data products can be viewed in 2D and 3D, and can be staked and blended together rendering optimal visualization that reveals details that no single data set can show. Data sets can be plotted and compared against each other. In addition to keyboard and mouse control, standard gaming and 3D mouse controllers allow users to maneuver first-person visualization of flying across the moons' surface. The portals also provide users the ability to specify any area of terrain for generation of STL/OBJ files that can be sent to 3D printers to make 3D models. 3D prints and the data visualization capabilities of these portals are particularly valuable in engaging students, educators and general public to personally explore the moons. In addition to the web portals, standard Application Programmable Interfaces (API) are available to facilitate access and dissemination of the data products to external applications and use.

Seeing Titan with VIMS infrared eyes during 13 years : from changing atmospheric features over the poles to global surface mapping

S. **Le Mouélic**[1], S. Rodriguez[2], C. Sotin[3], T. Cornet[4], B. Rousseau[5], R. Robidel[1], J. W. Barnes[6], R. H. Brown[7], B. J. Buratti[3], K. H. Baines[3], R. N. Clark[8], P. D. Nicholson[9], P. Rannou[10].

[1]Laboratoire de Planétologie et Géodynamique, CNRS UMR 6112, Université de Nantes, Nantes, France (stephane.lemouelic@univ-nantes.fr). [2]Laboratoire AIM, CEA/Saclay, Gif/Yvette, France. [3]JPL, Pasadena, USA. [4]ESA, European Space Astronomy Centre, Madrid, Spain. [5]Univ. Grenoble Alpes, CNRS, IPAG, Grenoble, France, [6]University of Idaho, Moscow, ID, USA. [7]University of Arizona, Tucson, AZ, USA. [8]PSI, Tucson, AZ, USA. [9]Cornell University, Ithaca, NY, USA, [10]GSMA, UMR CNRS 6089, Université de Reims Champagne-Ardenne, France.

Introduction: Cassini entered in Saturn's orbit in July 2004. In thirteen years, 127 targeted flybys of Titan have been performed. We have analyzed of the complete Visual and Infrared Mapping Spectrometer data set with two objectives : the first is to document the atmospheric seasonal changes over the poles during the mission [1]. The second objective is to merge all the observations in synthetic global color maps of the surface.

Results: For the study of the poles, we have computed individual color mosaics for each of the 127 targeted flybys, using VIMS wavelengths sensitive both to clouds and surface features. This series of maps reveal the systematic changes that progressively occurred in the 2004-2017 timeframe. First evidences for a vast ethane cloud covering the North Pole is seen as soon as the first and second targeted flyby in October 2004 and December 2005 [2]. The first detailed imaging of this north polar feature with VIMS was obtained in December 2006, thanks to a change in inclination of the spacecraft orbit [3]. At this time, the northern lakes and seas of Titan were totally masked to the optical cameras, whereas the southern pole was well illuminated and mostly clear of haze and vast clouds. The vast north polar feature progressively vanished around the equinox in 2009 [3,4,5], in agreement with the predictions of Global Circulation Models [6], revealing the underlying lakes and seas. First evidences of a giant cloud growing over the south pole occurred in May 2012 (T82), with a high altitude cloud being detected consistently at each flyby up to the last T126 targeted flyby. Our maps show that this feature grew up month after month until the end of the mission in 2017, with a poleward latitudinal extent of 75°S in 2013 ranging up to 58°S in April 2017. Thanks to the spectral capabilities of VIMS, we have detected HCN spectral signatures over the north pole in almost all flybys between 2004 and 2008. These HCN signatures started then to show up over the south pole in almost all flybys between 2012 and 2017.

For the study of the surface, we have developed an empirical approach to mitigate the effects of the atmosphere, which otherwise induce significant seams between individual images due to the scattering and absorption of atmospheric gases and aerosols. Global maps at 32 pixels per degrees have been produced at specific wavelength, revealing the surface heterogeneity of Titan. Polar surveys and global maps will be shown at the meeting.

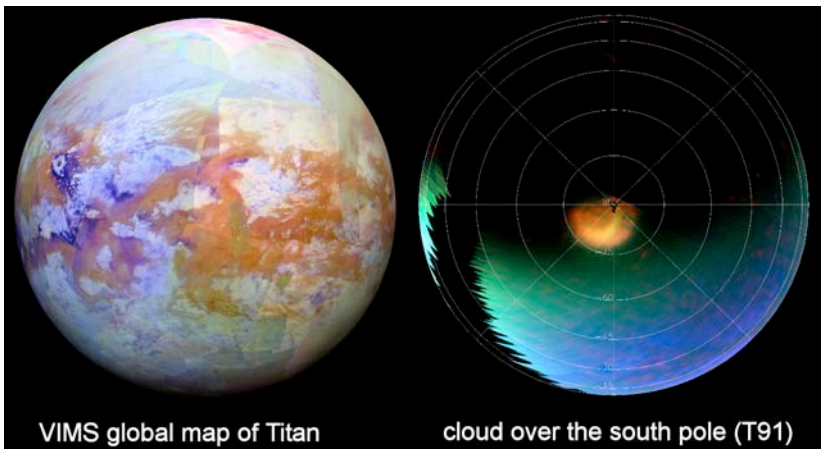

[1] Le Mouélic et al., Icarus, accepted with minor revisions [2] Griffith et al., Science, 2006. [3] Le Mouélic et al., PSS, 2012. [4] Rodriguez et al., Nature, 2009. [5] Rodriguez et al., Icarus 2011. [6] Rannou et al., Science 2005.

Enigmatic electron densities in Titan's ionosphere: Is ion transport a solution?

S. A. Ledvina[1], S. H. Brecht[2] and J. M. Bell.
[1]Space Sciences Lab, University of California, Berkeley CA, 94720, Ledvina@berkeley.edu. [2]Bay Area Research Corp., Orinda CA, 94563, (Sbrecht@pacbell.net). [2]National Institute of Aerospace, Hampton, VA, 23666, (Jared.m.bell@gmail.com).

Introduction: Galand et al., [2010] analyzed data from multiple Cassini instruments collected during four Titan encounters to investigate the formation of Titan's ionosphere. They found that the electron densities in Titan's deep ionosphere (below 1200 km altitude) were lower than models predicted.

Titan's ionosphere is created when solar photons, energetic magnetospheric electrons or ions, and cosmic rays ionize the neutral atmosphere. Electron densities generated by current theoretical models are much larger than densities measured by the Cassini instruments [cf. Richards et al., 2015a,b; Shebanits et al., 2017; and Mukundan and Bhardwaj, 2018]. The overabundance of the modeled electron densities must result either from overproduction or from insufficient loss of ions. The general consensus is that the models are not overproducing ions, leaving an unknown ion loss process as the most likely candidate for the discrepancy.

We investigate if ion transport is a viable explanation for the extra loss of ions. A three-dimensional hybrid simulation of Titan's plasma interaction is used for this investigation. The simulations include a simplified ion-neutral chemical reaction network, Hall and Pederson conductivities, and ion-neutral collisions. The atmospheric neutral densities and winds are taken from the three-dimensional Titan-Global Ionosphere Thermosphere Model of Bell et al., [2010]. Our focus will be on ion and electron densities below 1200 km altitude. We will determine what role Titan's plasma interaction and the atmospheric winds play in determining the ion and electron densities in this region, and if they can explain the enigmatic electron densities.

Comparison of modeled alkane abundances in Titan's atmosphere using different spectral windows with Cassini CIRS spectra

N. A. **Lombardo**[1,2], C. A. Nixon[1], R. K. Achterberg[1], K. Sung[3], P. G. J. Irwin[4].
[1]Goddard Space Flight Center, 8800 Greenbelt Road, Greenbelt, MD, 20770, USA (nicholas.lombardo@nasa.gov), [2]Center for Space Science and Technology, University of Maryland, Baltimore County, Baltimore, MD, 21250, USA, [3]Jet Propulsion Laboratory, California Institute of Technology, Pasadena, CA, 91109, USA, [4]Clarendon Laboratory, University of Oxford, Oxford, United Kingdom

Introduction: The Composite Infrared Spectrometer (CIRS) instrument on Cassini has been used to determine the abundance of trace gases in Titan's atmosphere. The instrument has three focal planes, each sensitive to a different wavenumber range – FP1 in the far infrared from 10 to 600 cm^{-1}, and FP3 and FP4 in the mid infrared from 600 to 1100 and 1100 to 1400 cm^{-1}, respectively. Across the spectral range covered by CIRS, molecules may show several transition features. By the nature of certain observing geometries and detector design, we can model different bands at a range of altitudes in Titan's atmosphere.

The three simplest alkanes, methane, ethane, and propane, have been studied extensively in Titan's atmosphere. Methane is assumed to have a nearly constant 1.41 x 10^{-2} mixing ratio in the stratosphere (*Niemann, 2005*). Ethane has been shown to vary seasonally, concentrating near the winter pole due to Titan's large circulation cell, and has a stratospheric abundance near 10^{-5}. Propane is also shown to vary seasonally, and has a stratospheric abundance near 10^{-6} (*Vinatier, 2015*).

Presentation: In this work, we compare the abundance of ethane modeled from several spectral bands in the far and mid infrared using the NEMESIS radiative transfer algorithm (*Irwin, 2008*). By combining FIR nadir spectra observed near the equator over the entire mission, we are able to increase the SNR of the data, allowing us to model the weak v4 band of ethane (289 cm^{-1}) and sound the ethane abundance at an altitude of 90 km. We also retrieve abundance profiles of propane using FP3 and FP4 spectra to determine the range of sensitive altitudes for each focal plane.

Conclusion: By making use of the large CIRS dataset, we are able to sound the ethane abundance deeper in Titan's atmosphere than before. Combing these values with current ethane abundance profiles at higher atltidues, we can constrain the vertical variation in the abundance of the gas. Constraining the range of sensitive altitudes for ethane and propane between Focal Planes 3 and 4 will help in the modeling of these features in the future, and may also extend the altitude range where the abundance of these gases is well known.

Uncovering the influence of surface and subsurface hydrology on Titan's climate system

J. M. **Lora**[1], S. P. Faulk[2], and J. L. Mitchell[2],
[1]UCLA (jlora@ucla.edu); 595 Charles Young Drive, Los Angeles, CA 90095), [2]UCLA (595 Charles Young Drive, Los Angeles, CA 90095.

Introduction: Comparisons of models of Titan's climate to various data acquired by Cassini have revealed that Titan's surface liquid distribution greatly influences the hydrologic cycle. Simulations with the Titan Atmospheric Model (TAM) with imposed polar methane "wetlands" reproduce observed cloud activity in Titan's atmosphere, whereas simulations with a globally-moist surface are not as successful. In addition, wetlands simulations indicate a strong correlation between extreme rainfall and observed geomorphic features, implicating the influential role of precipitation in shaping Titan's surface. The wetlands configuration is, in part, motivated by Titan's large-scale topography featuring low-latitude highlands and high-latitude lowlands, with the implication being that methane may concentrate in the high-latitude lowlands by way of runoff and subsurface flow of a global or regional methane table. But the extent to which topography controls the surface liquid distribution and thus impacts the global hydrologic cycle is unclear.

Coupled Atmosphere–Surface Hydrology Modeling: In order to make progress on understanding the interactions of Titan's dynamic atmosphere with the surface, we have developed a new coupled model for Titan's climate system. Here we present climate simulations of Titan wherein we incorporate a fully self-consistent surface hydrology scheme with infiltration, groundmethane evaporation, and surface and subsurface flow into the previously validated TAM. This allows simulated surface liquids to naturally redistribute under the influence of topography, capturing an essential set of processes. We assess the impact of surface hydrology on the surface liquid distribution over seasonal timescales, and compare the resulting hydrologic cycle to Cassini observations of cloud and surface features. This more realistic representation of Titan's hydrology provides insights into the complex interaction between Titan's atmosphere and surface, demonstrates the influence of surface hydrology on Titan's global climate, and lays the groundwork for further developments in planetary climate models.

Seasonal changes in the middle atmosphere of Titan from 2004 to 2017 using Cassini/CIRS observations

C. **Mathé**[1], S. Vinatier[1], B. Bruno[1], M. Sylvestre[2], C. A. Nixon[3], D E. Jennings[3], N. Gorius[3,4], J. C. Brasunas[3]. [1]LESIA (Observatoire de Paris, Université PSL, CNRS, Sorbonne Université, Univ. Paris Diderot, Sorbonne Paris Cité, 5 place Jules Janssen, 92195 Meudon, France, (christophe.mathe@obspm.fr), (sandrine.vinatier@obspm.fr), (bruno.bezard@obspm.fr), [2]School of Earth Sciences, University of Bristol,Wills Memorial Building, Queen's Road, Bristol BS8 1 RJ, UK, melody.sylvestre@bristol.ac.uk, [3]Planetary Systems Laboratory (NASA Goddard Space Flight Ctr., Greenbelt, MD 20771 , (conor.a.nixon@nasa.gov), (Donald.E.Jennings@nasa.gov), (nicolas.gorius@nasa.gov), (john.c.brasunas@nasa.gov). [4]The Catholic University of America, Washington, DC 20064

Due to Saturn's obliquity, Titan experiences strong seasonal variations that were monitored by the Cassini mission during almost 2 seasons, from the northern winter in 2004 to the summer solstice in 2017. Global circulation of the middle atmosphere reversed within two years after the northern spring equinox (Vinatier et al., 2015). The descending branch above the South pole brought enriched air from the upper atmospheric levels down to the stratosphere where strong molecular enhancements have been observed since 2012 (Coustenis et al., 2016, Teanby et al., 2017, Vinatier et al., 2015).

We present here a study of the seasonal variations of the temperature and molecular abundance profiles in the middle atmosphere of Titan from 2004 to 2017 using the entire CIRS limb mid-infrared dataset acquired at 0.5-cm-1 resolution. These data allow us to retrieve, using a line-by-line radiative transfer code coupled with a constrained linear inversion algorithm, the mixing ratio profiles of C2H2, C2H4, C2H6, C3H8, CH3C2H, C4H2, C6H6, HCN, HC3N and CO2. Using the same dataset, we also inferred the isotopic ratios of 14N/15N and 12C/13C in HCN.

References: Coustenis et al., "Titan's temporal evolution in stratospheric trace gases near the poles", Icarus, 2016,vol. 270; Teanby et al., "The formation and evolution of Titan's winter polar vortex", Nature Communications, 2017, vol. 8; Vinatier et al., "Seasonal variations in Titan's middle atmosphere during the northern spring derived from Cassini/CIRS observations", Icarus, 2015, vol. 250.

Is Titan's hemispheric surface-liquid dichotomy an equilibrium state?

J. L. **Mitchell**[1,2], S. P. Faulk[1] and J. M. Lora.
[1] Earth, Planetary and Space Sciences, 595 Charles Young Drive, UCLA (jonmitch@g.ucla.edu), [2]Atmospheric and Oceanic Sciences, UCLA.

Introduction: Cassini revealed a dramatic dichotomy in surface liquids on Titan that likely oscillates with the orbital and spin precession of the Saturn system.

Discussion: We will examine the possibility that the present hemispheric surface-liquid dichotomy is an equilibrium state using simulations of Titan's climate, and then speculate on the implications for the various modes of inter-hemispheric methane transport.

Titan's atmosphere: How to bake a five-layered cake

Conor A. **Nixon**[1].
[1]Planetary Systems Laboratory, NASA Goddard Space Flight Center, Greenbelt, MD 20771,, (conor.a.nixon@nasa.gov).

Introduction: Titan, long the most mysterious moon in the solar system due to its hazy atmosphere, yielded up many secrets to the Cassini-Huygens mission (2004-2017). With eighteen instruments, the two spacecraft comprehensively investigated Titan from the interior to the exosphere. This presentation summarizes the current picture of Titan's atmosphere, and what we still wish to know.

Atmospheric structure: The atmospheric temperature structure of Titan can be compared to the Earth, with five layers (Fig. 1), each controlled by different physical processes. These are inextricably linked to the chemistry, which is quite different on Titan from the Earth, yet results in some similar features.

Troposphere: the lowest layer exhibits a negative temperature gradient, controlled by convection. The temperature decreases from ~94 K (surface), to ~70 K (tropopause, ~45 km). Surface methane is evaporated by sunlight, and rises to ~30 km where clouds form and occasionally become large storms. Precipitation empties excess methane and wets the surface, slowly carving river channels into icy bedrock.

Stratosphere: the second, stably-stratified layer shows warming from the tropopause (70 K, 45 km) to the stratopause (~180 K, 300 km). Heating is due to methane and organic haze, which absorb solar UV, and reradiate strongly at thermal infrared wavelengths. Many trace gases are detected, most prominently hydrocarbons and nitriles, which originate higher up in the atmosphere and percolate downwards to condense in the lower stratopause.

Mesosphere: above 300 km, temperatures fall due to radiative cooling. The haze prominent at lower levels is seen here as a 'detached' layer, whose mechanism is still debated. At ~550 km, a weak temperature minimum occurs - the mesopause – where rising air currents in the global circulation reach their peak and begin to flow polewards.

Thermosphere: above the mesopause the thin thermosphere extends to the boundary with space, characterized by gradually increasing temperatures as molecules absorb short-wavelength solar radiation. Ionization and ion chemistry results, now understood to be a major process contributing to Titan's chemical inventory. Methane and nitrogen are broken apart and recombined to form heavier organic molecules and haze particles that eventually filter down to the surface. Gases begin diffusive separation, taking on different scale heights according to their molecular weight.

Exopshere: at ~1500 km is the *exobase*, the transition from atmosphere to space. Here the molecular mean free path exceeds the scale height, and molecules with velocities exceeding the escape velocity (~1.5 km/s) can leave the atmosphere. Light atoms and molecules escaping form a tenuous torus in Titan's orbit, while other atoms and molecules, including O and OH from Enceladus enter the atmosphere, contributing to the trace oxygen species such as CO, CO_2 and H_2O.

Conclusions: Cassini and Huygens have shown Titan to be Earthlike in some important respects, with a Hadley circulation and exobase, and five distictive atmospheric layers. Future missions and investigations will elucidate the mechanism for the rising and falling of the detatched haze, the microstructure of the haze particles, the composition of tropospheric and stratospheric clouds, and the long-term co-evolution of atmosphere and surface landforms.

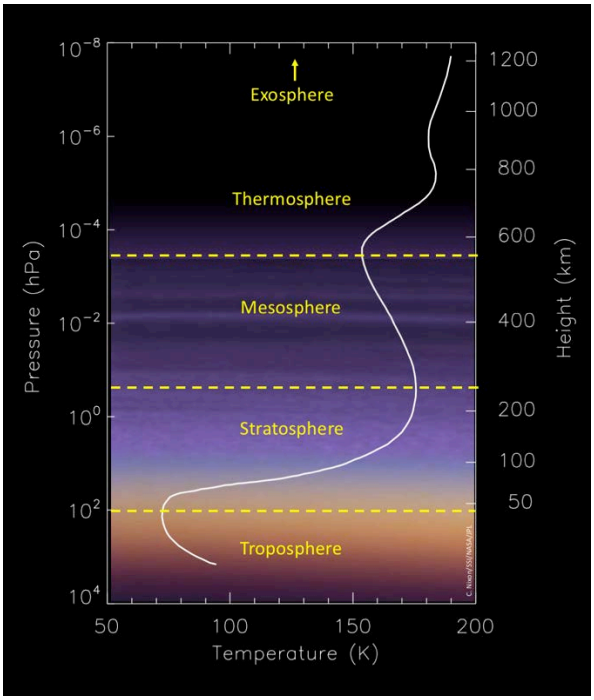

Figure 1: Titan vertical atmospheric thermal structure, showing transitions between canonical layers, and approximation of visible haze as a function of altitude. Image: PIA 06160 NASA/JPL./SSI.

Regional mapping of aerosol population and surface albedo of Titan by the massive inversion of the Cassini/VIMS dataset

S. **Rodriguez**[1], T. Cornet[2,3], L. Maltagliati[1,4], T. Appéré[1,5], S. Le Mouélic[6], C. Sotin[7], J.W. Barnes[8], R.H. Brown[9],
[1] IPGP, University Paris Diderot, France. (sebastien.rodriguez76@gmail.com). [2] Laboratoire AIM, CEA/Saclay, Gif/Yvette, France. [3] European Space Agency (ESA), European Space Astronomy Center (ESAC), Villanueva de la Cañada, Madrid, Spain. [4] Nature Publishing Group, London, United Kingdom. [5] Institut de Planétologie et d'Astrophysique de Grenoble, Université J. Fourier, CNRS/INSU, Grenoble, France. [6] LPG Nantes, UMR 6112 CNRS, Université de Nantes, Nantes, France. [7] Jet Propulsion Laboratory (JPL), Pasadena, CA. [8] University of Idaho, Moscow, ID,. [9] University of Arizona, Tucson, AZ.

Mapping Titan's surface albedo is a necessary step to give reliable constraints on its composition. However, even after the end of the Cassini mission, surface albedo maps of Titan, especially over large regions, are still very rare, the surface windows being strongly affected by atmospheric contributions (absorption, scattering). A full radiative transfer model is an essential tool to remove these effects, but too time-consuming to treat systematically the ~50000 hyperspectral images VIMS acquired since the beginning of the mission.

We developed a massive inversion of VIMS data based on lookup tables computed from a state-of-the-art radiative transfer model in pseudo-spherical geometry, updated with new aerosol properties coming from our analysis of observations acquired recently by VIMS (solar occultations and emission phase curves). Once the physical properties of gases, aerosols and surface are fixed, the lookup tables are built for the remaining free parameters: the incidence, emergence and azimuth angles, given by navigation; and two products (the aerosol opacity and the surface albedo at all wavelengths). The lookup table grid was carefully selected after thorough testing. The data inversion on these pre-computed spectra (opportunely interpolated) is more than 1000 times faster than recalling the full radiative transfer at each minimization step.

We present here the results from selected flybys. We invert mosaics composed by couples of flybys observing the same area at two different times. The composite albedo maps do not show significant discontinuities in any of the surface windows, suggesting a robust correction of the effects of the geometry (and thus the aerosols) on the observations. Maps of aerosol and albedo uncertainties are also provided, along with absolute errors. We are thus able to provide reliable surface albedo maps at pixel scale for entire regions of Titan and for the whole VIMS spectral range.

Integrated laboratory, modeling and observational investigations of the condensation of benzene on Titan's stratospheric aerosols

E. **Sciamma-O'Brien**[1,2], E.L. Barth[3], L.T. Iraci[1], F. Salama[1] and S. Vinatier[4],
[1]NASA Ames Research Center Moffett Field, CA 94035, [2]Bay Area Environmental Research Institute, Moffett Field, CA 94035,
[3]Southwest Research Institute, Boulder, CO 80301, [4]LESIA, Observatoire de Paris, Meudon 92195, France
(ella.m.sciammaobrien@nasa.gov), (ebarth@boulder.swri.edu), (laura.t.iraci@nasa.gov), (farid.salama@nasa.gov),
(sandrine.vinatier@obspm.fr).

Aerosols in Titan's atmosphere play an important role in determining its thermal structure and can act as condensation nuclei for the formation of clouds. The global circulation of Titan's atmosphere reversed within the two years following the northern spring equinox in August 2009, increasing the mixing ratios of benzene (C_6H_6) and other species at the South pole. A simultaneous strong cooling above the south pole (dropping temperatures below 120 K) resulted in conditions where molecules could condense at unusually high altitudes (>250 km). C_6H_6 and HCN ices have been detected by the Composite Infrared Spectrometer (CIRS) and the Visible and Infrared Mapping Spectrometer (VIMS), respectively, in the South polar cloud system, but the existing laboratory data is insufficient to allow models to reproduce the formation of the observed cloud system.

We will present the preliminary results and overall scope of a newly funded research project which combines laboratory, modeling and observational studies to investigate the condensation of benzene on Titan's aerosol as an important component of the cloud system that appeared during the autumn at 300 km above Titan's South pole. The project goals are: 1) to measure the vapor pressure of benzene at Titan-relevant temperatures using the Ames Atmospheric Chemistry Laboratory (ACL – Iraci et al. 2010), 2) to produce analogs of Titan's aerosols using the Titan Haze Simulation experiment developed on the NASA Ames COSmIC facility (Sciamma-O'Brien et al. 2017) and investigate the conditions required for condensation of benzene on their surface using the ACL, 3) to use the experimental data to constrain nucleation and condensation in microphysical models (Barth 2017), in order to determine expected cloud altitudes and particle sizes and 4) to compare our experimental data and modeling output with observations from CIRS in the 9-17 µm spectral region (Vinatier et al. 2017), to better understand the molecular composition of this cloud system.

References: Barth E. L. Modeling Survey of Ices in Titan's Stratosphere, *Planet. Space Sci.* **127**, 20-31, 2017. Iraci, L. T., Phebus, B. D., Stone, B. M., Colaprete, A. Water Ice Cloud Formation on Mars is More Difficult than Presumed: Laboratory Studies of Ice Nucleation on Surrogate Materials, *Icarus* 210 (2), 985-991, 2010. Sciamma-O'Brien, E., Upton, K. T., Beauchamp, J. L., Salama, F. The Titan Haze Simulation (THS) experiment on COSmIC. Part II. Ex-situ analysis of aerosols produced at low temperature. *Icarus* 289, 214-226, 2017. Vinatier, S., Schmitt B., Bézard, B., Rannou, P., Dauphin, C., de Kok, R., Jennings, D.E., Flasar, F.M. Study of Titan's fall southern stratospheric polar cloud composition with Cassini/CIRS: Detection of benzene ice, *Icarus* (in press).

Ackowledgements: This research is supported by the NASA SMD CDAP program.

Frozen hydrocarbons on Titan

J. M. **Soderblom**[1], V.F. Chevrier[2], K. Farnsworth[2], J. K. Steckloff[1,3,4], J. W. Barnes[5], R. H. Brown[6], T. Cornet[7], A. G. Hayes[8], J. Perry[6], S. Rodriguez[9], L. A. Soderblom[10], A. Soto[11], and E. P. Turtle[12],
[1]Massachusetts Institute of Technology, Cambridge, MA 02139 (jms4@mit.edu), [2]University of Arkansas, Fayetteville, AR. [3]Planetary Science Institute, Tucson, AZ, [4]University of Texas at Austin, Austin, TX, [5]University of Idaho, Moscow, ID [6]Univversity of Arizona, Tucson, AZ [7]European Space Astronomy Centre, Madrid, Spain. [8]Cornell University, Ithaca, NY [9]Institut de Physique du Globe de Paris (IPGP), Paris, France, [10]U.S. Geological Survey, Flagstaff, AZ [11]Southwest Research Institute, Boulder, CO [12]Applied Physics Laboratory, Laurel MD.

Introduction: Cassini ISS observations revealed widespread darkening of Titan's surface believed to result from rainfall, in 2004–2005 at Arrakis Planitia (~75–80°S), [1], and in 2010 in the tropics [2]. ISS and VIMS observations show that, following the initial darkening, these regions increased in albedo, becoming significantly brighter than their original albedo [3–4]. In the tropics event, the surface reverted back to its original albedo over a period of months [3]. Here, we present a comprehensive study of these events. We present an analysis of the observations, particularly those of the Arrakis event, and the relevant environmental conditions. We then discuss ongoing theoretical modeling and laboratory experiments designed to provide insight into the proposed processes.

Observations: The ISS observations of Arrakis were acquired in 2004 and 2005, in between which, ground-based images of Titan revealed an extensive cloud outburst near Arrakis [5]. The ISS-observed darkening closely correlates with topography apparent in Cassini SAR images, suggesting sufficient quantities of liquid to pool (Fig. 1). Arrakis was observed by VIMS four times, between 2007 and 2009. In all of these observations, the regions of interest were observed to be significantly brighter than the surrounding terrain (Fig. 1), indicating that the brightening in the south was much longer lived than that in the tropics. In 2007, VIMS observed a specular reflection on the margin of the bright material, suggesting some liquid was still present. Comparison of the bright surfaces' spectra with each other and with laboratory spectra is challenging because of extreme viewing geometries [4, 6].

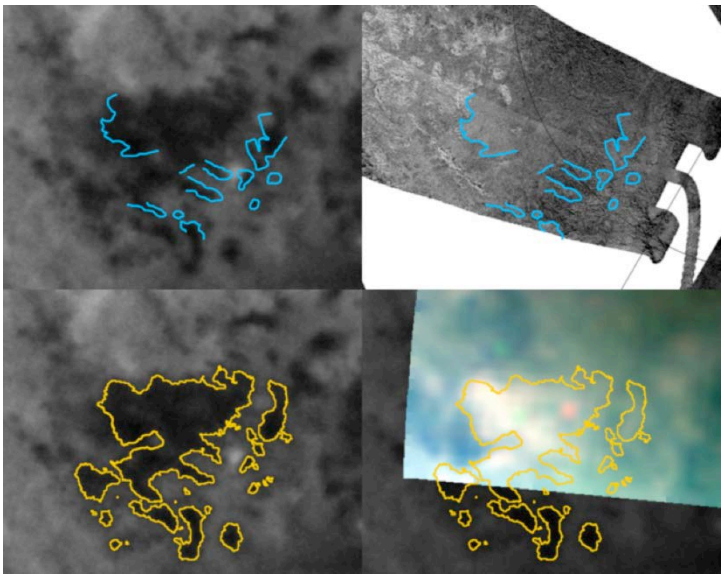

Figure 1. Arrakis Planitia. Top: Blue lines mark the topographic depressions observed in SAR images (right) and superimposed on the ISS image (left) showing darkened regions. Bottom: Yellow outlines drawn from the ISS (left) demarking the boundaries of the darkened terrain superimposed on a 2009VIMS color image.

Laboratory and modeling work: Based on the timescale and magnitude of the albedo changes, and the correlations between the timescale and temperature, we favor a thermodynamically controlled process for the brightening. To study the possibilities, we employ theoretical modeling [7] and laboratory experiments [8]. We have developed a thermodynamic model to study the temperature-dependent dissolution of nitrogen in methane-ethane mixtures and the associated impact on the liquids density and freezing temperature [7]. As the methane evaporates, the pond cools, causing the solubility of nitrogen to increase, which increases the liquid density. As this continues, it is possible to form an ethane-rich surface layer that becomes buoyant. Given the right conditions, this ethane-rich layer can then begin to precipitate ethane ice [7]. Finally, we present results from laboratory experiments that support the modeling work and suggest that it might be possible to isolate and freeze ethane from a methane-ethane mixture on Titan under certain circumstances [8].

References: [1] Turtle, E.P., et al. (2009), GRL, 36, L02204. [2] Turtle, E.P., et al. (2011), Science, 331, 1414–1417. [3] Barnes, J.W., et al. (2013), Planet. Space Sci., 2, 1. [4] Soderblom, J.M. et al. (2016), DPS, 502.04. [5] Schaller, E.K., et al. (2006) Icarus, 182, 224–229. [6] Farnsworth, K. et al. (2018), LPSC, 2739. [7] Steckloff, J.K. et al. (2017), DPS, 301.05. [8] Farnsworth, K. et al., 2017, LPSC, 1974.

Titan's interior structure inferred from analysis of topographic and gravity data

C. **Sotin**[1], N. Rambaux[2], O. Cadek[3], K. Kalousova[3], A. Neri[4], and B. Reynard[4].
[1]Jet Propulsion Laboratory–California Institute of Technology, Pasadena, CA, USA (Christophe.sotin@jpl.nasa.gov), [2]IMCCE, Observatoire de Paris – PSL Research University, Sorbonne Université, 77 Avenue Denfert-Rochereau, 75014 Paris, France, [3]Charles University, Faculty of Mathematics and Physics, Department of Geophysics, V Holešovickách 2, 180 00 Praha 8, Czech Republic,

[4]Laboratoire de Géologie de Lyon : Terre, Planète, Environnement, Campus de la Doua, 2 rue Raphaël Dubois, 69622 Villeurbanne Cedex, France.

Introduction: The Cassini mission has provided Titan's shape [1] and gravity coefficients [2,3] that are combined to infer the interior structure. Non compensated topography can be an important component of the gravity field. If correlated with the degree 2 gravity coefficients, non compensated topography can alter the interpretation of the degree 2 gravity coefficients in terms of the moment of inertia and thus the density profile inside Titan [4]. Using additional information such as the Huygens data on the electric field measurements during the descent and equations of state (EoSs), the Cassini observations provide density profile that help constrain Titan's geological evolution and interior dynamics.

Analysis of gravity and shape data: Titan's shape has been measured by radar altimetry, synthetic-aperture radar topography and stereo radargrammetry [1]. It is turned into a topographic map by substracting an ellipsoid that contains the rotational and tidal potentials. The difference between this ellipsoid and an equipotential surface calculated with the gravity coefficients up to degree 4 [3] is less than 25 m. The topographic map shows a strong degree (2,0) corresponding to the polar depressions, but no obvious equatorial degree (2,2). The interior is composed of a series of layers: icy crust, ocean, High-Pressure ice layer, silicate core. The position of each interface is calculated by solving the the Clairaut equations. A 3D spherical code is used to compute the gravity coefficients with non-hydrostatic components. The effect of non compensated topography at the pole is investigated for both Airy and Pratt models based on geodynamical processes that are discussed. The effect of equatorial topography is also investigated.

Implications for the interior structure: The interior models are constrained by the EoSs of water (ice and liquid water) and silicates. It is found that if the equatorial topography is non compensated, then Titan's silicate core would be 125 km smaller and 270 kg/m^3 denser compared to a model of compensated topography. Such a model allows for the presence of reasonable amount of iron in the hydrated silicate core compared to previous models. The data also suggest that the High-Pressure ice layer is convecting with the formation of liquids at the HP ice/silicate core interface, which would permit the rapid transfer of salts and volatiles such as ^{40}Ar or CH_4 to the surface.

This work has been performed at the Jet Propulsion Laboratory, California Institute of Technology, under contract to NASA.

[1] P. Corlies et al. (2018) GRL, 44, 11,754-11,761 [2] Iess L. et al. (2010) Science, 327, 1367 [3] Iess L. et al. (2012) Science 337, 457. [4] P. Gao and D.J. Stevenson (2013) Icarus, 226, 1185–1191.

Pond hockey on Titan? How to stratify Titan's vernal ponds and form ethane ice deposits

J. K. **Steckloff**[1,2,3], J. M. Soderblom[1], V. F. Chevrier[4], K. Farnsworth[4], A. Soto[5], [1]Massachusetts Institute of Technology, Cambridge, MA 02139 USA (jordan1@mit.edu), [2]Planetary Science Institute, Tucson, AZ USA [3]University of Texas at Austin, Austin, TX USA, University [4]of Arkansas, Fayetteville, AR USA, [5]Southwest Research Institute, Boulder, CO USA.

Introduction: Cassini ISS observations revealed regions on Saturn's moon Titan that become significantly darker (lower albedo) following storm events [1–2]. The regions in at least one of the events are observed to be topographically low [3], indicating that liquid (predominantly methane-ethane-nitrogen) is pooling on Titan after these storm events. These dark ponds, however, are then observed to significantly brighten (higher albedo relative to pre-storm albedo), before fading to their pre-storm albedos [3–4]. We interpret these data to indicate ethane ice formation, which cools from evaporation of methane. Through our numerical modeling and laboratory effort, we have found that the formation of ethane ices requires a unique sequence of thermophysical and thermochemical conditions.

Stratification Dynamics: Initially, the methane in the methane-ethane-nitrogen mixture evaporates, cooling the pond. Nitrogen, which dissolves preferentially in methane-rich mixtures, exsolves, further cooling the liquid. However, nitrogen's solubility increases as the temperature of the mixture drops. Thus, relatively more methane than nitrogen leaves the fluid, increasing the relative fraction of nitrogen. This increased nitrogen fraction increases the density of the liquid. At ~85 K and below, further evaporative cooling at the pond's surface leads to a chemical stratification, with an increasingly ethane-rich epilimnion (surface layer) overlying a denser, methane-rich hypolimnion (subsurface layer). Depending on the thermochemical conditions of the mixture, this stratification can be either permanent or episodic. Overturn events can lead to a rapid exsolution of nitrogen, which would rapidly cool the mixture.

Ethane Ice Formation/Precipitation: Further evaporation of methane from the ethane-rich epilimnion drives its temperature and composition toward the methane-ethane-nitrogen liquidus curve, causing pure ethane ice to precipitate out of solution. Ethane ice is denser than the liquid, and thus settles to the bottom of the pond. This growing ethane ice deposit would be obscured by the overlying liquid, and remain undetectable by Cassini VIMS and ISS. Eventually, all ethane precipitates and settles into the ice deposit as the residual liquid evaporates away. The now exposed ethane ice, would appear to Cassini VIMS and ISS as a dramatic brightening of the surface, consistent with observations.

References: [1] Turtle et al. 2009, GRL; [2] Turtle et al. 2011, Science; [3] Soderblom et al. 2014, DPS; [4] Barnes et al. 2013 Planet. Sci.

Insights into Titan's surface and subsurface methane reservoirs at the end of the Cassini Mission

E. P. **Turtle**[1], J. E. Perry[2], E. Karkoschka[2], A. S. McEwen[2], S. M. MacKenzie[1], S. Rodriguez[3], S. Le Mouélic[4], C. Sotin[5], R. D. Lorenz[1], A. G. Hayes[6], M. Mastrogiuseppe[7], J. D. Hofgartner[5], J. I. Lunine[6], J. M. Barbara[8], A. D. Del Genio[9], P. Corlies[6], J. Kelland[6], J. M. Lora[10], S. Faulk[10], R. A. West[5], J. Pitesky[5], T. L. Ray[5], M. Roy[5],
[1]Johns Hopkins Applied Physics Laboratory, Laurel, MD (Elizabeth.Turtle@jhuapl.edu), [2]University of Arizona, Tucson, AZ, [3]Institut de Physique du Globe de Paris (IPGP), CNRS-UMR 7154, Université Paris-Diderot, USPC, Paris, France, [4]CNRS-UMR 6112, Université de Nantes, Nantes, France, [5]Jet Propulsion Laboratory, Pasadena, CA, [6]Cornell University, Ithaca, NY, [7]Sapienza University of Rome, Italy, [8]SciSpace, LLC., NASA Goddard Institute for Space Studies, New York, NY, [9]NASA Goddard Institute for Space Studies, New York, NY, [10]University of California, Los Angeles, CA.

Introduction: Over the course of the *Cassini-Huygens* mission, our understanding of Titan's surface and geology has changed from low-resolution near-infrared maps that revealed broad regions of brighter and darker terrain [*e.g.*, 1] to familiar territory with a very Earth-like combination of landforms and processes, including organic dunes [*e.g.,* 2,3], high-latitude hydrocarbon lakes and seas [*e.g.,* 4,5], and rare methane rain [*e.g.*, 6,7].

Surface observations: *Cassini* ISS, VIMS, and RADAR [8-10] have documented Titan's surface at 938 nm, atmospheric windows 1-5 µm, and 2.2 cm respectively. Global maps have been produced by ISS and VIMS, and synthetic aperture radar (SAR) imaging covers well over 60% of the surface. Recent photometric analysis [11] of the entire ISS equatorial dataset (±30°) has improved the signal-to-noise ratio by a factor of 4-5, along with the effective resolution, and produced calibrated surface albedos (Fig. 1). VIMS' global hyperspectral mosaic of Titan's surface [12] is empirically corrected for atmospheric contribution and improves the coverage and resolution of the northern lake district. In addition to RADAR mapping, altimetric observations also provided bathymetric measurements of Titan's lakes, constraining depths to be >100 m [13] and demonstrating hydrological connections between lakes that are perched hundreds of meters higher than the equipotential surface of the maria [14].

Subsurface methane reservoirs: ISS and VIMS also documented seasonal changes in weather patterns from Titan's late southern summer through its early northern summer [*e.g.*, 15-18]. Such observations constrain aspects of atmospheric circulation models, including the roles of surface and subsurface reservoirs. The behavior observed from 2004-2017 is consistent with models that include a widespread near-surface methane reservoir in addition to the observed maria, suggesting a broader subsurface methane table is accessible to the atmosphere. An interpretation that is in agreement with other results suggesting connected hydrology at Titan's north pole [*e.g.*, 5,19-22].

References: [1] Roe H.G. *et al.* (2004) *GRL 31.* [2] Lorenz R.D. *et al.* (2006) *Science 312.* [3] Radebaugh J. *et al.* (2008) *Icarus 194.* [4] Stofan E.R. *et al.* (2007) *Nature 445.* [5] Hayes A.G. *et al.* (2017) *GRL 44.* [6] Lunine J.I. and Lorenz R.D. (2009) *AREPS 37.* [7] Turtle E.P. *et al.* (2011) *Science 331.* [8] Porco C.C. *et al.* (2004) *SSR 115.* [9] Brown R.H. *et al.* (2004) *SSR 115.* [10] Elachi *et al.* (2004) *SSR 115.* [11] Karkoschka E. *et al.* (2017) *DPS 49*, #301.06. [12] Le Mouélic S. *et al.* (2018) *LPSC 49.* [13] Mastrogiuseppe M. *et al.* (2017) *AGU,* #P12B-08. [14] Hayes A.G. *et al.* (2017) *GRL 44.* [15] Turtle E.P. *et al.* (2011) *GRL 38.* [16] Rodriguez S. *et al.* (2011) *Icarus 216.* [17] Corlies P. *et al.* (2017) *DPS 49*, #304.12. [18] Kelland J. *et al.* (2017) *DPS*, #304.09. [19] Hayes A.G. *et al.* (2008) *GRL 35.* [20] Jennings D.E. *et al.* (2016) *ApJ 816.* [21] Birch S.P.D. *et al.* (2017) *Icarus 282.* [22] Lora J.M. and Ádámkovics M. (2017) *Icarus 286.*

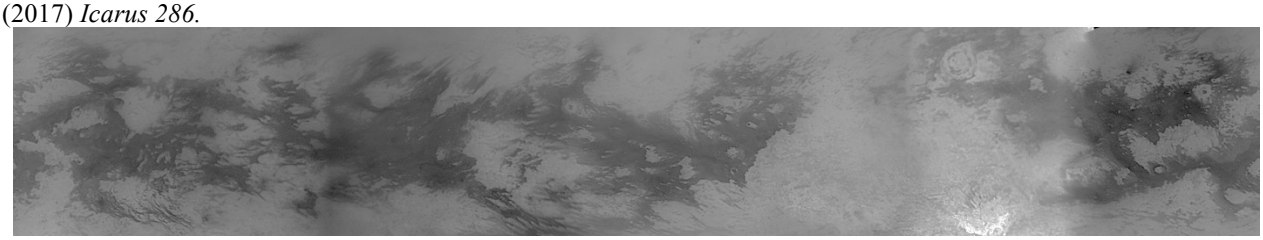

Figure 1: ISS equatorial map. Albedos, calibrated to DISR [11], range from 0.25 in the dunes to 0.9 at Hotei.

Seasonal effects in Titan's stratosphere analyzed through Global Climate Modelling

J. **Vatant d'Ollone**[1], S. Lebonnois[2] and J. Burgalat[3],
[1]Sorbonne Université, École normale supérieure, PSL Research University, École polytechnique, CNRS, Laboratoire de Météorologie Dynamique, LMD / IPSL, Box 99, 4 place Jussieu, F-75005 Paris, France (jan.vatant-dollone@lmd.jussieu.fr), [2]Sorbonne Université, École normale supérieure, PSL Research University, École polytechnique, CNRS, Laboratoire de Météorologie Dynamique, LMD / IPSL, Box 99, 4 place Jussieu, F-75005 Paris, France (sebastien.lebonnois@lmd.jussieu.fr), [3]GSMA, UMR 7331, BP1039, Université de Reims Champagne-Ardenne, 51687 REIMS cedex, France (jeremie.burgalat@univ-reims.fr).

Observations of Titan through Cassini's overall mission allowed to map Saturn's moon stratospheric thermal structure and composition over almost half a Titan's year. Former analysis of these observations revealed many seasonal variations among which

some features remained unexplained or partially understood, such as the mechanisms in place in the polar vortex, the evolution of the thermal structure at high latitudes and the impact of the strong observed enrichment in trace compounds in winter polar nights.

The latest improvements in the IPSL Titan's Global Climate Model (GCM) radiative transfer, now based on a flexible correlated-k method and up-to-date gazes spectroscopic data, lead to a correct modeling of the temperature profiles in the middle atmosphere.

Given this, it is now possible to tackle some scientific issues about thermal structure in polar regions. Special interest will be bear on the destabilization of lower polar winter stratosphere, such as observed by Cassini radio-occultations, which is now reproduced in simulations without any latitudinal variation of composition neither radiative coupling with haze.

We will also present the coupling of this new version of the GCM with our photochemical solver, extended up to 1300 km, and the consequences of the improved thermal structure and mixing in the middle atmosphere on the seasonal distribution of trace compounds. On the light of the results of coupled simulations, we will discuss questions raised by observations, such as the delay between circulation reversal at the equinox and reversal of the chemical enrichment as well as the strength of this enrichment for various species.

Finally, as the former microphysical model needed to be switched off so far in this new version of the GCM, focus will be put on the challenges addressed by re-coupling a new microphysical moments scheme – in the perspective of having a fully interactive microphysical-chemical-dynamical coupled model – and first results of this work will be presented.

Seasonal variations in Titan's stratosphere observed with Cassini/CIRS during northern spring

S. **Vinatier**[1], B. Bézard[1], C. Mathé[1], N. Teanby[2], M. Sylvestre[2], S. Lebonnois[3], R. Achterberg[4], N. Gorius[5], F.M. Flasar[5] and the CIRS Team.

[1]LESIA, Observatoire de Paris, PSL Research University, CNRS, Sorbonne Universités, UPMC Univ. Paris 06, Univ. Paris Diderot, Sorbonne Paris Cité, 5 Place Jules Janssen, 92195 Meudon Cedex France, (sandrine.vinatier@obspm.fr), (bruno.bezard@obspm.fr), (christophe.mathe@obspm.fr), [2] School of Earth Science, University of Bristol (Wills Memorial Building, Queen's Road, Bristol, BS8 1 RJ, UK, (n.teanby@bristol.ac.uk), (melody.sylvestre@bristol.ac.uk), [3] LMD, CNRS, IPSL (UMR 8539, 4 Place Jussieu, 75005, Paris, France, (sebastien.lebonnois@lmd.jussieu.fr), [4] University of Maryland, Department of Astronomy, College Park, MD 20742, (richard.k.achterberg@nasa.gov), [5] NASA/GSFC, Greenbelt, MD, (nicolas.gorius@nasa.gov, f.m.flasar@nasa.gov).

Since 2004, Cassini performed 127 close Titan flybys, observing its atmosphere with instruments including the Cassini Composite InfraRed Spectrometer (CIRS). We know from CIRS observations that the global dynamics drastically changed after the northern spring equinox that occurred in August 2009 ([1], [2], [3], [4]). The pole-to-pole middle atmosphere dynamics (above 100 km) experienced a global reversal in less than 2 years after the equinox [4], while the northern hemisphere was entering spring. This new pattern, with downwelling at the south pole, has resulted in an enrichment of almost all molecules inside the southern polar vortex from 2011. According to General Circulation Model calculations, this single circulation cell pattern should remain until 2025.

We will present an analysis of CIRS limb observations during the entire northern spring up to the beginning of northern summer, in September 2017. We show that many species (C_2H_2, HCN, HC_3N, C_6H_6, C_4H_2, CH_3CCH, C_2H_4) experienced their highest enrichments near the south pole near 500 km in March 2015, with abundances similar to in situ results from INMS at 1000 km [5], suggesting that the air inside the confined polar vortex (observed at latitudes higher than 80°S) was very efficiently transported downward from very high altitudes. In September 2015, an extension of the polar vortex towards lower latitudes (~65°S) was observed, while the molecular abundances decreased by a factor of 10 at 500 km. Simultaneously, in the northern hemisphere, after the disruption of the north polar vortex following the equinox, the enriched air that was previously confined at very high latitude gradually expanded towards mid latitudes at altitudes higher than 300 km. Since the beginning of 2016, a zone depleted in molecular gas and aerosol is observed in the entire northern hemisphere between 400 and 500 km, suggesting some complex unknown dynamical effect. We also show that an enriched region persistes at high northern latitude below 350 km during the entire northern spring, probably due to the confinement of the enriched air by a small circulation cell.

References:[1] Teanby, N. et al., 2012, Nature, 491, pp. 733-735.[2] Achterberg et al., DPS 46, abstract 102.07,Tucson, 2014.[3] Coustenis et al., 2016, Icarus 270, 409-420.[4] Vinatier et al., 2015, Icarus, 250, 95-115.[5] Cui et al., 2009, , Icarus, 200, 581-615.

Highlights and open questions on Titan's atmospheric chemistry

V. **Vuitton**[1], R.V. Yelle[2], S.J. Klippenstein[3], S.M. Hörst[4] and P. Lavvas[5],

[1]Institut de Planétologie et d'Astrophysique de Grenoble, Univ. Grenoble Alpes, CNRS, CNES, Grenoble, 38000, France, veronique.vuitton@univ-grenoble-alpes.fr, [2]Lunar and Planetary Laboratory, Univ. of Arizona, Tucson, AZ 85721, (yelle@lpl.arizona.edu), [3]Chemical Sciences and Engineering Division, Argonne National Lab., Argonne, IL 60439, (sjk@anl.gov), [4]Department of Earth and Planetary Sciences, Johns Hopkins Univ., Baltimore, MD 21218, (sarah.horst@jhu.edu), [5]Groupe de Spectrométrie Moléculaire et Atmosphérique, Univ. Reims Champagne-Ardennes, CNRS, Reims, 51687, France, panayotis.lavvas@univ-reims.fr.

Cassini demonstrated the existence in Titan's upper atmosphere of a new regime for organic chemistry in the solar system. INMS and CAPS unexpectedly discovered a complex ionospheric chemistry dominated by large organic molecules with m/z greater than 1000 Da but their mass resolving power was insufficient for unique identifications. Photochemical models provided assignments for the complex positive and negative ions present in the thermosphere, up to m/z ~ 100 Da. They notably inferred that ions are nitrogen rich. They showed that neutral and ion chemistry are intimately coupled, the latter being a substantial source of neutral species. They provided some fairly good understanding of the neutral composition, at the notable exception of oxygen-bearing species.

New outstanding questions raised by Cassini include:

- Why is there a factor of 2-3 disagreement between the observed and modeled positive ions (and electron) densities?
- What is on the nightside the relative contributions and characteristics of in situ ionization and transport of ions from the dayside?
- What is the chemical nature of the macromolecules? Are they nitrogen rich and resemble HCN polymers? Do they contain polyaromatic and/or heterocyclic subunits?
- What are the processes responsible for the growth of the aerosols? What are the relative contributions of ion-neutral vs. radical reaction pathways?
- What is the nature, intensity and time variability of the source(s) of oxygen in the atmosphere? Can biological precursors such as amino acids and nucleotide bases or other chemical species with some prebiotic potential be synthesized in the atmosphere?
- How do ions and neutral species interact with the photochemical haze and various condensates in the lower atmosphere?

A new generation of very-high resolution mass spectrometers with a mass resolving power ($m/\Delta m$ at FWHM) of 100,000 at m/z = 100, a sensitivity of 10^{-3} molecule cm^{-3} and a mass range up to 1000 u in orbit around Titan with extended flyby coverage would provide some answers to these open questions.

Bibliography: 1. C.A. Nixon, R.D. Lorenz, R.K. Achterberg, A. Buch, P. Coll, R.N. Clark, R. Courtin, A. Hayes, L. Iess, R.E. Johnson, R.M.C. Lopes, M. Mastrogiuseppe, K. Mandt, D.G. Mitchell, F. Raulin, A.M. Rymer, H. Todd Smith, A. Solomonidou, C. Sotin, D. Strobel, E.P. Turtle, V. Vuitton, R.A. West, R.V. Yelle, "Titan's cold case files - Outstanding questions after Cassini-Huygens", *Planet. Space Sci.*, in press. 2. V. Vuitton**,** R.V. Yelle, S.J. Klippenstein, S.M. Hörst, P. Lavvas, "Simulating the density of organic species in the atmosphere of Titan with a coupled ion-neutral photochemical model", *Icarus*, submitted.

EVENTS

Reception

Free for all attendees, pre-registration required
Sunday, August 12
6:00-8:00pm
Hotel Boulderado Mezzanine – 2115 13th Street

Please join us at a kick-off reception Sunday evening, on the beautiful Mezzanine of the Hotel Boulderado. There will be assorted hors d'oeuvres and a cash bar.
See map in Getting Around section.
Assorted hors d'oeuvres and a cash bar.

Public Lecture

Free for all attendees and the public
Tuesday, August 14
7:30-8:30pm
CU's Glenn Miller Ballroom, in the UMC, 1669 Euclid Avenue – 2115 13th Street

Linda Spilker, NASA-JPL planetary scientist and project scientist for the Cassini mission, will give a talk titled *Cassini and the future exploration of the outer Solar System*.
See map in Getting Around section.

Banquet

$70 per person for attendees and guests, pre-registration required
Wednesday, Aug. 15
7:30 – 9:00pm (Cash bar opens at 7:00pm)
Hotel Boulderado Conference Center – 2115 13th St, Boulder

Menu
Organic Mixed Greens – Poached Pears, Roasted Heirloom Tomatoes, Daikon Sprouts, Citrus Vinaigrette
Choice of Entree (chosen during registration)

- *Roasted Spaghetti Squash – White Bean cassoulet, grape tomato, Garlic and Basil Relish*
- *Burgundy Braised Short Ribs – Pearl Onions, Carrots & Leeks – Oyster Mushroom Jus*
- *Seared Colorado Striped Bass – Saffron White Beans – Smoked Tomato Beurre Blanc*

Chef's choice of sides
Local artisan bread
Mascarpone Creme Fraiche Berry Parfait
Local Organic Coffee & Hot Tea

Getting Around

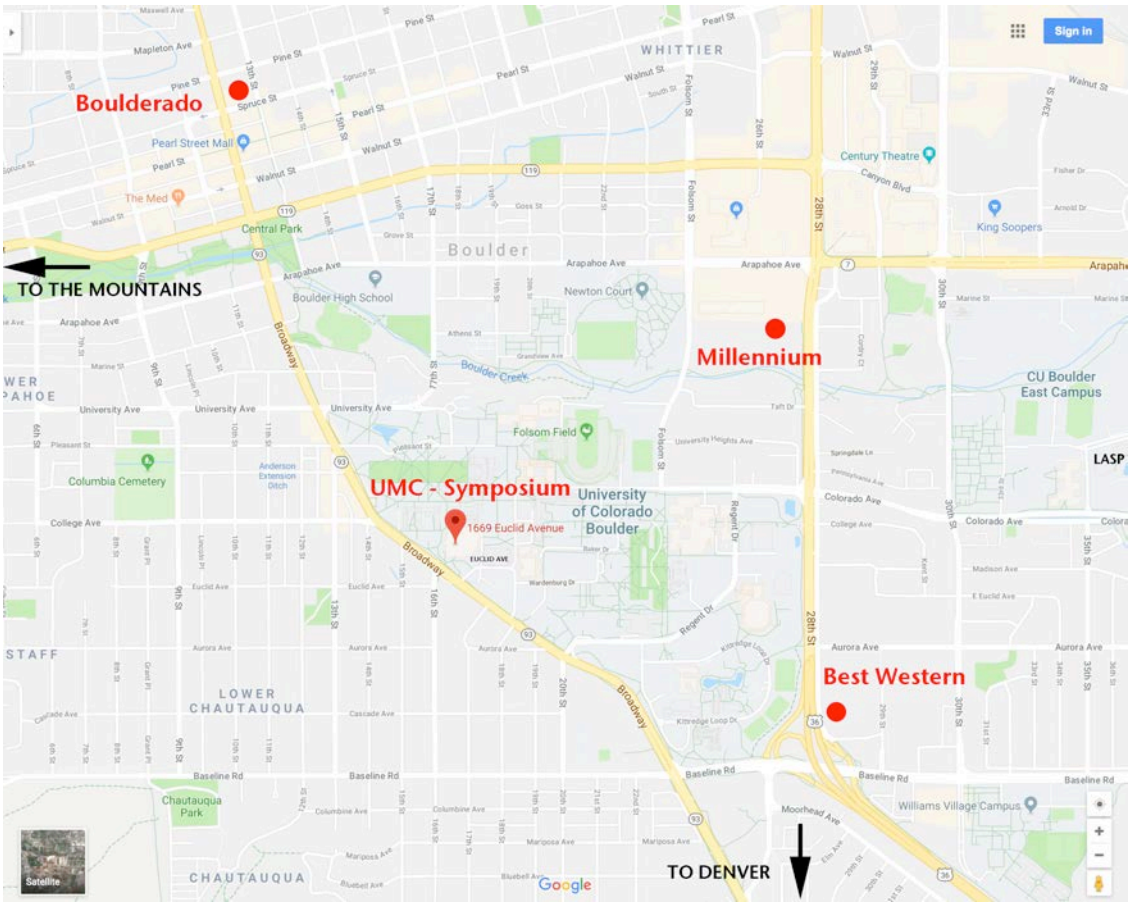

Symposium and Public Lecture

The Glenn Miller Ballroom in the University Memorial Center (UMC) on the University of Colorado Boulder campus. 1669 Euclid Ave., just off Broadway.

Parking: Euclid Auto Park, 1725 Euclid Ave., just east of the UMC, under the Case Building. Buy a $25 parking pass for the week here: https://cuboulder.pmreserve.com/. You will need the make/model/plate of the car so if you are renting a car, it's best to do this after you pick up your rental. You may come and go at your own risk (it's a busy lot and you may lose your space). If you do it in advance, enter any car information, then call Parkmobile at 866-330-7275 to update it. Or you can pay a daily ~$35 fee through a kiosk in the lot.

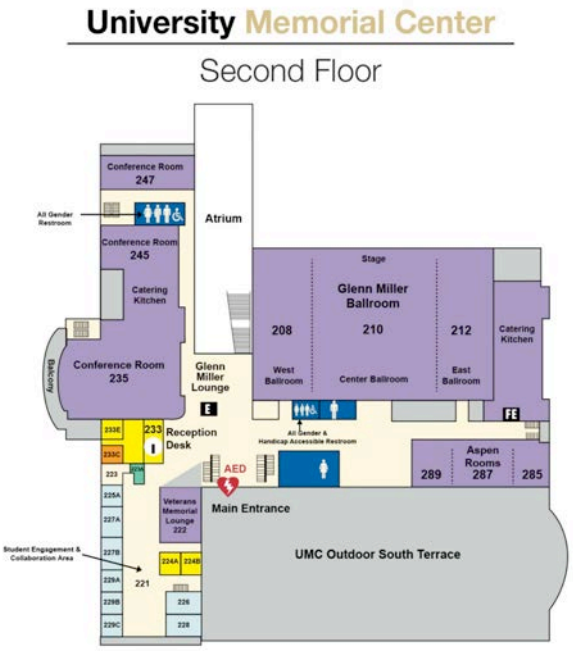

Reception and Banquet

The Hotel Boulderado is in downtown Boulder, just off the Pearl Street Mall. 2115 13th Street.
From the symposium, head north on Broadway (mountains are west) and take a right on Spruce and a left on 13th. There is valet parking, or there is paid parking on the streets or in local lots.

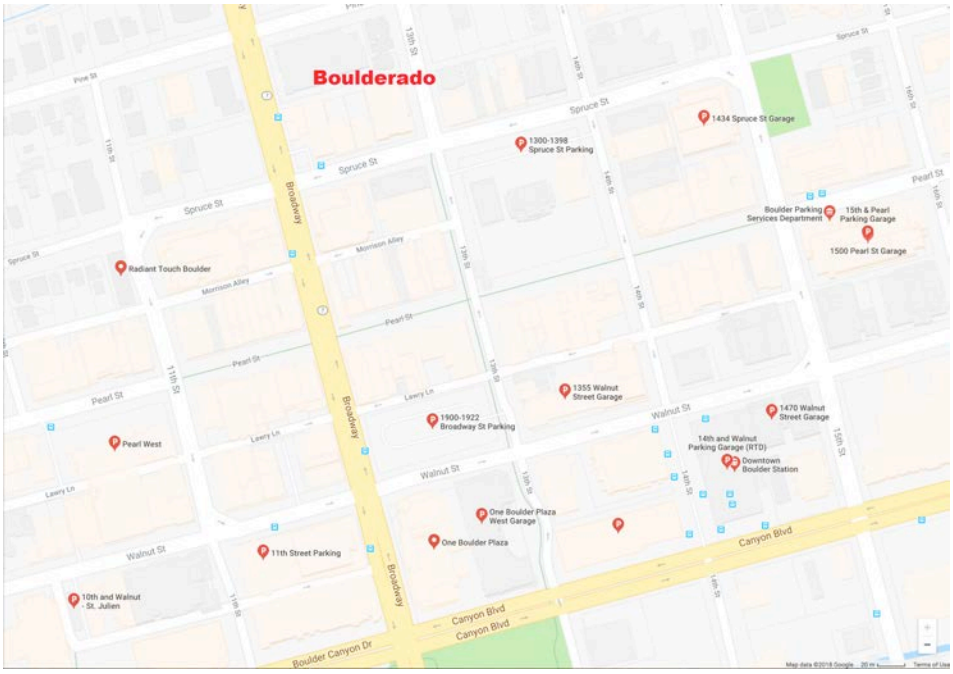

The Hill area (restaurants for lunch)